The Influence of an Improved Soil Scheme on the Arctic Climate in a Regional Climate Model (RCM)

Der Einfluss eines verbesserten Bodenschemas auf das arktische Klima in einem regionalen Klimamodell

---

Subodh Kumar Saha

Ber. Polarforsch. Meeresforsch. 519 (2006)
ISSN 1618 - 3193

Subodh Kumar Saha
Stiftung Alfred-Wegener-Institut für Polar- und Meeresforschung
Forschungsstelle Potsdam
Telegrafenberg A43
14473 Potsdam

Die vorliegende Arbeit ist die inhaltlich unveränderte Fassung einer Dissertation in der Wissenschaftsdisziplin Physik der Atmosphäre, die im Januar 2005 der Mathematisch-Naturwissenschaftlichen Fakultät der Universität Potsdam vorgelegt wurde.

Contents

Abstract

The regional climate model HIRHAM4 has been used for investigating the Arctic land-surface processes and their influences on the Arctic climate. The model simulated soil temperature is quite good during summer but, during winter it has large cold bias up to maximum 20 °C. However the model simulated 2m air temperature is very close to the observation, except in some selected regions. Due to the low model surface albedo in the costal region during summer, the 2m air temperature is warmer compared to the observation. Use of temperature dependent polynomial scheme for surface albedo of bare ground, has reduced the surface albedo bias in the costal region and hence improved the summer 2m air temperature simulation.

The model is able to capture meso-scale features of horizontal snow distribution patterns and also the maximum, minimum snow fall regions, but it underestimates snow water equivalent everywhere in the domain. The model does not take into account the soil moisture freezing/thawing during the seasonal transition periods. Therefore, lake of snow coupled with the absence of soil moisture freezing/thawing scheme causing excessive cooling of soil. Several model sensitivities has been performed but, none of these sensitivity studies (planetary boundary layer stability function, soil thermal conductivity, snow density) was able to remove model winter soil temperature bias completely. Therefore in the next step coupling between a complex land surface model (LSM) and HIRHAM4 has been designed to improve the simulation of Arctic soil processes and to assess the influence of new land-surface scheme on the future projection of Arctic climate.

The NCAR (National Center for Atmospheric Research) LSM has been used for this study. The stand alone version of LSM was driven by HIRHAM4 output at each time step. The stand alone LSM improved the winter soil temperature everywhere in the domain. During winter at 10 cm depth of soil, the LSM was warmer by a maximum of 5 °C compared to the HIRHAM4 and at 320 cm depth, the LSM soil was warmer by a maximum of 10 °C. There was also an increase in snow water equivalent. The LSM showed that, the soil moisture content, soil moisture freezing/thawing process and the amount of snow over ground are important for the winter soil temperature evolution. Interactive coupling between HIRHAM4 and LSM was through the exchange of variables in each model time step. The HIRHAM4 coupled LSM simulation was also able to reduce the winter cold soil temperature bias. There were large changes in the HIRHAM4 coupled LSM simulated surface sensible, latent and radiative fluxes compared to the HIRHAM4. The surface sensible and latent heat flux changes were mainly due to the different spatial distribution of soil moisture content in HIRHAM4 and LSM. The surface radiative fluxes were indirectly influenced by the changed surface sensible and latent heat fluxes.

Model soil and 2m air temperature in the permafrost regions were found sensitive to the use of different land surface schemes during scenario simulations. We show that, the future projection of Arctic soil and near surface air temperature is uncertain by $\pm 2\,^{\circ}C$ purely due to the use of land-surface scheme and it's coupling with the atmosphere. Also there are differences in the future projection of tow model's (HIRHAM4 and HIRHAM4 coupled LSM) summer precipitation by $\pm 12\ mm\,month^{-1}$. Future projection of mean sea level pressure was differed between tow models by a maximum of 4 hPa over the ocean. It is clearly seen that, the land-surface scheme not only has influence regionally but also in a remote area and the future projection of large-scale circulation pattern is also uncertain significantly due to the use of land-surface scheme.

Zusammenfassung

Das regionale Klimamodell HIRHAM wurde benutzt, um arktische Landober fläechenprozesse und ihren Einfluss auf Klimasimulationen zu untersuchen. Die simulierten Bodentemperaturen stimmen im Sommer gut mit Beobachtungen üeberein, wäehrend sie im Winter um bis zu 20 °C zu kalt sind. Die simulierte 2m Lufttemperatur ist in guter Üebereinstimmung mit Beobachtungen, ausser an einigen ausgewäehlten Regionen. In Küestenregionen ist die simulierte Lufttemperatur im Sommer wäermer als Beobachtungen, und zwar aufgrund von einer kleineren simulierten Oberfläechenalbedo. Die Einfüehrung einer Temperaturabhäengigen Oberfläechenalbedoparameterisierung füehrt zur Reduktion des Albedofehlers und daher zur Verbesserung der Temperatursimulation in den Küestenregionen.

Das Modell simuliert mesoskalige Muster der horizontalen Schneeverteilung, sowie eine realistische Darstellung der Regionen mit maximalen/minimalen Schneefall. Die Schneedicke (snow water equivalent) wird durch das Modell jedoch unterschäetzt. Das Bodenschema berüecksichtigt nicht die Prozesse des Bodengefrierens und -auftauens. Diese fehlenden Prozesse, wie auch die unterschäetzte Schneedecke füehren zum starken Abküehlen des Bodens. Es wurden verschiedene Sensitivitäetsstudien durchgefüehrt, unter anderem die Sensitivitäet der Bodentemperatur bzgl. der planetaren Grenzschicht-Stabilitäet, der Wäermeleitfäehigkeit des Bodens, und der Schneedichte. Keines dieser Prozesse konnte den winterlichen Fehler in der simulierten Bodentemperatur komplett beseitigen. Daher wurde im näechsten Schritt, ein komplexes Landoberfläechenmodell (LSM) an das HIRHAM interaktiv gekoppelt.

Das NCAR (National Center for Atmospheric Research) LSM wurde benutzt. Die stand-alone Version des LSM Modells wurde jeden Zeitschritt mit dem HIRHAM Output angetrieben. Das stand-alone LSM verbesserte die simulierte winterliche Bodentemperatur. Im Winter, in 10 cm (320 cm) Bodentiefe sind die simulierten Bodentemperaturen maximal 5 °C (10 °C) wäermer als die HIRHAM simulierten Werte. Die simulierte Schneedicke (snow water equivalent) wurde gröesser. Die LSM Simulationen zeigten, dass der Bodenwassergehalt, die Bodengefrier- und auftauprozesse, und die Schneedecke füer die winterliche Bodentemperaturentwicklung von Bedeutung sind. Die interaktive Kopplung zwischen LSM und HIRHAM wurde üeber den Austausch von Variablen zu jedem Zeitschritt realisiert. Das HIRHAM-LSM gekoppelte Modell konnte den kalten winterlichen Bodentemperaturfehler reduzieren. Die simulierten sensiblen, latenten und Strahlungsflüesse äenderten sich gegenüeber der HIRHAM Simulation. Die Äenderungen der sensiblen und latenten Wäermefluesse sind hauptsäechlich durch die verschiedene räeumliche Verteilung des Bodenwassergehaltes in den beiden Modellen. Die Strahlungsflüesse am Erdboden sind indirekt durch die genderten sensiblen und latenten Wäermeflüesse beeinflusst.

Die Boden- und 2m Lufttemperaturen üeber Permafrostregionen sind in Szenarien-Simulationen sensitiv bzgl. des benutzten Landoberfläechenschemas. Die zukünftige Projektion der Boden- und 2m Lufttemperaturen hat bzgl. des verwendeten Landoberfläechenschemas und seiner Kopplung mit der Atmosphäere eine Ungenauigkeit von 2 °C. Die Abschäetzungen der Äenderungen des zukünftigen sommerlichen Niederschlages mit beiden Modellen (HIRHAM und HIRHAM-LSM) unterscheiden sich um 12 mm pro Monat. Auch die Abschäetzung der zukünftigen Bodenluftdruckäenderung ist verschieden, mit maximal 4 hPa unterschied üeber dem Ozean. Die verschiedenen Landoberfläechenmodelle zeigen nicht nur regionale Äenderungen üeber Land, sondern auch Äenderungen in den gross-skaligen Zirkulationsmustern, sowie Äenderungen üeber dem Ozean.

1 Introduction

1.1 Motivation

The land surface of the Earth represents a large source and sink of heat, moisture and greenhouse gases. There exist close interactions between the atmosphere and the land surface. Therefore a change in atmospheric circulations influences the land surface and vice versa. Instrumental records show an increase in the global averaged surface air temperature (the average of near surface air temperature over land and sea surface temperature) in the 20^{th} century by about 0.6 °C. The IPCC (Intergovernmental Panel on Climate Change) projects an increase in global averaged surface temperature in the 21^{st} century by 1.4 to 5.8 °C. The increase in surface temperature is larger in the Northern Hemisphere and the land areas are projected to warm more rapidly than the global average, particularly during the cold season (*Cubasch et al.*, 2001). The Arctic is a host of a vast amount of permafrost and a largest warming signal is projected here. In the last few years many studies have been made to understand the climate processes of the Arctic and the possible regional climate changes as well as the feedbacks to the global climate (*Dorn et al.*, 2003; *Kiilsholm et al.*, 2003). The future projected warming is vulnerable to the stability of Arctic permafrost. Permafrost is a product of severe climate conditions and is a very sensitive part of the Arctic climate. About one third of the land area of the Northern Hemisphere contains permafrost and the major parts of it are found in the circumpolar Arctic region. Numerous studies have shown that both large-scale patterns and regional details of the permafrost distribution are very sensitive to climate change at different temporal and spatial scales (*Hinkel and Nelson*, 2003; *Pavlov and Moskalenko*, 2002; *Anisimov and Nelson*, 1996). The active layer of permafrost is the upper layer that thaws in every summer and refreezes in every winter. An increase in annual mean temperature at the base of the active layer from 0 °C, increases the thaw depth in successive summers and often these depths become larger than the refreezing depths in the following winter. This is known as "permafrost degradation". There are evidences that the permafrost in some regions of the Arctic have started to melt. The degradation of the permafrost or melting is a big threat to infrastructure, regional hydrology and ecosystems. It may act as a positive feedback to the global warming through the release of greenhouse gases to the atmosphere.

Interactions between the atmosphere and the permafrost are very complex. Snow cover, vegetation type, soil type, soil moisture content, phase changes of soil moisture and planetary boundary layer (PBL) structure above the surface are involved in the

interaction between the atmosphere and permafrost. Permafrost and the active layer influence the atmosphere by affecting the surface heat fluxes, evaporation, surface runoff and trace gas exchange. The atmosphere influences the active layer and permafrost through precipitation (snow and rain), PBL structure and clouds. The seasonal freezing and melting of active layer account for a large amount of latent heat. Therefore, the thermal inertia of active layer becomes high and it does not get warmed up or cooled down rapidly during the phase transition of soil moisture (i.e. around 0 °C). Vegetation cover and snow season also make the difference in active layer and permafrost temperature.

The regional climate model HIRHAM4 does not take account of freezing and thawing of the active layer. The moisture transport between the soil layers is also not considered in the HIRHAM4. Therefore the true description of active layer and permafrost and hence the true feedback processes between the atmosphere and the permafrost are missing in HIRHAM4. Representations of seasonal soil moisture freezing, thawing and soil moisture at each layer in the HIRHAM4 will improve the description of feedback processes between the atmosphere and the land surface in a more realistic way. Also the future changes in the permafrost and the role of permafrost in climate change over the circumpolar Arctic can be addressed in a better way.

The Arctic is a data-poor region and many variables, particularly the soil temperatures are measured at few stations only. There are also difficulties in snow fall measurements. In the mountain regions, observations may underestimate the winter precipitation by as much as 40% (*Legates and Willmott*, 1990). Therefore, it is difficult to assess the performance of a climate model in this region. Nevertheless only numerical climate models can deliver important *climate* information in the Arctic. The newly developed active layer and permafrost schemes can be studied using complex numerical climate models.

1.2 Objectives of this work

The regional climate model HIRHAM4 has been applied to the circumpolar Arctic by *Dethloff et al.* (1996) and also been used to understand several aspects of the Arctic climate (*Rinke et al.*, 1999; *Dorn et al.*, 2000; *Dethloff et al.*, 2001). So far the soil processes in the HIRHAM4 did not get much attention. The HIRHAM4 has been validated for a small region in the East European Arctic and the indices of soil freezing and thawing were found quite good (*Christensen and Kuhry*, 2000). But little is known about permafrost, active layer and it's interactions with the atmosphere. The main objectives of this work are therefore the following:

- to assess the HIRHAM4 soil simulations, particularly the seasonal evolution of soil temperature and the interaction of soil processes with the atmosphere
- to identify the key processes responsible for the active layer and permafrost temperatures
- to improve the descriptions of soil processes in HIRHAM4 by using a new complex land-surface scheme (NCAR Land Surface Model)
- to apply the HIRHAM4 with a new soil scheme for IPCC scenario simulation and to assess the possible changes in permafrost temperatures due to the improved soil scheme.

It has been documented that the absence of seasonal soil moisture freezing and thawing can add biases to the soil and near surface air temperature (*Viterbo et al.*, 1999). The timing of snow fall, snow season and snow amount on the ground surface largely determine the soil temperature (*Ling and Zhang*, 2003). The HIRHAM4 winter Arctic surface air temperature depends very strongly on the choice of the planetary boundary layer scheme (*Dethloff et al.*, 2001). A positive feedback in the land surface boundary-layer coupling during winter may further stratify the planetary boundary layer and this can introduce a cold bias to the surface and soil temperature (*Viterbo et al.*, 1999).

For an Alaskan region a more advanced land surface model (NCAR LSM version 1.0) has been applied to assess the model soil processes and interactions with the atmosphere. *Beringer et al.* (2001) applied the LSM to the Alaskan Arctic and found that the mosses are important for the Arctic soil. The LSM has been coupled with CCM2 global model (T42 resolution) by *Bonan* (1998) and it was shown that it improved the precipitation, soil water, particularly during transition periods. The surface albedo depends on the spectral band of incident solar radiation. The use of spectral surface albedo in climate model was recommended by *Roesch et al.* (2002) for minimizing the uncertainty in surface albedo calculation. The LSM uses the spectral apporach for calculating surface albedo, whereas the HIRHAM4 uses the total surface albedo approach.

Here we have used the LSM for the entire Arctic with a high horizontal resolution ($0.5\,° \times 0.5\,°$). The LSM simulation have been performed in a stand alone mode and in a coupled way with the model HIRHAM4. The influences of new land-surface scheme and its coupling with the atmosphere on the future permafrost temperature have been investigated. The study is organized as follows:

The second chapter provides a general introduction to regional climate modeling, a brief description of the HIRHAM4 governing equations and a detailed description of soil processes involved in the model.

In the third chapter, the HIRHAM4 simulated mean sea level pressure, $2\,m$ air temperature, precipitation, snow water equivalent and soil temperature are compared with the available observations.

Sensitivity studies with changed HIRHAM4 soil thermal conductivity, snow density, new snow albedo scheme for bare land and revised stability function in the PBL

are discussed in the fourth chapter.

A brief description of NCAR land surface model is given in chapter five. Here the results from the stand alone version of LSM, driven by the HIRHAM4 output are analyzed and validated against the observations.

The HIRHAM4, coupled with the NCAR Land Surface Model (LSM version 1.0) is described in chapter six. The current coupling between HIRHAM4 and LSM and the possible future coupling procedure are described. The results from the new coupled model are compared with the HIRHAM4 results and with the observations.

In the seventh chapter, IPCC (Intergovernmental Panel on Climate Change) B2 emission scenario simulations for the two negative NAO and one positive NAO phases have been simulated using the HIRHAM4 and the coupled model (NCAR land surface model coupled with the HIRHAM4). The possible changes in the soil and surface air temperature, precipitation and mean sea level pressure are investigated. The eighth chapter describes the summary and conclusions of this work.

2 HIRHAM4 Model Description & Soil Processes

2.1 Introduction

The global circulation models (GCMs) are widely used for climate simulations and also for the future climate scenarios. The scatter between these model is large and often they contain large biases particularly in the meso-scale climate features. The physical processes in the Earth climate systems are very complex in nature, they range from the molecular scale (e.g. micro-physical cloud formation) to the planetary scale (e.g. cyclones) and there exist close interactions between the large-scale and the small-scale processes. The common practice of describing the physical processes on scales beyond the models resolution is *parametrization*. There are large model to model variations in the parametrization schemes and also in the numerical techniques. Therefore, the performance of each model differs from the others. Since the spatial and temporal resolutions of the GCMs are coarse, they need less computer power but they do contain also less regional information. So to include meso-scale features into the numerical climate model, one needs a high resolution climate model, which will be able to take into account the small scale orography, vegetation, soil moisture, soil type, snow distributions etc. Current GCM's can reach a horizontal resolution of 1 degree, but this resolution is not enough for mountain regions to capture steep orography, snow and vegetation distributions. There are also some unique regional climate features, which are not given enough importance or which are not parameterized in the GCMs. For example permafrost and seasonally frozen and melted active soil layer are unique features of the Arctic climate and an Arctic model needs to take care of that processes in a realistic way.

One of the several down-scaling techniques is dynamic down-scaling by regional climate modeling, which enables to resolve climate processes with very high resolution for a smaller (limited) area with affordable computer resources. With this technique, a climate model with hydrostatic approximation can reach about 10 km horizontal resolution. A regional climate model with the same physics and dynamics as in the GCM can be applied for a smaller domain with high temporal and spatial resolution. The high resolution model can be embedded either in a GCM or initial conditions and lateral boundary forcing can be provided from observed analysis data. The high resolution model is forced by the large scale signal at its boundary, which will carry the large scale information into the integration domain and the local processes inside the model domain will evolve according to its dynamics and

parameterizations of physical processes. the HIRHAM4 is such a regional climate model (RCM) and used here for the present study.

The choice of the RCM integration area is critical and depends very much on the chosen location (*Jones et al.*, 1995). A larger domain may not be able to carry the large-scale information from the lateral forcing field at the boundary to the interior of the domain. A small domain will not be suitable for developing small scale processes but it will be influenced largely by the lateral forcing fields. The RCM solution also depends on the resolution of the driving boundary fields. The mismatch between the driving coarse-resolution model and the high-resolution RCM does not cause fundamental problems if proper boundary condition procedure is applied, as demonstrated by *Denis et al.* (2002). The maximum acceptable spatial resolution jump between the driving and the nested models is six to twelve fold, i.e. T60 to T30 resolution of the coarse driving model for a 45 km resolution RCM (*Denis et al.*, 2003). For choosing the HIRHAM4 domain and the resolution of lateral forcing data, the above limitations are fulfilled.

2.2 Model description

The regional climate model HIRHAM4 was developed by *Christensen and van Meijgaard* (1992) and improved by *Christensen et al.* (1996). The adiabatic formulation is based on the high resolution limited area model HIRLAM (*Machenhauer et al.*, 1998; *Gustafsson*, 1993) and the physical parameterizations are taken from the general circulation model ECHAM (*Roeckner et al.*, 1992, 1996). The HIRHAM4 has been applied for the circumpolar Arctic region by *Dethloff et al.* (1996), which covers all areas North of about ~65 °N. The standard model version has a horizontal grid resolution of 0.5 degree in rotated latitude and longitude. In the vertical, a hybrid sigma coordinate with 19 or 25 levels is used. Top of the model level is at about 10 hPa. The HIRHAM4 is a standard primitive equation Eulerian staggered grid point model. The physical parameterizations are taken from ECHAM4 and include radiation, cumulus convection, land surface processes, planetary boundary layer turbulence, gravity wave drag and condensation.

2.2.1 Governing equations

The dynamical part of HIRHAM4 is based on the prognostic momentum, thermodynamic and moisture equations. It is a hydrostatic model. Two metric coefficients (h_x, h_y) have been used in the model equations for any orthogonal coordinate system or map projection with axis (x, y). On the Earth surface, a distance δX, δY can be written as:

$$\delta X = a\, h_x \delta x \quad \text{and} \quad \delta Y = a\, h_y \delta y. \tag{2.1}$$

In the case of a rotated spherical coordinate on the Earth surface (λ, ϕ), the above metric coefficients can be written as:

$$\delta X = a\, cos\lambda\, d\phi \quad \text{and} \quad \delta Y = a\, \delta\lambda, \tag{2.2}$$

where a is the radius, ϕ the longitude and λ the latitude of the Earth. In the cartesian coordinate the model horizontal momentum and thermodynamic equations are:

$$\frac{\partial u}{\partial t} = (f+\xi)v - \dot{\eta}\frac{\partial u}{\partial \eta} - \frac{R_d T_v}{a h_x}\frac{\partial \ln P}{\partial x} - \frac{1}{a h_x}\frac{\partial}{\partial x}(\Phi + E) + PH_u + K_u, \tag{2.3}$$

$$\frac{\partial v}{\partial t} = -(f+\xi)u - \dot{\eta}\frac{\partial v}{\partial \eta} - \frac{R_d T_v}{a h_y}\frac{\partial \ln P}{\partial y} - \frac{1}{a h_y}\frac{\partial}{\partial y}(\Phi + E) + PH_v + K_v, \tag{2.4}$$

$$\frac{\partial T}{\partial t} = -\frac{u}{a h_x}\frac{\partial T}{\partial x} - \frac{v}{a h_y}\frac{\partial T}{\partial y} - \dot{\eta}\frac{\partial T}{\partial \eta} + \frac{\kappa T_v \omega}{(1+(\delta-1)q_v)P} + PH_T + K_T, \tag{2.5}$$

where

$$\xi = \frac{1}{a h_x h_y}\Big\{\frac{\partial}{\partial x}(h_y v) - \frac{\partial}{\partial y}(h_x u)\Big\}, \tag{2.6}$$

$$E = \frac{1}{2}(u^2 + v^2), \tag{2.7}$$

$$\dot{\eta} = \frac{\partial \eta}{\partial t}, \tag{2.8}$$

where u, v are the zonal and meridional velocities, T the air temperature, R_d the dry air gas constant, f the Coriolis force, Φ the geopotential height, κ the von Kármán's constant, T_v the virtual air temperature, PH_u, PH_v, PH_T are the tendencies from physical parametrization, K_u, K_v, K_T are the tendencies from horizontal diffusion. The water vapor and cloud water equations are:

$$\frac{\partial q_v}{\partial t} = -\frac{u}{a h_x}\frac{\partial q_v}{\partial x} - \frac{v}{a h_y}\frac{\partial q_v}{\partial y} - \dot{\eta}\frac{\partial q_v}{\partial \eta} + PH_{q_v} + K_{q_v}, \tag{2.9}$$

$$\frac{\partial q_w}{\partial t} = -\frac{u}{a h_x}\frac{\partial q_w}{\partial x} - \frac{v}{a h_y}\frac{\partial q_w}{\partial y} - \dot{\eta}\frac{\partial q_w}{\partial \eta} + PH_{q_w} + K_{q_w}, \tag{2.10}$$

where q_v is the water vapor mixing ratio, $q_w = q_l + q_i$ is the cloud water mixing ratio including the liquid q_l and the solid fraction q_i. The hydrostatic equation is

$$\frac{\partial \Phi}{\partial P} = -\frac{R_d T_v}{P} \tag{2.11}$$

and the continuity equation is

$$\frac{\partial}{\partial \eta}\Big(\frac{\partial P}{\partial t}\Big) + \nabla\cdot\Big(\vec{V_h}\frac{\partial P}{\partial \eta}\Big) + \frac{\partial}{\partial \eta}\Big(\dot{\eta}\frac{\partial P}{\partial \eta}\Big) = 0, \tag{2.12}$$

where $\vec{V_h}$ is the horizontal wind vector and the definition of divergence operator is

$$\nabla\cdot\vec{V_h} = \frac{1}{a\,h_x h_y}\Big\{\frac{\partial}{\partial x}(h_y u) + \frac{\partial}{\partial y}(h_x v)\Big\}. \tag{2.13}$$

By integrating the continuity equation, using the boundary conditions $\dot{\eta} = 0$ at $\eta = 0$ and $\eta = 1$, we obtain the equation for the surface pressure tendency

$$\frac{\partial P_S}{\partial t} = -\int_0^1 \nabla\cdot(\vec{V_h}\frac{\partial P}{\partial \eta})d\eta. \tag{2.14}$$

The pressure coordinate vertical velocity is

$$\omega = \frac{\partial P_S}{\partial t} + \int_\eta^1 \nabla \cdot (\vec{V_h}\frac{\partial P}{\partial t})d\eta + \vec{V_h} \cdot \nabla P \tag{2.15}$$

and the equation for $\dot{\eta}$ is

$$\dot{\eta}\frac{\partial P}{\partial \eta} = (1 - \frac{\partial P}{\partial P_S})\frac{\partial P_S}{\partial t} + \int_\eta^1 \nabla \cdot (\vec{V_h}\frac{\partial P}{\partial \eta})d\eta. \tag{2.16}$$

A detailed description of model governing equations can be found in *Machenhauer* (1988) and in *Dorn* (2002).

2.2.2 Surface radiation and atmospheric heating

The principal quantity determined in the radiation calculation is the temperature tendency, i.e. the atmospheric heating or cooling rate. It is related to the flux divergence according to

$$\left(\frac{\partial T}{\partial t}\right)_{rad} = \frac{g}{c_p}\frac{\partial F}{\partial P}, \tag{2.17}$$

where F is the total radiative flux (short wave and long wave), g and c_p are the constant of gravity and the specific heat of air respectively. The model radiative transfer equations are not calculated in each time step but only in every 2 hours. To take into account the change in temperature and solar zenith angle between the time when the full radiation is calculated, effective transmissivity τ_e and emissivity ϵ_e are defined at each model level such that

$$F_T = \epsilon_e \cdot \sigma \cdot T^4, \tag{2.18}$$

$$F_S = \tau_e \cdot S_0, \tag{2.19}$$

where F_T and F_S are the net thermal (long wave) and solar (short wave) fluxes respectively. σ is the Stefan-Boltzmann constant and S_0 is the solar flux at the top of atmosphere. The values ϵ_e and τ_e are kept constant between the full radiation time steps and the net fluxes are recomputed at every time step using equations (2.18) and (2.19) with the correct temperature and solar zenith angle. Further descriptions of HIRHAM4 radiative transfer equations can be found in *Fortman* (2004).

2.2.3 Boundary relaxation

The lateral boundary forcing in the model is according to *Davies* (1976). Surface pressure, wind, specific humidity and air temperature are relaxed in a 10 grid points wide boundary zone and the formulation for a field f, at each time step and at k^{th} grid point is

$$f_k = (1 - \alpha_k)f_k^{HIRHAM4} + \alpha_k f_k^{ERA15}. \tag{2.20}$$

The coefficient α_k is the relaxation weight, which joins the boundary forcing data with the model data linearly within the relaxation zone. Fields f_k with superscript

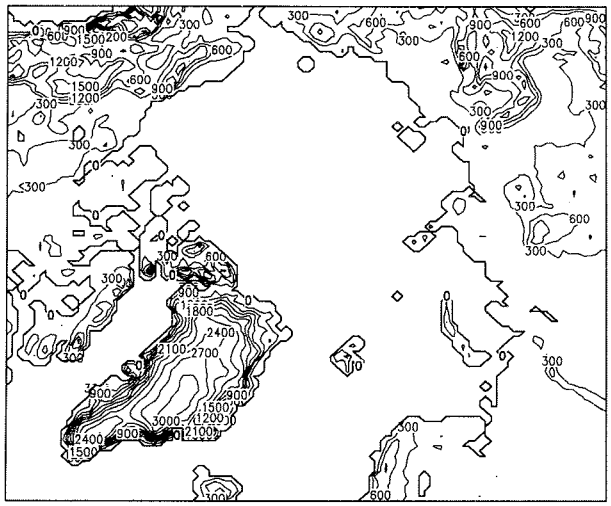

Figure 2.1: The HIRHAM4 integration area and orography (in m) in $50 \times 50\,km$ model horizontal resolution.

$HIRHAM4$ and $ERA15$ are representing the model values and lateral forcing values respectively. α_k depends on the grid point distance from the boundary and is given by

$$\alpha_k = 1 - tanh(ak), \tag{2.21}$$

where a is a constant and depends on the number of relaxation points. Moisture and cloud water are relaxed according to so called inflow/outflow scheme, where only values on the edge of the domain are modified. If the flow is towards out of the integration area, a value extrapolated from the four nearest points located upstream and inside the model domain is applied at the model levels otherwise the boundary field value is assigned to this outer point. The model lower boundary was forced by daily ERA-15 sea surface temperature and sea ice fraction. Except IPCC B2 scenario run, the model initial condition and lateral forcing were from ECMWF re-analysis ERA-15 (*Gibson et al.*, 1999), with spectral T106 resolution, 31 vertical hybrid levels and 6 hourly data.

2.2.4 Numerical schemes

The HIRHAM4 is a rotated grid coordinate model, pole has been brought to the equator (0 °N, 0 °E) and then horizontally it is discretized into a 0.5 ° by 0.5 ° grid. The model integration area and the topography are shown in Figure 2.1. The model horizontal formulations are in Arakawa C-grid.

Vertical discretization

The model's vertical coordinate is a hybrid sigma coordinate $\eta(P, P_S)$, which follows the sigma coordinate near the surface and pressure coordinate at the upper layers. This is a monotonic function of pressure P and also depends on surface pressure P_S where:

$$\eta(0, P_S) = 0 \quad \text{and} \quad \eta(P_S, P_S) = 1. \tag{2.22}$$

If the atmosphere is divided into $NLEV$ layers (for HIRHAM4 it is 19 or 25), then these are defined by the pressures of the interface between "half levels" and the "half level" pressures are given by

$$P_{k+1/2} = A_{k+1/2} + B_{k+1/2}\, P_S, \tag{2.23}$$

for $k = 0, 1, 2.....NLEV$. The $A_{k+1/2}$ and $B_{k+1/2}$ are constants (the values are given in the Table 2.1). The model follows the pressure coordinate when $B_{k+1/2} = 0$ (i.e. level 1,2), sigma coordinate when $A_{k+1/2} = 0$ (level 17, 18,....25) and hybrid sigma coordinate for the rest (level 3, 4,....16). The values of constant A's and B's are determined using a reference sea-level pressure $P_S = 1015$ hPa. The model prognostic variables are described in "full level" pressure P_k and though the values for P_k are not required explicitly in the vertical finite difference scheme, they are used for interpolating data to the pressure levels. A simple form of "full level" pressure is adopted by using

$$P_k = \frac{1}{2}\Big(P_{k+1/2} + P_{k-1/2}\Big). \tag{2.24}$$

Horizontal discretization

The *centered difference* scheme is used here for the horizontal discretization of model equations. In cartesian coordinate if ψ is the variable and Δx is the horizontal distance between two grid points in the x-axis, then the first-order derivative of ψ with respect to x and with truncation error δx^2 is represented by

$$\frac{\partial \psi}{\partial x} \simeq \frac{\psi(x + \Delta x) - \psi(x - \Delta x)}{2\Delta x} \tag{2.25}$$

and the second-order derivative of ψ with truncation error δx^2 is represented by

$$\frac{\partial^2 \psi}{\partial x^2} \simeq \frac{\psi(x + \Delta x) - 2\psi(x) + \psi(x - \Delta x)}{(\Delta x)^2}. \tag{2.26}$$

In the Arakawa C staggered grid T, q_v, q_w and p are calculated at the grid point (x, y), u and v are calculated at the grid point $(x+\Delta x, y)$ and $(x, y+\Delta y)$ respectively.

k	$A_{k+1/2}$	$B_{k+1/2}$	Lev.	Height (m)	Pressure (hPa)	Lev.	Height (m)	Pressure (hPa)
0	0.000	0.0000000						
1	2000.000	0.0000000	1	26195	10.0	1	26195	10.0
2	4000.000	0.0000000	2	22226	30.0	2	22226	30.0
3	6046.110	0.0003389	3	19927	50.4	3	19927	50.4
4	8267.927	0.0033571	4	18086	73.4	4	18086	73.4
5	10609.513	0.0130700	5	16306	102.7	5	16306	102.7
6	12851.100	0.0340771	6	14489	141.2	6	14489	141.2
7	14698.498	0.0706498	7	12639	190.9	7	12639	190.9
8	15861.125	0.1259166	8	10811	252.6	8	10811	252.6
9	16116.236	0.2011954	9	9048	325.9	9	9048	325.9
10	15356.924	0.2955196	10	7389	409.4	10	7389	409.4
11	13621.460	0.4054091	11	5862	500.6	11	5862	500.6
12	11101.561	0.5249322	12	4490	595.8	12	4490	595.8
13	8127.144	0.6461079	13	3289	690.4	13	3289	690.4
14	5125.141	0.7596983	14	2273	779.7	14	2273	779.7
15	2549.969	0.8564375	15	1455	858.6	15	1455	858.6
16	783.195	0.9287469	16	836	922.6	16	836	922.6
17	0.000	0.9432648				17	545	954.0
18	0.000	0.9580097				18	409	964.9
19	0.000	0.9729851	17	409	969.0	19	308	980.0
20	0.000	0.9793752				20	212	990.8
21	0.000	0.9858072				21	155	997.3
22	0.000	0.9922814	18	155	997.4	22	97	1003.9
23	0.000	0.9948476				23	56	1008.5
24	0.000	0.9974205				24	34	1011.0
25	0.000	1.0000000	19	34	1011.1	25	12	1013.7

Table 2.1: Height, standard pressure and the corresponding coordinate parameters of vertical levels in HIRHAM4. The 19-*level* and 25-*level* version of HIRHAM4 are shown and the reference sea-level pressure $P_S = 1015$ hPa is used.

Time discretization

In HIRHAM4 the semi-implicit "Leap-Frog" scheme is used for solving the prognostic equations. An equation of the form, similar to equation (2.17) with a prognostic variable ψ can be written as

$$\frac{\partial \psi}{\partial t} = F. \tag{2.27}$$

Using the semi-implicit scheme, ψ at the future time step $n+1$ can be written as

$$\psi^{n+1} = \psi^{n-1} + 2\Delta t \cdot (F^n - S_\psi), \tag{2.28}$$

where F^n represents the local temporal derivative of ψ, S_ψ is the semi-implicit correction term and formulation of this quantity varies from one equation to the other. The explicit formulation of time derivative of ψ is used as a first approximation and subscript 'e' is denoting the explicit term. Therefore from equation 2.27 we get the following

$$\psi_e^{n+1} = \psi^{n-1} + 2\Delta t \cdot F^n. \tag{2.29}$$

Now using equations (2.28) and (2.29), we have the complete solution for ψ at the future time step $n+1$

$$\psi^{n+1} = \psi_e^{n+1} - 2\Delta t \cdot S_\psi. \tag{2.30}$$

Finally, a time filter is for the values ψ at the n^{th} time step (this value in the next time step will be treated as $(n-1)^{th}$ time step value) is

$$\psi_f^n = \psi^n + \epsilon_f(\psi_f^{n-1} + \psi^{n+1} - 2\psi^n), \tag{2.31}$$

where subscript f represents the time filtered value and $\epsilon_f = 0.05$.

2.3 Land surface processes

The land surface parametrization scheme comprises the evolution of soil temperature profile, soil moisture, surface water vapor flux, planetary boundary layer momentum and heat transfer and snow pack over land. If there is snow on the ground surface, then the snow surface temperature, otherwise ground surface temperature acts as an interface between atmosphere and soil.

2.3.1 Soil temperature

The model soil column of total depth 9.834 m is divided into 5 layers. The thickness of the individual soil layer increases with depth as shown in Figure 2.2. Thermal heat conduction is the main process for heat transfer into the soil and the equation for the soil layers follows the form

$$\begin{aligned}
\frac{\partial T_1}{\partial t} &= \frac{F_s}{\rho_g C_g \Delta z_1} + \frac{2\kappa(T_2 - T_1)}{\Delta z_1(\Delta z_1 + \Delta z_2)} && \text{(For layer 1)} \\
\frac{\partial T_i}{\partial t} &= -\frac{2\kappa(T_i - T_{i-1})}{\Delta z_i(\Delta z_{i-1} + \Delta z_i)} + \frac{2\kappa(T_{i+1} - T_i)}{\Delta z_i(\Delta z_i + \Delta z_{i+1})} && \text{(For layers 2 to 5)}
\end{aligned} \tag{2.32}$$

with

κ	heat diffusivity in the soil,
T_1	temperature for soil layer 1,
T_2	temperature for soil layer 2,
T_i	temperature for soil layer i,
F_s	sum of radiative and turbulent fluxes at the surface and
$\rho_g \cdot C_g$	heat capacity of soil per unit volume.

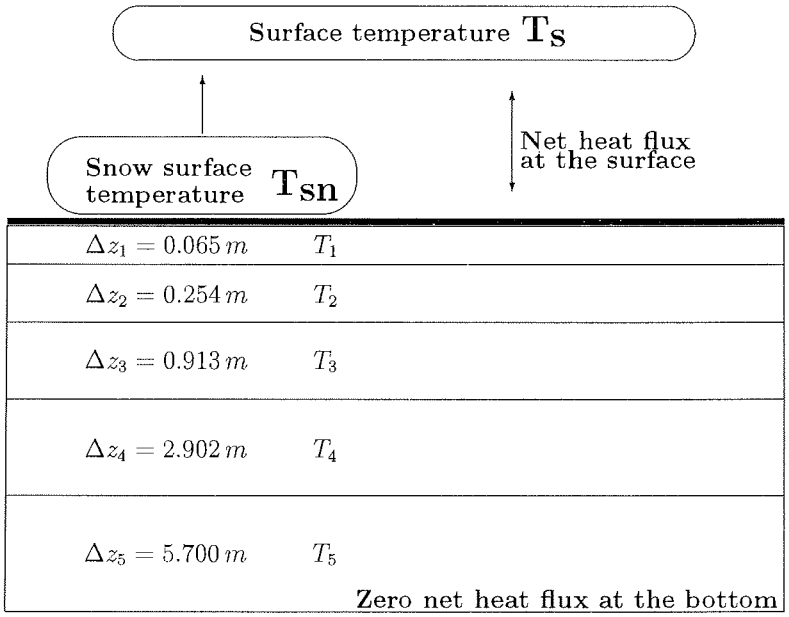

Figure 2.2: Schematic diagram of HIRHAM4 soil layers.

The top boundary condition is determined by the net fluxes of latent heat, sensible heat and radiation at the ground surface. The bottom boundary condition is prescribed by introducing zero net heat flux at the bottom in order to close the energy budget of the Earth-atmosphere system. Thermal properties of the soil i.e. temperature, thermal conductivity ($= \frac{\kappa}{\rho_g \cdot C_g}$), volumetric heat capacity are defined at the center of each soil layer. Thermal conductivity and volumetric heat capacity vary horizontally according to the soil type, which is a field generated by FAO (the United Nations Organization for Food And Agriculture) soil type distribution (*Wilson and Henderson-Sellers*, 1985). The horizontal distributions of the soil thermal characteristics (thermal conductivity, volumetric heat capacity) are assumed to be the same for all layers.

2.3.2 Snow pack temperature

In the presence of snow pack over land with a depth exceeding 9 m water equivalent, the surface is considered to be covered with ice and soil temperature equations are solved with the characteristic of ice. These areas are prescribed in the model and identified as glaciers. For snow depth deeper than 0.025 m, an extra heat conduction equation evolves according to

$$\frac{\partial T_{Sn}}{\partial t} = \frac{F_S}{\rho_{Sn} \cdot C_{Sn} \cdot S_n}, \tag{2.33}$$

with

T_{Sn}	Temperature in the middle of snow pack,	
F_S	sum of radiative and turbulent fluxes at the surface,	
$\rho_{Sn}C_{Sn}$	heat capacity of snow per unit volume	0.6345×10^6 J m^{-3} K^{-1}
	computed using snow density ρ_{Sn} of	300 kg m^{-3} and
S_n	depth of the snow pack.	

The skin temperature of the snow, which serves as an interface to the atmosphere, is obtained through a linear extrapolation from the snow layer and the upper soil layer. This temperature may not exceed the snow melt temperature. If $T_{Sn} > 273.16$ K, the energy is first used to warm the soil underneath and only if both the snow temperature and the upper soil temperature reach the melting point, further energy will be used to melt the snow.

2.3.3 Surface moisture flux

Evaporation from the snow surface, bare soil, vegetated surface or skin reservoir is generally parameterized at potential rate as:

$$J_q = \rho \cdot C_h \cdot \mid \nu_h \mid \cdot \Big(q_v - q_s(T_S, P_S)\Big), \tag{2.34}$$

where C_h is the heat transfer coefficient, $\mid \nu_h \mid$ the magnitude of the horizontal wind vector at the lowest model level, T_S the surface temperature, P_S the surface pressure, q_v the water mixing ratio and q_s the saturation water mixing ratio at the surface. Over land, each grid square is divided into 4 fractions:

1. fraction C_{Sn} covered with snow,
2. fraction $(1 - C_{Sn}) \cdot C_l$ covered with water in skin reservoir,
3. fraction $(1 - C_{Sn}) \cdot (1 - C_l) \cdot (1 - C_v)$ covered with bare soil,
4. fraction $(1 - C_{Sn}) \cdot (1 - C_l) \cdot C_v$ covered with vegetation.

Where C_{Sn}, the snow cover fraction, depends on snow depth S_n.

$$C_{Sn} = min\Big(1, \frac{S_n}{S_{n_{cr}}}\Big). \tag{2.35}$$

$S_{n_{cr}}$ is the critical snow depth (0.015 m equivalent water depth). The wet skin fraction C_l is derived from the skin reservoir water content:

$$C_l = min\Big(1, \frac{W_l}{W_{lmx}}\Big). \tag{2.36}$$

Where W_l is the skin reservoir content and W_{lmx} is the maximum skin reservoir content. The vegetation fraction C_v is equal to the climatological field C_{vcl} except in dry conditions when vegetation is reduced according to the following empirical expression:

$$C_v = min(C_{vcl}, C_{vcl} \cdot \frac{W_S}{0.4 \cdot W_{Smax}}). \tag{2.37}$$

W_S represent the total amount of water available in the root zone and W_{Smax} is the total water holding capacity. Therefore evaporation from the snow and skin reservoir is at the potential rate:

$$J_{q_{vi}} = \rho \cdot C_h \cdot \mid \nu_h \mid \cdot \Big[\Big\{q_v - q_s(T_S, P_S)\Big\}\Big\{C_{Sn} + (1 - C_{Sn}) \cdot C_l\Big\}\Big]. \tag{2.38}$$

For the evaporation from bare soil (no water in skin reservoir) it is assumed that the relative humidity h at the surface is related to the water content W_S of the soil:

$$\begin{aligned} J_{q_{vb}} = {} & \rho \cdot C_h \cdot \mid \nu_h \mid \cdot \Big\{q_v - h \cdot q_s(T_S, P_S)\Big\} \\ & \Big\{(1 - C_{Sn}) \cdot (1 - C_l) \cdot (1 - C_v)\Big\}, \end{aligned} \tag{2.39}$$

where

$$\begin{aligned} h = \max\Big[0.5\Big(1 - \cos\{\pi \frac{W_S - (W_{Smax} - W_{stop})}{W_{Stop}}\}\Big), \\ \min\Big(1, \frac{q_v}{q_s(T_S, P_S)}\Big)\Big]. \end{aligned} \tag{2.40}$$

To avoid evaporation from a deep layer, the total reservoir W_{Smax} is split into two parts: an upper layer W_{Stop} and a lower one $(W_{Smax} - W_{Stop})$. The evaporation from dry (no water in skin reservoir) vegetated area is proportional to evaporation efficiency E, based on *Sellers et al.* (1986):

$$\begin{aligned} J_{q_{vd}} = {} & \rho \cdot C_h \cdot \mid \nu_h \mid \cdot E \cdot \Big\{q_v - q_s(T_S, P_S)\Big\} \\ & \Big\{(1 - C_{Sn}) \cdot (1 - C_l) \cdot C_v\Big\}. \end{aligned} \tag{2.41}$$

The total evaporation in a grid square (equations 2.38, 2.39, 2.40, 2.41) is given by

$$\begin{aligned} J_{q_v} = J_{q_{vi}} + J_{q_{vb}} + J_{q_{vd}} = \rho \cdot C_h \cdot \mid \nu_h \mid \cdot \Big[& \Big\{C_{Sn} + (1 - C_{Sn}) \cdot C_l\Big\} \cdot \Big\{q_v - q_s\Big\} \\ & + \Big\{(1 - C_{Sn}) \cdot (1 - C_l) \cdot (1 - C_v)\Big\} \cdot \Big\{q_v - h \cdot q_s\Big\} \\ & + \Big\{(1 - C_{Sn}) \cdot (1 - C_l) \cdot C_v \cdot E \cdot \Big\{q_v - q_s\Big\}\Big]. \end{aligned} \tag{2.42}$$

2.3.4 Soil hydrology

The parameterizations of soil hydrology comprise three budget equations for i) snow depth S_n (snow water equivalent in meter) accumulated at the surface, ii) water amount W_l intercepted by the vegetation during rain or snow melt episodes (the so called skin reservoir), iii) soil water amount W_S. The water equivalent of the snow layer is computed over land and glacier areas from

$$\frac{\partial S_n}{\partial t} = \frac{J_{qSn} + P_{Sn} - M_{Sn}}{\rho_w}, \tag{2.43}$$

with

J_{qSn} evaporation rate per unit area over the snow pack,
P_{Sn} snow fall rate per unit area,
M_{Sn} snow melt rate per unit area and
ρ_w density of water.

Rain water and melting snow on the leaves are intercepted by the vegetation until its water holding capacity W_{lmx} is exceeded. The corresponding budget equation is given by

$$\frac{\partial W_l}{\partial t} = \frac{J_{q_{vi}} + C_{ip} \cdot C_v \cdot (C_a \cdot P_R + M_{sn})}{\rho_w}, \tag{2.44}$$

with

$J_{q_{vi}}$ evaporation rate from the skin reservoir (eqn. 2.38),
P_R rainfall rate per unit area,
C_v fraction of the grid box covered by vegetation,
C_{ip} coefficient of efficiency of rain and snow melt interception,
C_a fractional area wetted by rain during a time step (100 % for large scale rain and 50 % for convective rain).

$$W_{lmx} = W_{lmax}[(1 - C_v) + C_v \cdot LAI], \tag{2.45}$$

where LAI is the leaf area index and W_{lmax} is the maximum amount of water that can be held on one layer of leaf or bare ground ($2.0 \times 10^{-4}\ m$).

The amount of rain and snow melt which does not enter the skin reservoir is used to calculate the amount of soil infiltration and surface runoff. The soil water reservoir evolves according to

$$\frac{\partial W_S}{\partial t} = \frac{J_{q_v} - J_{q_{vi}} + P_R - P_{Ri} + M_{Sn} - M_{Sni} - R_R - R_D}{\rho_w}, \tag{2.46}$$

with

J_{q_v} grid mean evaporation rate per unit area,
P_{R_i} rainfall rate per unit area intercepted by the skin reservoir,
M_{Sni} snow melt rate per unit area intercepted by the skin reservoir,
R_R surface runoff rate per unit area from precipitation events and snow melt,
R_D runoff rate per unit area from drainage processes.

The surface runoff is calculated following the scheme by *Dümenil and Todini* (1992). The scheme takes into account the sub-grid scale heterogeneity of a grid area by introducing a terrain steepness dependent structure parameter b. Using the total water holding capacity W_{Smax}, the fractional saturated area $\frac{s}{S}$ in a grid box is defined as

$$\frac{s}{S} = 1 - \left(1 - \frac{W_S}{W_{Smax}}\right)^b. \tag{2.47}$$

Runoff due to rainfall or snow melt will occur in the fractional saturated area $\frac{s}{S}$ of a grid box, while in the $(1 - \frac{s}{S})$ fractional grid box area rain or snow melt will infiltrate. The amount of surface runoff in the saturated part of the grid area during a time step Δt is computed from

$$\frac{1}{\rho}\int_t^{t+\Delta t} R_R dt = Q - (W_{Smax} - W_S) + W_{Smax}\left[\left(1 - \frac{W_S}{W_{Smax}}\right)^{\frac{1}{1+b}} - \frac{Q}{(1+b)\cdot W_{Smax}}\right]^{1+b}, \text{ if } [...] > 0 \tag{2.48}$$

or

$$\frac{1}{\rho}\int_t^{t+\Delta t} R_R dt = Q - (W_{Smax} - W_S), \text{ if } [...] \leq 0 \text{ and } Q + W_S > W_{Smax}, \tag{2.49}$$

where Q is the total water available for infiltration and runoff after skin reservoir interception and represented as

$$Q = \int_t^{t+\Delta t} \frac{P_R - P_{Ri} + M_{Sn} - M_{Sni}}{\rho_w} dt. \tag{2.50}$$

Runoff due to drainage processes occurs independently of the water input Q if the soil wetness is between 5% and 90% of the field capacity (slow drainage) or larger than 90% (fast drainage)

$$\frac{R_D}{\rho_w} = \begin{cases} d_{min}\cdot\frac{W_S}{W_{Smax}} & \text{if } (0.05\cdot W_{Smax} < W_S < 0.9\cdot W_{Smax}) \\ d_{min}\cdot\frac{W_S}{W_{Smax}} + (d_{max} - d_{min})\left(\frac{W_S - 0.9\cdot W_{Smax}}{W_{Smax} - 0.9\cdot W_{Smax}}\right)^{1.5} & \text{if}(W_S \geq 0.9\cdot W_{Smax}), \end{cases} \tag{2.51}$$

where
$d_{min} = 2.8\cdot 10^{-10}\ m\,s^{-1}$ and $d_{max} = 2.8\cdot 10^{-8}\ m\,s^{-1}$.

2.3.5 Land surface albedo

Over snow free land areas, specified seasonal means of background albedo are used (*Christensen et al.*, 2001). A 1 km global data set of major ecosystem types according to *Olson* (1994a) and *Olson* (1994b) has been made available by U.S. Geological Survey (USGS,1997). It has been derived from the International Geosphere Biosphere programme (IGBP) 1 km AVHRR data set and the background albedo is from these data sets, which is used in HIRHAM4.

In the snow covered areas, the surface albedo is modified according to

$$\alpha_{Surf} = \alpha_{Sb} + (\alpha_S - \alpha_{Sb}) \cdot \frac{S_n}{S_n + S_n^*}, \tag{2.52}$$

where

α_S	snow albedo,
α_{Sb}	background albedo,
S_n	simulated snow depth (in water equivalent),
S_n^*	critical snow depth ($= 0.01\,m$).

For $S_n \gg S_n^*$ the surface albedo approaches the albedo of snow. The albedo of snow (α_S) is a function of surface type (t_s), surface temperature (T_S) and fractional forest area (a_f). For $T_S \geq T_m = 273.15K$ (i.e., for melting of snow or ice), α_S is fixed at a relatively small value, $\alpha_S = \alpha_{Smin}(t_s, a_f)$, where α_S is larger, $\alpha_S = \alpha_{Smax}(t_s, a_f)$, for cold surface ($T_S \leq T_\circ = 263.15K$) according to *Robock* (1980). Over land the respective snow albedo are assumed to depend on the fractional forest area ($0 \leq a_f \leq 1$) according to

$$\begin{aligned} \alpha_{Smin}(a_f) &= 0.3 \times a_f + 0.4 \times (1 - a_f), \\ \alpha_{Smax}(a_f) &= 0.4 \times a_f + 0.8 \times (1 - a_f). \end{aligned} \tag{2.53}$$

In the temperature range $T_\circ < T_S < T_m$,
$\alpha_S = \alpha_S(T_S, t_s, a_f)$ is obtained by linear interpolation

$$\alpha_S = \alpha_{Smax} - (\alpha_{Smax} - \alpha_{Smin}) \frac{T_S - T_\circ}{T_m - T_\circ}. \tag{2.54}$$

For glacier ($a_f = 0.0$), $\alpha_{max} = 0.8$ and $\alpha_{min} = 0.6$. Therefore for glacier, equation 2.54 is given by

$$\alpha_S = 0.8 - 0.2 \times \frac{T_S - T_\circ}{T_m - T_\circ}. \tag{2.55}$$

2.3.6 Boundary layer transport

The planetary boundary layer transports in the surface layers are parameterized by the Monin-Obukhov similarity theory as described by *Abegg* (1999). Parameterizations of boundary layer fluxes of momentum, heat and humidity above the surface layer are based on *Louis* (1979) and updated by *Louis et al.* (1982). The transfer coefficients of heat, moisture and momentum depend on the roughness length $z_\circ$,

the von Kármán's constant κ and an empirical stability function f. The transfer coefficients of heat C_h and momentum C_m are given by

$$C_m = \left(\frac{\kappa}{\ln(z/z_o)}\right)^2 \cdot f_m(R_i, z/z_o), \tag{2.56}$$

$$C_h = \left(\frac{\kappa}{\ln(z/z_o)}\right)^2 \cdot f_h(R_i, z/z_o). \tag{2.57}$$

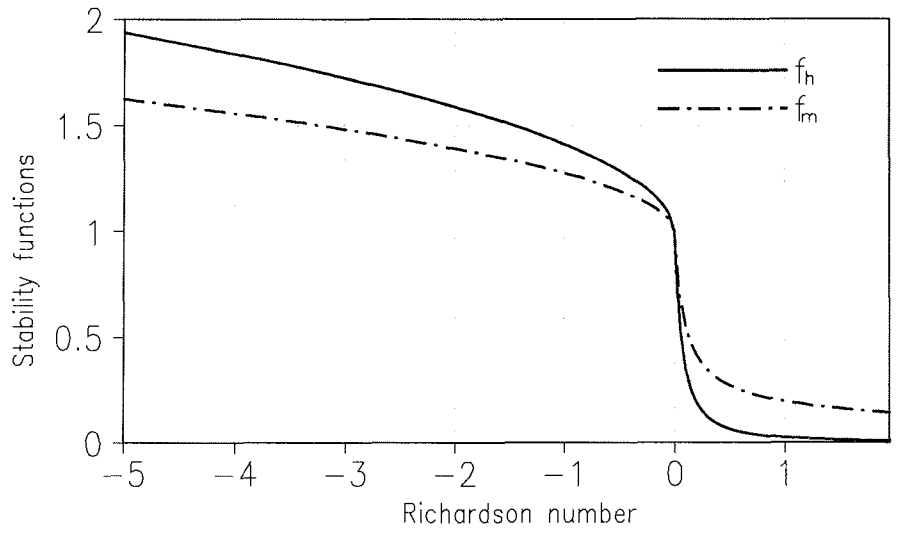

Figure 2.3: Stability functions for momentum f_m and heat f_h, for positive and negative Richardson numbers.

For stable conditions, when Richardson number $R_i \geq 0$, the stability functions are parameterized as follows

$$f_m = \frac{1}{1 + (2 \cdot b \cdot R_i)/(\sqrt{1 + d \cdot R_i})}, \tag{2.58}$$

$$f_h = \frac{1}{1 + (3 \cdot b \cdot R_i)/(\sqrt{1 + d \cdot R_i})}, \tag{2.59}$$

with $b = 5, d = 5$.

For the near neutrality conditions (i.e. when $R_i \rightarrow 0$), the stability functions are

$$f_m = 1 - 2 \cdot b \cdot R_i, \tag{2.60}$$

$$f_h = 1 - 3 \cdot b \cdot R_i, \tag{2.61}$$

with $b = 5$.

In the highly unstable cases ($R_i < 0$), i.e. for the free convection case, the stability functions are:

$$f_m = 1 - \frac{2 \cdot b \cdot R_i}{1 + 3 \cdot b \cdot c[\frac{\kappa}{log(z/z_0+1)}]^2 \sqrt{(z/z_0+1)(-R_i)}}, \tag{2.62}$$

$$f_h = 1 - \frac{3 \cdot b \cdot R_i}{1 + 3 \cdot b \cdot c[\frac{\kappa}{log(z/z_0+1)}]^2 \sqrt{(z/z_0+1)(-R_i)}}, \tag{2.63}$$

where κ is the von Karman's constant and $b = c = 5$. Figure 2.3 shows the stability functions for momentum and heat for both positive and negative Richardson numbers. Here for simplicity $z = z_0$ is used.

3 Validation of HIRHAM4

3.1 Introduction

Often the numerical model simulated climate do contain biases compared to the observations. The performance of one model differs from the other in space and time. The discrepancy may come from different parameterizations of physical processes, different initial and boundary conditions and different numerical schemes. The main objective of this chapter is to analyze and detect the errors in the model's surface and soil variables against available observations. The Arctic is a data-poor region with many unique climate features. In such a region model inter-comparison may improve the understanding of physical processes along with observations (*Rinke et al.*, 2000). Due to the sparse observational network in the Arctic, the spatial interpolation of the observed data may contain biases or smooth out the very local profiles. Also there are limited number of directly measured climate variables. While comparing a model simulation with station measurements, station data may not be representative of that area, which is resolved in the model by $50 \times 50\,km$ grid box.

A 15 year (1979-1993) HIRHAM4 simulation with ERA-15 (1979-1993) lateral and lower boundary conditions has been performed. The standard HIRHAM4 version of horizontal resolution 0.5 by 0.5 degree and vertical 19 atmospheric levels is used for this simulation. Here, mainly monthly mean soil and surface variables are analyzed and compared with the observations. The variables compared are mean sea level pressure, precipitation, 850 hPa. and $2\,m$ air temperatures, soil temperature, snow water equivalent (SWE) and surface albedo. For the comparison of recent periods (1999-2002) soil and air temperatures at Lena Delta station, operational ECMWF analysis data driven HIRHAM4 simulations have been used.

3.2 Observational data

The model validation has been carried out by using both the gridded and station data from different sources. For the soil temperature validation, only few station measurements were available.

3.2.1 Station data

The station measurements of $2\,m$ air & soil temperatures, precipitation and SWE from several stations situated at Western Russia (WR, WRII), Eastern Siberia (ES),

Lena Delta (LD) and North Canada (NC) are used here. The locations of all stations are shown in Figure 3.1. The available station data are divided into total 5 sets of data. The detailed description of each data set is shown in Table 3.1 and the individual station's description is given in Appendix A. The soil temperature data of 5 different depths (20, 40 ,80, 160, 320 cm) are used. Except for the Lena Delta station and West Russian (WR) stations, monthly mean data (variables are mentioned in the Table 3.1) from all other 3 locations are used for 15 years (1979-1993). The Lena Delta monthly mean soil and $2\,m$ air temperatures are available from August 1998 to August 2002. The West Russian (WR) stations soil temperatures of 12 years (1979-1990) are used.

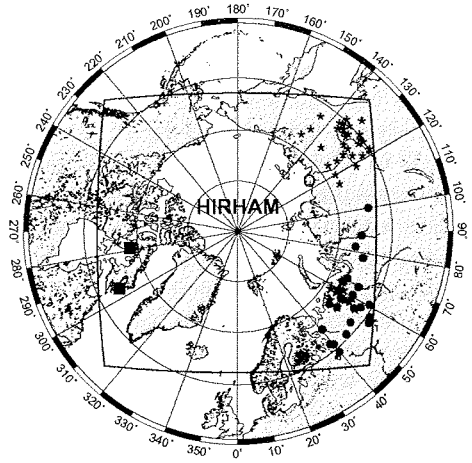

Figure 3.1: The locations of all stations in the HIRHAM4 integration area. The details of each data set are given in the Table 3.1.

3.2.2 Gridded data

Near surface and 850 hPa air temperature

Near surface gridded monthly climatology mean air temperature for the whole Arctic domain was available from *Willmott and Rawlins* (1999) (*http://climate.geog.udel.edu /~climate/html_pages/download.html*). A total of 4517 land-surface weather stations located north of 43 °N were interpolated with the *Willmott and Matsuura* (1995) DEM-assisted algorithm to a 0.5 by 0.5 degree grid resolution. The 850 hPa monthly mean air temperature was from ECMWF re-analysis ERA-15 (*Gibson et al.*, 1999), with spectral T106 resolution and 31 vertical hybrid levels.

Precipitation

Two sets of gridded land surface monthly precipitation data, interpolated from observations are used here. *Matsuura and Willmott* (2004) (*http://climate.geog.udel.edu/~*

Data Location	Data Source	Variable	Time period	Symbol
East Siberia **ES**	V. E. Romanovsky (personal communication)	T_{2m}, T_{soil}, S_n	1979-93	*
West Russia **WR**	NSIDC (*Barry et al.*, 2001) http://nsidc.org/data/arcss078.html	T_{soil}	1979-90	●
West Russia (**WRII**)	Peter Kuhry (*Christensen and Kuhry*, 2000)	T_{2m}, T_{soil}, S_n, P_R	1979-93	★
Lena Delta (**LD**)	Julia Boike (*Boike and Becker*, 2000)	T_{2m}, T_{soil}	1988-02	○
North Canada (**NC**)	Peter Kuhry (personal communication)	T_{2m}, S_n, P_R	1979-93	■

Table 3.1: The different sources of station data sets, their locations, symbols in the map, time period and variables ($T_{2m} = 2\,m$ air temperature,T_{soil} = soil temperature, S_n = snow depth or SWE and P_R = precipitation). The description of each station is given in Appendix A.

climate/html_pages/download.html) monthly precipitation interpolated to a 0.5 by 0.5 degree grid resolution, is taken for the time slice 1979-1993. Xie-Arkin monthly precipitation (*Xie and Arkin*, 1997) interpolated to a 2.5 by 2.5 degree grid resolution for the same time slice is used.

Snow depth

For the model validation of snow water equivalent, the global snow depth climatology of the U.S. Air Force Environmental Technical Application Center (USAF/ETAC) is used here (*Foster and Davy*, 1988). This is a mid-monthly mean snow depth climatology with a $1\,° \times 1\,°$ equal-angle grid resolution. Since the HIRHAM4 produces snow water equivalent, the USAF/ETAC snow depth was converted into snow water equivalent according to *Verseghy* (1991),

$$\rho_s = 188.82 + 0.419 S_n \leq 450\ kg\,m^{-3}. \tag{3.1}$$

After some calculations we get

$$S_w = \frac{188.82}{1 - 0.419 S_n} \times \frac{S_n}{1000}, \tag{3.2}$$

where S_n is the snow depth in meter, S_w is the snow water equivalent in $m\,m^{-2}$, ρ_s is the density of snow, which does not exceed 450 $kg\,m^{-3}$ and a water density of 1000 $kg\,m^{-3}$ is used.

Surface albedo

The AVHRR Polar Pathfinder Twice-Daily 25 km EASE-Grid (Equal-Area Scalable Earth Grid) surface albedo (*Fowler et al.*, 2002) was used for the time period April 1981 to September 1998 (*http://nsidc.org/data/nsidc-0094.html*).

3.3 Mean sea level pressure

The monthly climatology mean (1979-1993), summer (JJA) and winter (DJF) averaged mean sea level pressure (MSLP) of HIRHAM4 simulation and ERA-15 are shown in Figure 3.2. During summer, there are no large variations in MSLP over the entire domain. However there is a high pressure centered over Greenland in both HIRHAM4 and ERA-15. This high pressure is due to the cold air masses situated over the Glacier. Over the central part of the Arctic, the HIRHAM4 MSLP overestimates the ERA-15 MSLP by a maximum of 3 hPa. Except Greenland, over the major land part, the HIRHAM4 MSLP underestimates the ERA-15 MSLP by about 2 hPa. The spatial distributions of winter MSLP are very different from the summer MSLP. There exists a high pressure of more than 1024 hPa over East Siberia. In both HIRHAM4 and ERA-15, the high pressure system is extended from East Siberia to North Canada and North Alaska, whereas a low pressure of maximum about 998 hPa is situated over the North Atlantic. There are very small differences between the HIRHAM4 and ERA-15 MSLP over the ocean, but over land the HIRHAM4 underestimates the ERA-15 MSLP by 2 - 8 hPa. Therefore the HIRHAM4 simulated MSLP is very similar to the ERA-15 reanalysis MSLP.

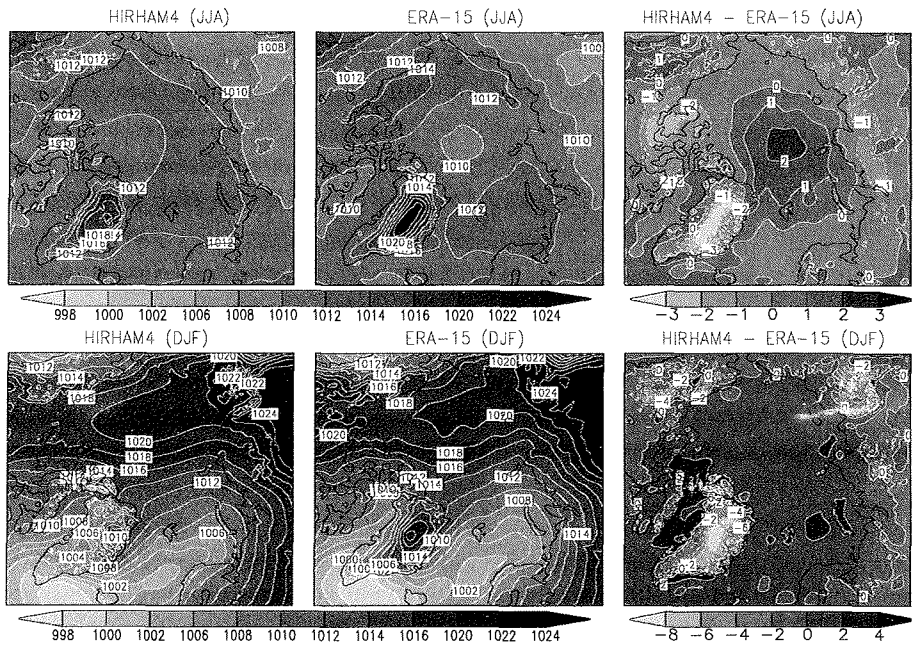

Figure 3.2: Monthly climatology mean (1979-1993) winter (DJF) and summer (JJA) averaged HIRHAM4 and ERA-15 mean sea level pressure in hPa.

3.4 Air and soil temperature

Surface air temperature is one of the most important climate variables and available from observations for most of the places. Figure 3.3 shows the domain averaged, model monthly climatology mean (1979 – 1993) $2\,m$ air temperature and Willmott-Rawlins climatology near surface air temperature. The model air temperature has a good agreement with the observation through out the year. However in summer, the model shows a slight warming of about 3 °C and a leading spring season by about one week.

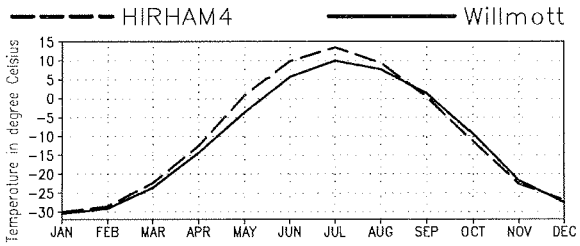

Figure 3.3: Domain averaged (excluding 10 grid points at the boundary and glacier parts) monthly climatology mean (1979-1993) HIRHAM4 2m air temperature in °C (dashed line) and Willmott-Rawlins climatology near surface air temperature (solid line).

Summer(JJA) and winter(DJF) averages of the model monthly climatology mean $2\,m$ air temperatures and Willmott-Rawlins climatology near surface air temperature are shown in Figure 3.4. During summer and winter, the large scale spatial patterns of maximum and minimum temperature zones are well captured by the model. Summer minimum air temperature pattern stayed over the central part of Greenland in both, model and observation but during winter the observed minimum is shifted further north. An extended cold region during winter in East Siberia, with temperature below −40 °C is seen in the observations. Though the model is not able to reproduce such cold air temperatures in this region. The model overestimates summer surface air temperature in the coastal region of Siberia, North Alaska, North Canada and Greenland by 2 - 8 °C. During winter the model shows a strong warm bias of maximum 10 °C in Alaska and part of Eastern Siberia.

Summer and winter averages of 850 hPa monthly climatology air temperature from HIRHAM4 simulation and ERA-15 reanalysis are shown in Figure 3.5. The summer and winter large scale patterns are very similar in both ERA-15 and HIRHAM4. Since the model's lateral forcing was from ERA-15, the temperature patterns in HIRHAM4 boundary region are very similar. However the model has been deviated from the ERA-15 in the central part of the domain and over the Greenland area. Over Greenland area, the model is colder by a maximum of 4 °C during summer and by a maximum of 10 °C during winter compared to ERA-15. However for the elevated surface, the 850 hPa will be within the land/glacier. Therefore over the Greenland and mountain regions in Alaska and East Siberia, the 850 hPa temperatures are of limited value. In summer, central part of the Arctic is warmer than the ERA-15 by a maximum of 4 °C.

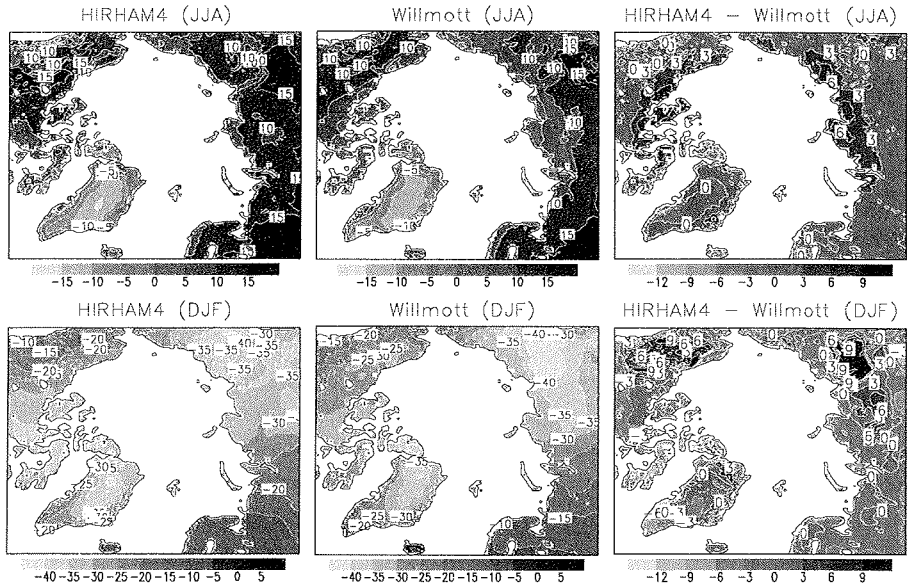

Figure 3.4: Summer (JJA) and winter (DJF) averages of HIRHAM4 monthly climatology mean (1979-1993) $2\,m$ air temperature and Willmott-Rawlins climatology (DEM algorithm) near surface air temperature in °C. The right hand side of upper and lower panels shows the difference between HIRHAM4 and Willmott-Rawlins climatology during summer and winter respectively.

Domain averaged HIRHAM4 soil temperatures of 5 layers during the years 1979 to 1993 are shown in Figure 3.6. The largest seasonal change in soil temperature is seen in the uppermost soil layer and the magnitude is damped as the soil depth increases, which is consistent with the Fourier heat conduction law. The time lag of lower layer soil temperature from the upper soil layer is also consistent with the Fourier heat conduction law.

The validation of the Arctic soil temperature is extremely difficult, as (1) only very few measurement sites are available and (2) the soil processes are very localized. A station soil temperature may not be representative for a region of $50 \times 50\ km$ used by the model. Using a small number of station data, it is difficult to compare them with model simulation of such resolution. The model data have been linearly interpolated to the all corresponding station locations (latitude, longitude). Only four nearest model grid point data around the station location have been used for the interpolation. Figure 3.7 shows time series of air and soil temperature for the station Lena Delta (72.37 °N, 126.48 °E), situated at the coast of Laptev Sea. The $2\,m$ air temperature of the model agrees very well with the observation. The soil temperature at $9\,cm$ depth is very close to the observation by magnitude but there is a slight time lead in the model. The deeper layers at $47\,cm$ and $58\,cm$ are also quite

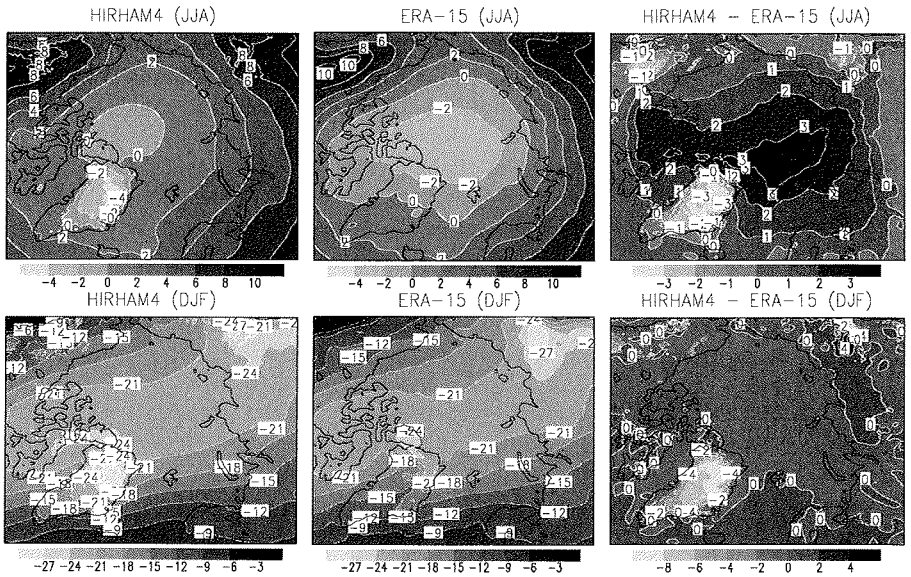

Figure 3.5: Summer (JJA) and winter (DJF) averages of HIRHAM4 and ERA-15 monthly climatology mean (1979-1993) 850 hPa air temperature in °C. The right hand side of the upper and lower panels shows the difference between ERA-15 and HIRHAM4 during summer and winter respectively.

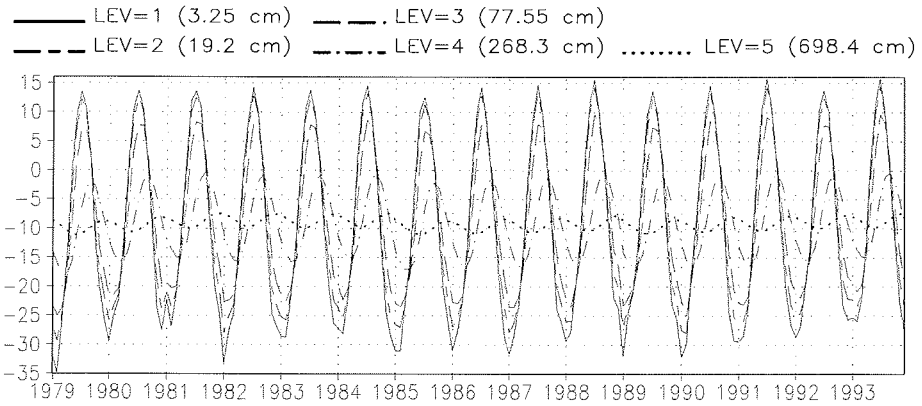

Figure 3.6: Domain averaged HIRHAM4 soil temperature at 5 vertical levels in °C for the years 1979 to 1993.

similar to the observation. Since the soil is seasonally melted and frozen up to 58 cm depth, there is no permafrost at this station up to this depth. At the beginning of winter, when soil temperature reaches 0 °C, the soil moisture starts to freeze. During the soil moisture freezing, the soil temperature does not decrease rapidly. A large amount of latent heat release (334 $J\,g^{-1}$ for pure water) is associated with the soil moisture freezing and hence almost all of the ground heat flux is used for the phase transition of soil moisture. Therefore the soil temperature curve near 0 °C becomes flat (Figure 3.7) at the beginning of winter, the temperature is not changing much with time and after some days or a month it decreases rapidly. This phenomenon is not seen in the model soil temperature, because the HIRHAM4 does not take into account the latent heat of soil moisture freezing. However, the HIRHAM4 simulation at the station Lena Delta shows a very good agreement with the observation.

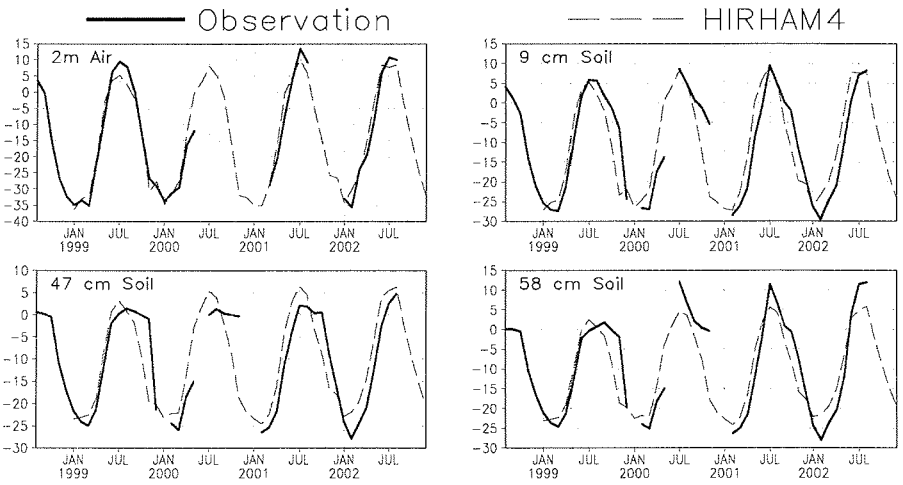

Figure 3.7: Time series of 2m air and soil temperature from a station in the Lena Delta. The solid lines are from observations and the dashed lines are from HIRHAM4. The model data have been linearly interpolated to the station grid.

Monthly climatology mean (1979 - 1993) of East Siberian (ES) 33 stations averaged 2 m air and soil temperatures are shown in Figure 3.8. The 2 m model air temperature shows a very good agreement with observation but the soil temperatures for all layers have small warm bias during summer and large cold bias during winter. The observations show a rapid damping of soil temperature as the depth increases and a leading time shift compared to the model. The model soil in winter is colder by about 15 °C to 20 °C, whereas in the summer it is warmer by about 5 °C. Unfortunately the latent heat of freezing effect is not seen in the observations. Due to the averaging effect, the temperature profile has been smoothed out. Monthly mean time series and the climatology monthly mean of each individual station has been also compared with the model. The soil temperature at all stations has shown a very similar strong cold model biases during winter and a small warm model bias during summer.

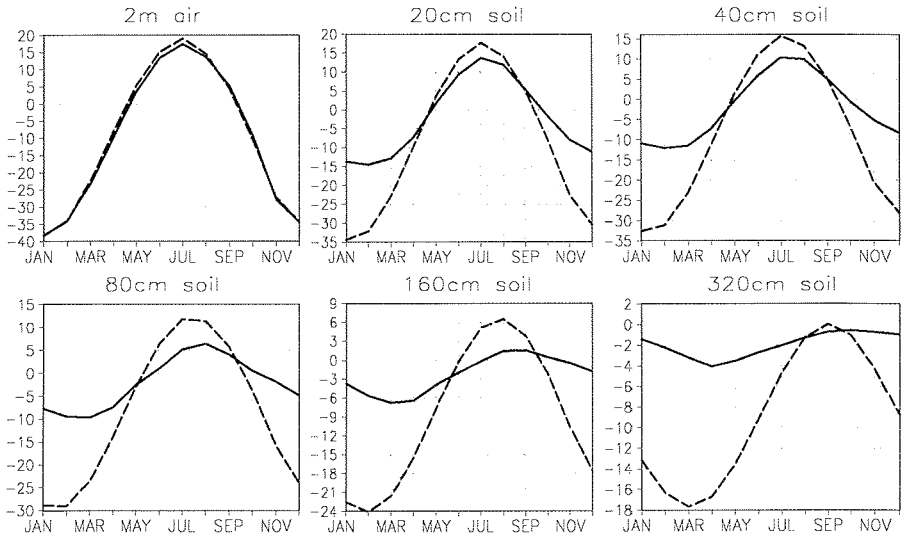

Figure 3.8: Monthly climatology mean (1979-1993), air and soil temperature averaged over East Siberian (ES) stations. The solid lines are from the observations and the dashed lines are from the HIRHAM4. The model data have been interpolated linearly to the station grid.

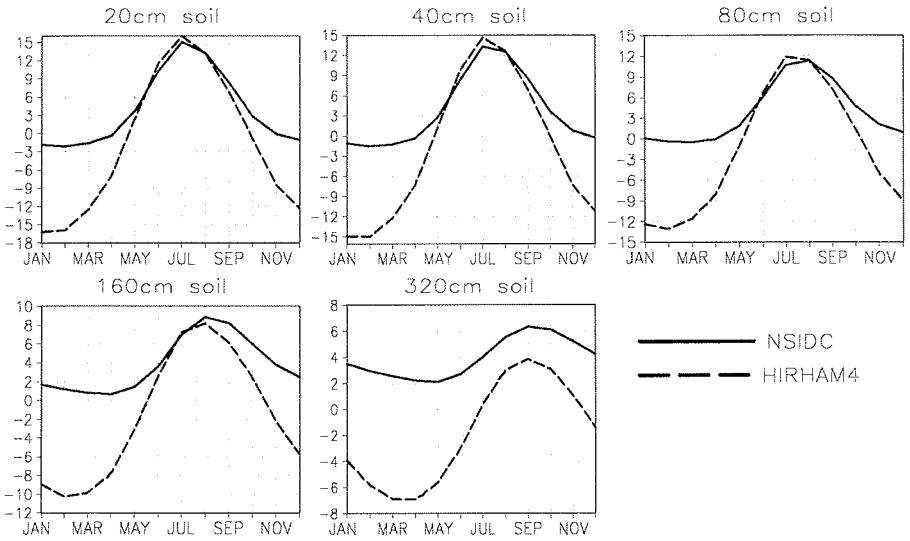

Figure 3.9: Monthly climatology mean soil temperature (1979-1990), averaged over West Russian (WR) stations. Solid lines are from observations and dashed lines are from HIRHAM4.

Total 22 stations from West Russian (WR) region are taken for the model soil temperature validation. This region has a climate different from East and far- East Siberia. The climate in West Russia is more influenced by cyclones originated over the ocean, whereas East Siberia has more continental influence. The winter air and soil temperatures in the East and far-East Siberia are much colder than in West Russia. Figure 3.9 shows the monthly climatology mean soil temperature, averaged over all stations along with the model simulations. Similar as for East Siberia, the model shows a strong winter cold bias by a maximum of 12 °C. The summer soil temperatures are quite satisfactory. Figure 3.10 shows the mean vertical soil temperature profile and its seasonal evolution in the East Siberia (ES) and West Russia (WR) regions using station measurements and model simulations. The seasonal cycle of warm and cold phase of soil is very clear. Although the model summer soil temperature and its vertical profile are quite good compared to the observations, the model is unable to reproduce the right winter soil temperatures in both regions.

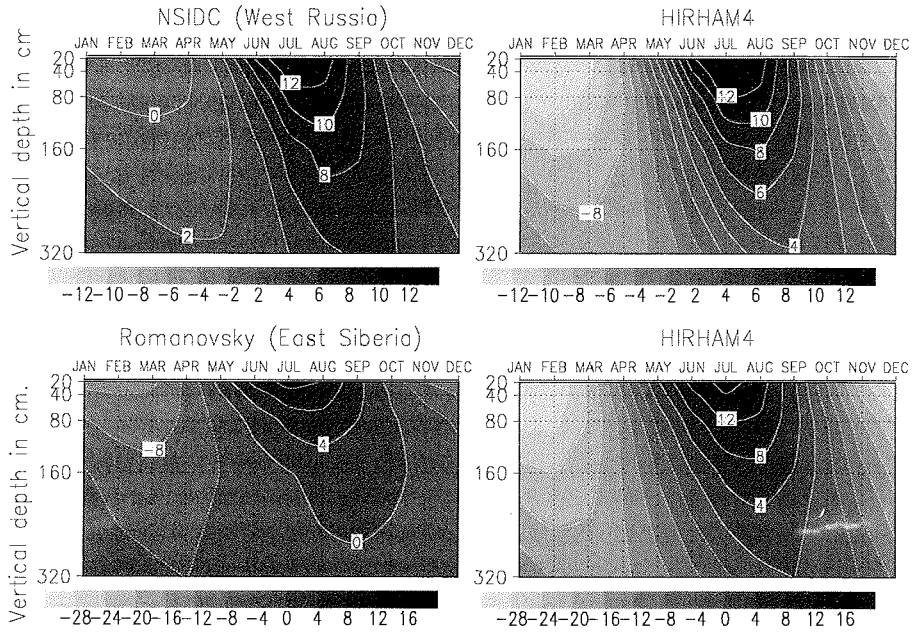

Figure 3.10: The first row shows the West Russian (WR) 22 stations averaged monthly climatology mean soil temperature and the HIRHAM4 simulations for these stations. The second row is similar to the first one but from East Siberian (ES) 33 stations average and from the HIRHAM4 simulations for these stations.

A different set of West Russian (WRII) air and soil temperature data, available from 4 stations are used here for further validation. The monthly climatology mean (1979-1993) of station averaged $2\,m$ air and $20, 40, 80, 160$ *and* 320 *cm* soil

temperatures are shown in Figure 3.11. This data set shows that, the NSIDC soil temperature (Figure 3.9) is very similar to it. Throughout the year, the model shows a very good agreement in $2\,m$ temperature with the observations. However in winter, the model shows a cold bias of maximum 12 °C at $20\,cm$ depth soil. The cold bias has been reduced at the deeper $320\,cm$ layer compared to the uppermost layer. Since the temperature signal at the surface is damped out very much when it propagates downward and hence the difference between seasonal temperature maxima and minima decreases. The amplitude of soil temperature decreases exponentially for vertically homogeneous and dry soil (*Yershov*, 1998). The sharp damping in soil temperature also can be seen in the model simulation (Figure 3.6).

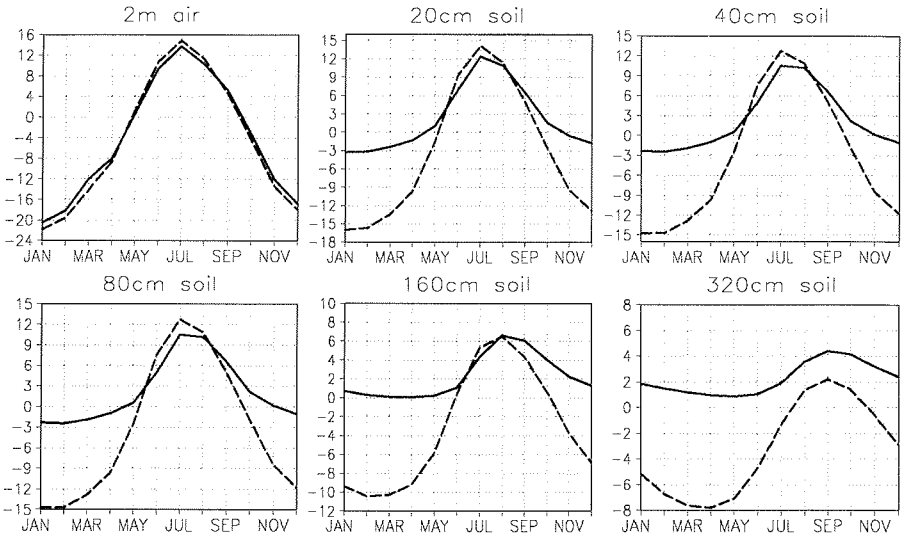

Figure 3.11: Monthly climatology mean (1979-1993) air and soil temperature averaged over 8 West Russian (WRII) stations. The solid lines are from observations and the dashed lines are from the HIRHAM4. The model data have been interpolated linearly to the station grid.

The monthly climatology mean (1979-1993) of model simulated and observed $2\,m$ air temperature at the 2 North Canadian (NC) stations are shown in Figure 3.12. Here again the model $2\,m$ air temperature is found good compared to the observations. However the winter model $2\,m$ air temperature is colder by a maximum of 5 °C at both stations. At "Baker Lake" station, the model is quite good during summer but at "Hall Beach" station, the model shows a summer cold bias of maximum of 5 °C.

The reason of the winter cold bias in the model simulated soil temperature could be partly due to the absence of soil moisture freezing scheme, as discussed before. This huge amount of latent heat associated with soil moisture freezing can damp

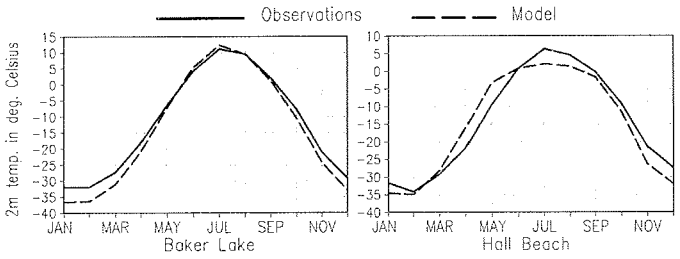

Figure 3.12: Monthly climatology mean 2m air temperature from two stations in north Canada in degree Celsius.

the soil temperature during winter, i.e it can decrease the soil cooling during winter. A similar process can be seen in the soil when spring starts. The soil will warm up and the frozen moisture in it will melt. After complete melting of the soil moisture, the soil temperature will start to increase. Therefore in the beginning of winter and spring, the temperature evolution of soil becomes very slow, which damps the amplitude of seasonal soil temperature.

The seasonal snow cover timing and it's duration is also very important for the winter Arctic soil temperature (*Ling and Zhang*, 2003). The insulation effect of snow in later autumn is much more important than in earlier autumn, since the air temperature in later autumn remains much lower than in early autumn. A delay in snowpack onset by 10 days in later autumn can decrease the ground surface temperature by about 3 °C and this cooling impact may last for the entire winter (*Ling and Zhang*, 2003). Since the solar elevation during seasonal snow cover onset in autumn is much lower than the spring snow melt time, the timing of snow cover onset has less influence on the surface net short wave radiation than does that of snow melt (*Zhang et al.*, 2001).

Also there is a possibility that, a stable stratified boundary layer can lead to an excessive cooling of soil and an accumulation of soil temperature error during winter time. There exists a positive feedback in the land surface-boundary layer coupling (*Viterbo et al.*, 1999). During winter, air above the land surface remains dense and stratified. Land surface emits long wave radiation to the space and becomes further colder. In this situation if the stratification is stable enough, there will be smaller amount of heat from the upper part of atmosphere to the lower surface through vertical mixing. This will further stratify the lower atmosphere and hence the soil will cool down further.

Except at the Lena-delta station, the model developed a strong cold winter soil temperature bias at all stations. However the summer soil temperatures were very close to the observations. Therefore, the model validation implies that, there might be missing key winter soil processes in the model as discussed above. The dependency of soil temperature on PBL stability function, soil thermal properties, snow depth and snow albedo will be discussed in details during model sensitivity studies (chapter 4).

3.5 Precipitation

Precipitation directly influences the soil water content, skin moisture and snow depth. The observational and numerical studies have shown that a soil moisture anomaly can alter the partitioning of surface latent and sensible heat fluxes, hence modify surface air temperature, humidity and precipitation (*Atlas et al.*, 1993; *Yang et al.*, 1994; *Beljaars et al.*, 1996; *Kanamitsu et al.*, 2003). Figure 3.13 shows the domain averaged (excluding 10 grid points from the boundary zone and glacier part) monthly climatology mean precipitation of HIRHAM4, Willmot-Rawlins and Xie-Arkin data sets. Willmott-Rawlins precipitation is slightly higher in August compared to Xie-Arkin precipitation and for the other months both observed data are quite similar. The model underestimates the winter precipitation by a maximum of 6 $mm\,month^{-1}$ and overestimates during May and June by a maximum of 12 $mm\,month^{-1}$.

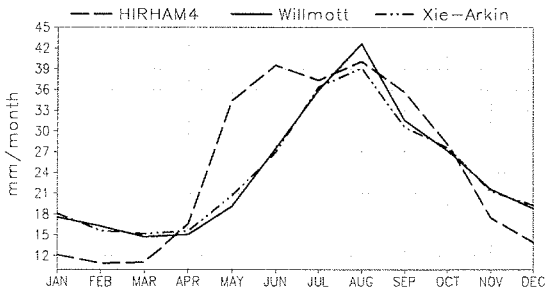

Figure 3.13: Domain averaged (excluding 10 grid points at the boundary and glacier part) monthly climatology mean precipitation in $mm\,month^{-1}$ for the year 1979-1993.

The spatial precipitation pattern for the summer (JJA) and winter (DJF) climatology mean are shown in Figure 3.14. The model monthly mean precipitation shows many regional scale patterns which are mostly not seen in observed data. The orographic model precipitation is clearly seen in the mountain regions. The observations in these mountain regions underestimate precipitation due to the lack of high elevation stations and the influence of under-catch due to the effects of wind and sublimations. *Legates and Willmott* (1990) suggested that winter precipitation may be underestimated by as much as 40% in mountain regions. The regions with maximum and minimum precipitation during summer are well captured by the model. The south and south-east coasts of Greenland get a lot of precipitation due to storm track in the north Atlantic (*Dorn*, 2002) and the model has a better agreement in this region with Willmott-Rawlins precipitation data than with Xie-Arkin data. Scandinavia, West Russia and Rocky mountain region with high precipitation zones in summer are captured well by the model. The coastal parts of Kara Sea, Laptev Sea and East Siberian Sea with minimum summer precipitation zones have quite good agreement with both observations. The Northern coasts of Alaska and Canada also get minimum summer precipitation, which is seen in both observations.

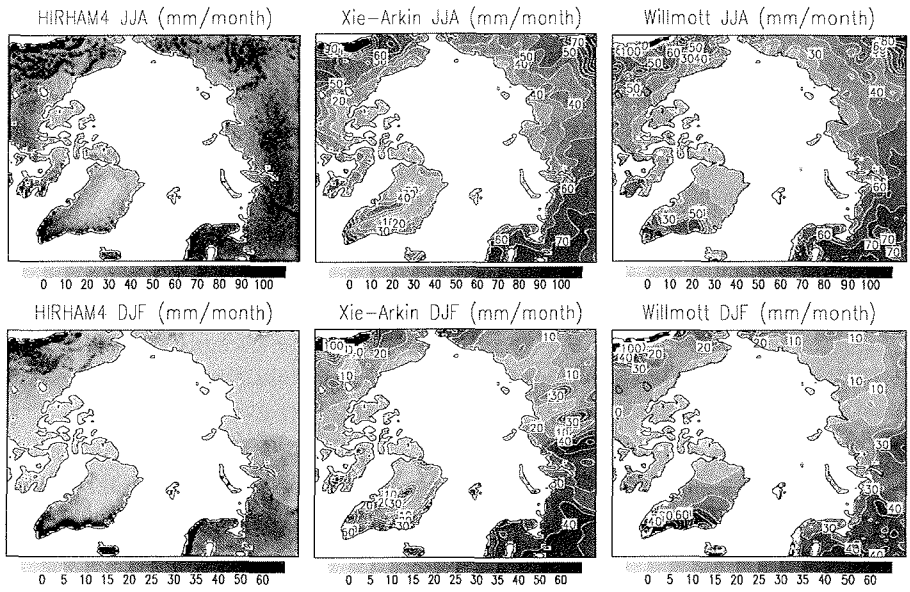

Figure 3.14: Monthly climatology mean (1979-1993) summer (JJA) and winter (DJF) average precipitation in $mm\,month^{-1}$. The first column is from HIRHAM4, the second column is from Xie-Arkin precipitation and the third column is from Willmott-Rawlins.

During winter, the maximum precipitation regions at the South and South-east coasts of Greenland, West coast of Scandinavia and in the Rocky mountains are captured by the model. The whole Scandinavia and west part of Russia get a lot of precipitations due to the winter cyclonic activities (*Serreze and Barry*, 1988), but the magnitudes are slightly underestimated by the model. A big discrepancy in the model winter precipitation arises at East and far-East Siberia and North-east Canada. In these regions, the model underestimates the precipitation by a maximum of $15\,mm\,month^{-1}$ (40-100% of observed precipitation).

Less precipitation during winter means decrease in snow and rain-on-snow(ROS) over ground. ROS is associated with large scale storm movement, which brings warmer air into the cold region and causes the rain fall over snow. Due to the exchange of sensible and latent heat between snow and rain, the existing snow starts to melt. Although the winter ROS events are infrequent, they are capable exerting a considerable influence on mean winter time soil temperature (*Putkonen and Roe*, 2003). The HIRHAM4 does not take into account ROS, which may introduce winter cold bias in soil temperature along with a thin snow layer. Higher precipitation during May, June can enhance the skin and soil moisture in snow free region, which again influence the surface heat budget.

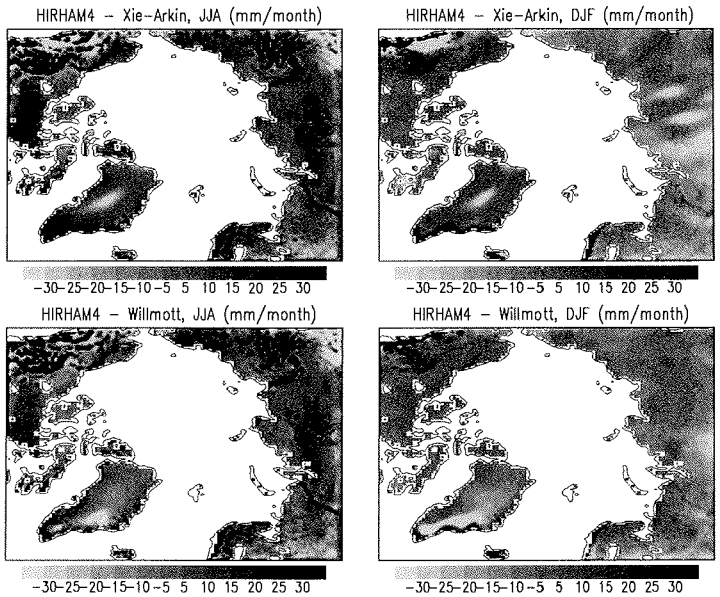

Figure 3.15: Difference between HIRHAM4 and Willmott-Rawlins, Xie-Arkin monthly climatology mean precipitation (in $mm\ month^{-1}$) during winter and summer seasons.

Figure 3.15 shows the difference between HIRHAM4 simulation and observed summer and winter monthly climatology mean precipitation. During summer, the model clearly overestimates precipitation by a maximum of $30\,mm\,month^{-1}$ in most of the mountain range regions and the coastal part of Greenland. The model winter precipitation is underestimated in the entire domain, except in the Rocky mountains, at the North coast of Scandinavia, and South-east coast of Greenland. The standard deviation of monthly mean summer and winter averaged precipitations for HIRHAM4, Willmott-Rawlins data and Xie-Arkin data are shown in Figure 3.16. The model shows a very low variability in Siberia, of the order of maximum $2\,mm\,month^{-1}$, connected with the model's small amount of precipitation. Since the model winter monthly mean precipitation is within $5\,mm\,month^{-1}$ as compared to a maximum of 15 to 20 $mm\,month^{-1}$ in the observation, the model's variability is expected to be below $5\,mm$. The other large scale variability pattern in Alaska, West Siberia, Scandinavia and all the South and South-east coast of Greenland are well captured. The summer variability in the model is slightly higher but the spatial patterns are very close to the observations.

Time correlations between monthly mean model and observed precipitations are calculated. This will further clarify the model's ability to capture the timing of precipitation. The correlation shows a high positive value, more than 0.5 in most of the domain land surface except in Greenland (Figure 3.17). Therefore the model's seasonal cycle of precipitation is quite good compared to the observations.

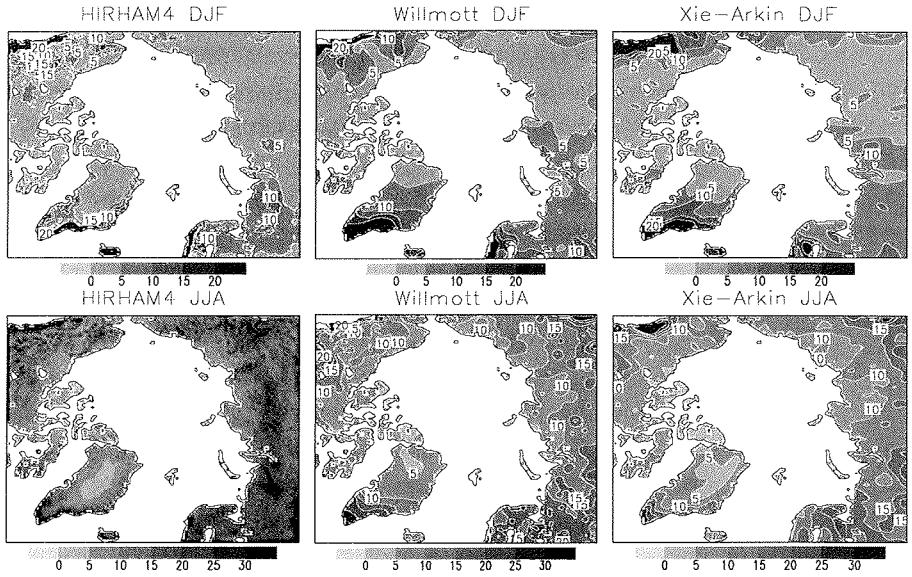

Figure 3.16: The standard deviation of winter and summer averaged monthly precipitation. 15 years monthly precipitation (in $mm\,month^{-1}$) from HIRHAM4, Willmott-Rawlins and Xie-Arkin are used.

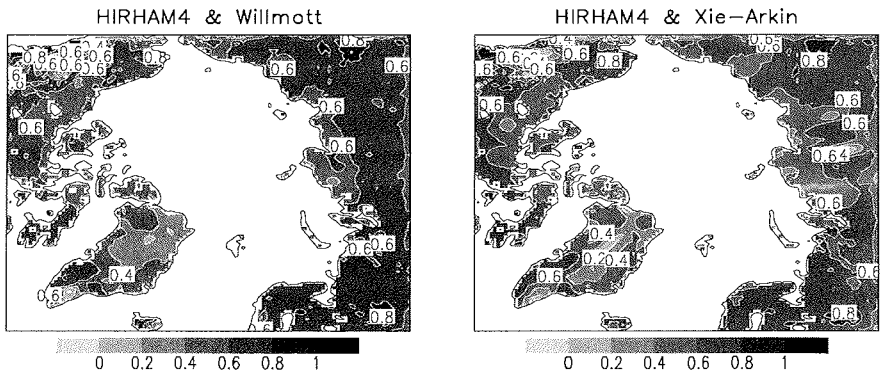

Figure 3.17: Time correlation between HIRHAM4, Willmott-Rawlins and HIRHAM4, Xie-Arkin monthly mean precipitation (1979-1993).

Precipitation measurements from two stations in North Canada (NC) (Table 3.1, Figure 3.1) are also available. Figure 3.18 shows the monthly climatology mean precipitation from these two stations and the HIRHAM4 simulation. Here at both stations, the model has a winter precipitation deficiency by a maximum of $5\,mm\,month^{-1}$. At "Baker Lake", the model overestimates the summer precipitation by $5-25\,mm\,month^{-1}$, whereas at "Hall Beach" station the model underestimates the summer precipitation by a maximum of $18\,mm\,month^{-1}$.

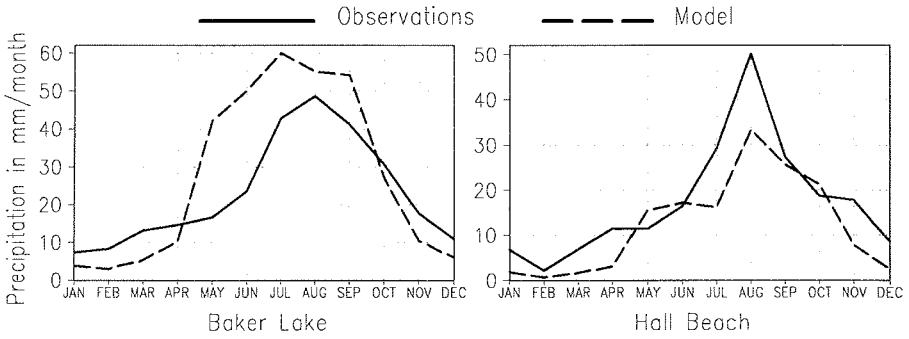

Figure 3.18: Monthly climatology mean precipitation from two stations in North Canada (NC) in $mm\,month^{-1}$.

The monthly climatology mean (1979-1993) precipitation from 14 West Russian (WRII) station measurements are shown in Figure 3.19. Here, the monthly climatology mean precipitation at individual station as well as the average over all stations are shown. The common feature of the model precipitation is that, there are two precipitation maxima, one around May-June and the other around September-October which are not seen in the observations. At most of the stations, the model shows an enhanced precipitation during May-June. The similar May-June precipitation maximum was found in the model domain averaged precipitation (Figure 3.13). Neither of the two gridded precipitations (Willmott-Rawlins and Xie-Arkin) have shown such high precipitation during May-June. The other common feature of the model is that it underestimates the winter precipitation at all stations. The precipitation, averaged over all stations shows that the model winter precipitation is underestimated by a maximum of $17\,mm\,month^{-1}$.

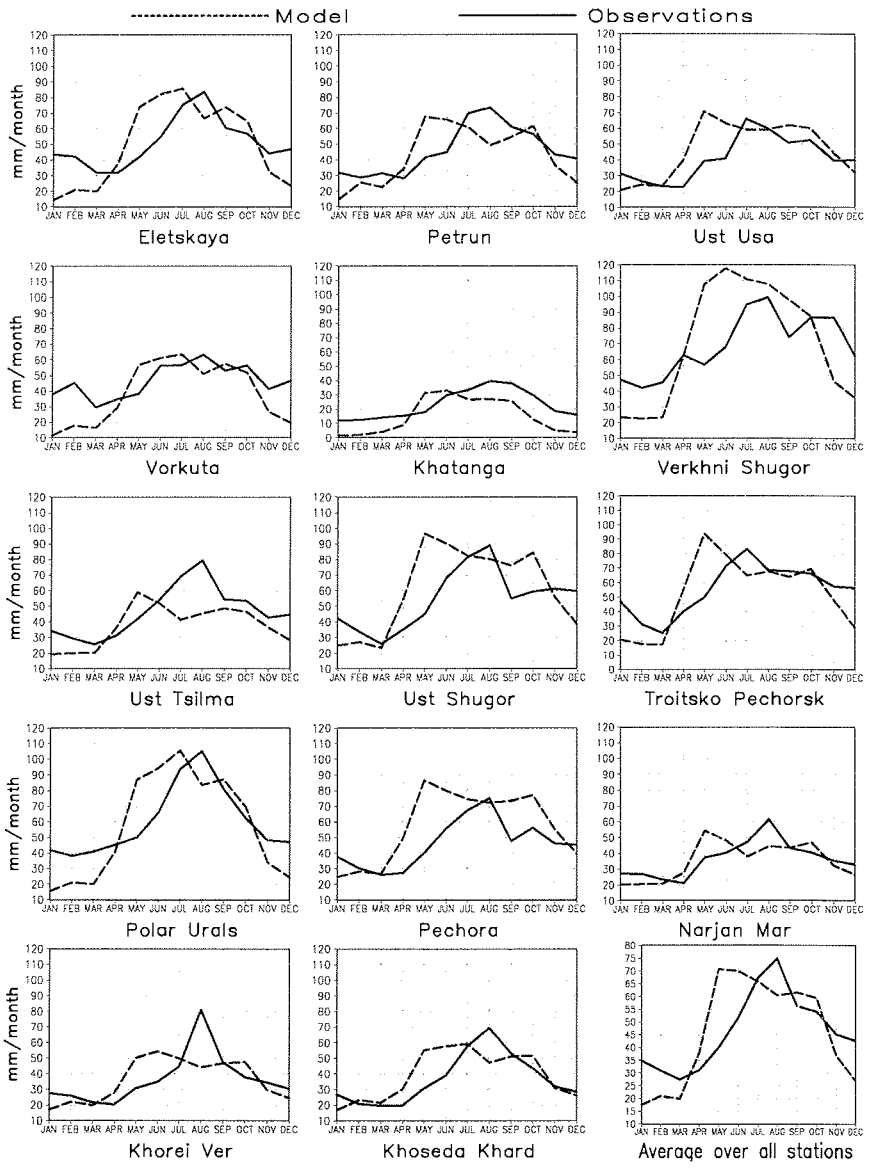

Figure 3.19: Monthly climatology mean (1979-1993) precipitation for 14 West Russian (WRII) stations in $mm\,month^{-1}$ and an average over all stations. The solid lines are from observations and the dashed lines are from model, interpolated to the station grid.

3.6 Snow depth

Since the Arctic is covered by seasonal and perennial snow, snow plays an important role in the surface heat budget of this region and hence the Earth surface heat budget. Snow and ice albedo are much higher (0.6 to 0.9) than the land and ocean part. So, snow/ice covered regions will reflect a large part of the incident solar radiation back to the space and hence further cool down the surface. Therefore the effect on the surface heat budget due to snow cover change is much larger than other albedo changes (e.g. albedo changes associated with land cover changes). Also the high thermal emissivity of snow enhances the cooling of surface during night. A small perturbation in the surface temperature can either increase or decrease snow amount but it depends very much on the snow surface temperature. If the temperature is well below the freezing point, a small perturbation will not change much in snow/ice. However if it is near the melting point, there will be a strong snow-albedo feedback mechanism, which will either increase or decrease the snow depth. In either case of increase or decrease in surface temperature around the melting point, the feedback loop is positive (Figure 3.20).

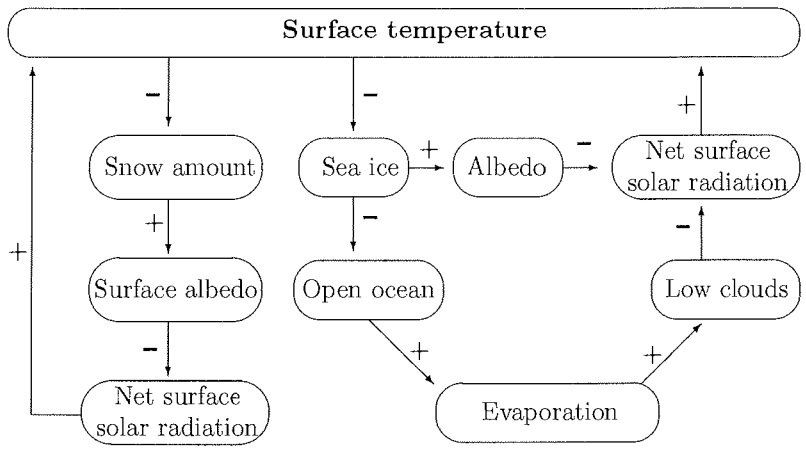

Figure 3.20: Temperature albedo feedback loop. If the direction of input and output changes are the same, then the feedback is positive (+), otherwise the feedback is negative (−).

In the Earth's hydrological cycle, snow plays also an important role. Unlike the tropics, a major part of the Arctic ground and river water comes in the form of solid precipitation (i.e. snow fall). The density of snow changes with time. After falling on ground, snow goes through several complex physical changes including density, shape and size of the ice crystal even in fixed temperature condition. So it is always

problematic to convert snow depth measured in meter or centimeter to snow water equivalent or vice versa. However here a formulation of snow density by *Verseghy* (1991) and 3 other fixed snow density have been used.

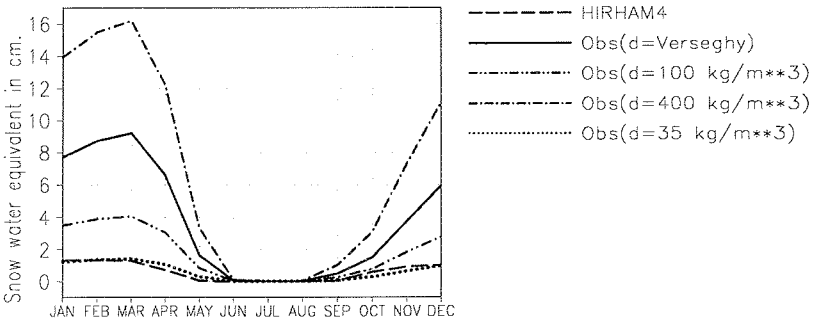

Figure 3.21: Snow water equivalent (SWE) averaged over 22 stations in East Siberia (ES). The observed snow depth is converted into SWE by using *Verseghy* (1991) algorithm and fixed snow densities $400\,kg\,m^{-3}$, $100\,kg\,m^{-3}$ and $35\,kg\,m^{-3}$.

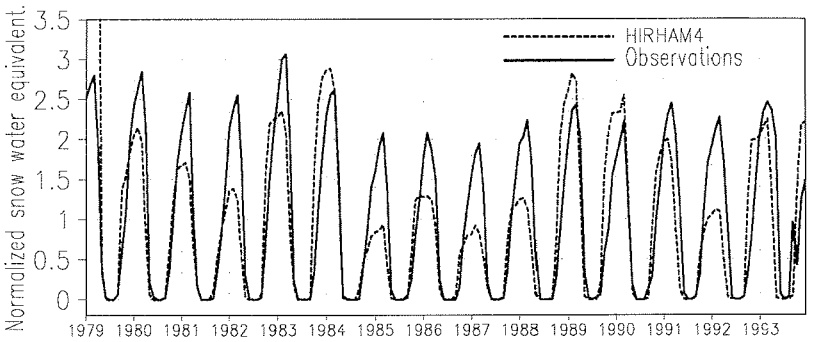

Figure 3.22: Monthly mean normalized snow water equivalent (SWE) averaged over 22 stations in East Siberia (ES). The HIRHAM4 and observed monthly SWE are divided by their 15 years (1979-1993) average monthly SWE respectively.

Figure 3.21 shows the monthly climatology mean of snow water equivalent, averaged over all East Siberian (ES) 22 stations. The SWE value, calculated by using the *Verseghy* (1991) algorithm is between the SWE values calculated by using maximum(400 $kg\,m^{-3}$) and minimum(100 $kg\,m^{-3}$) snow densities. The model clearly underestimates the winter snow water equivalent by 8 to 9 times (using Verseghy algorithm). It is clear from the figure that the large deficiency of snow (SWE) in the model can't be due to the snow density uncertainty. It may be largely

due to the lack of winter precipitation as described in section 3.5. However a suitable snow density which brings the observed snow depth very close to the model SWE is about 35 $kg\,m^{-3}$.

Although the model has shown a large snow deficiency at the East Siberian (ES) stations, the inter-annual snow variability is captured well by the model. Figure 3.22 shows the normalized station averaged monthly mean SWE. The normalization has been done by the monthly SWE, averaged over 15 *years*.

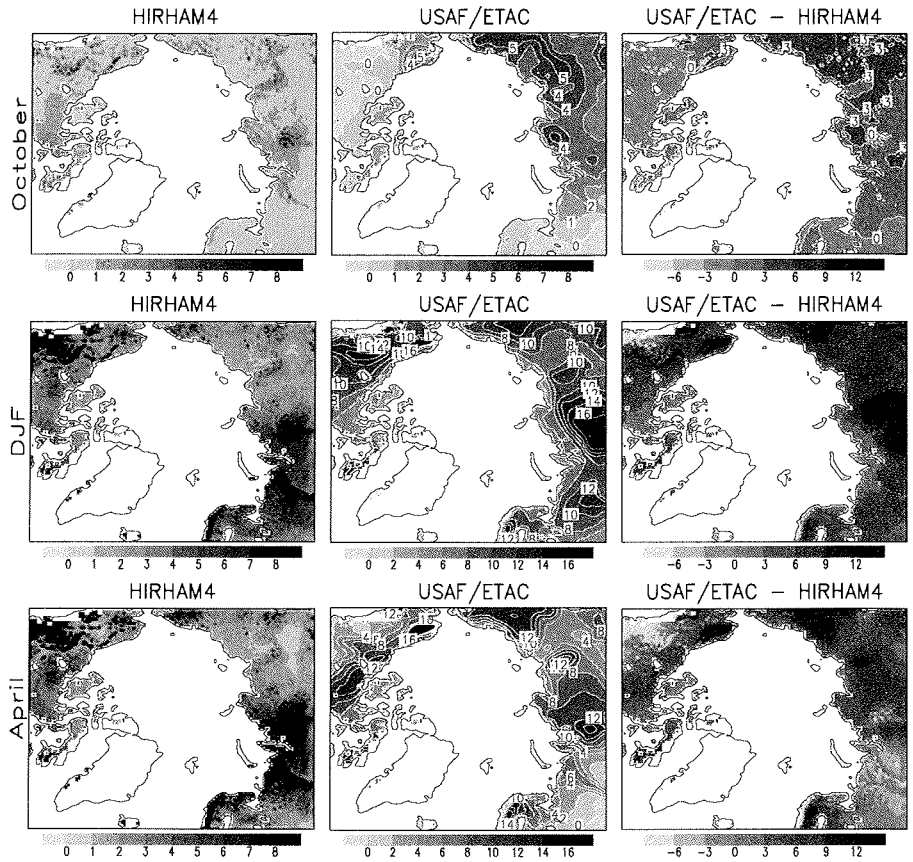

Figure 3.23: USAF/ETAC and HIRHAM4 snow water equivalent (SWE). The upper and lower panels are the climatology mean of October, April respectively and the middle panel is the average over the DJF climatology mean.

USAF/ETAC, HIRHAM4 and USAF/ETAC *minus* HIRHAM4 monthly climatology mean SWE of October, winter (December, January, February average) and April are shown in Figure 3.23. Snow fall in October is important, since the soil does not get very cold or may be in unfrozen state. Therefore a decrease in snow by

3 to 5 *cm* in the whole Siberia and western Russia compared to the USAF may enhance soil cooling in the model. The model shows a very nice small-scale horizontal SWE patterns, whereas the observations are very smooth. At the Ural mountain regions during winter and April, the model shows large SWE and also with small scale patterns. However the observation shows a rather smooth pattern. The large scale SWE patterns in the model during winter and April are very similar to the observations. Unfortunately, the model underestimates the SWE in the East Siberian region by a maximum of 5 *cm* from October through April. However during winter, this large snow deficiency in the permafrost region may not be crucial. Because the soil will be already in frozen condition during winter and a small amount of heat (i.e. heat capacity) is able to change the soil temperature. The model snow bias during April has been reduced slightly compared to winter.

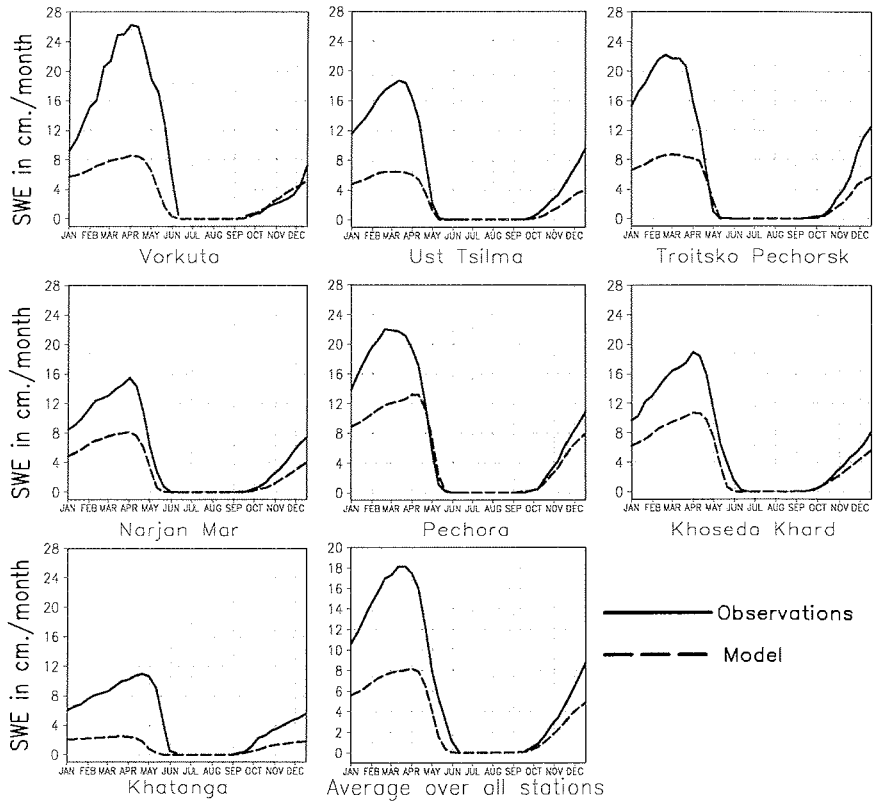

Figure 3.24: Monthly climatology mean (1979-1993) snow water equivalent (SWE) in $cm\,month^{-1}$ for seven stations in Western Russia (WRII) and averaged over all seven stations. Observed snow depth in *cm* has been converted in SWE by using *Verseghy* (1991) and the model SWE has been interpolated to the station grid.

The SWE at 7 individual West Russian (WRII) station and an average over all 7 stations are shown in Figure 3.24. At each of these stations, the model largely underestimates the SWE by an average of 5 to 10 *cm* during the snow season. Also at the 2 Canadian stations, a similar SWE bias (Figure 3.25) is seen. In the West Russian and East Siberian regions, the model has a similar SWE bias with respect to both the USAF/ETAC gridded data and the station data sets (WRII, ES). At the North Canadian (NC) stations, the maximum model SWE bias occurs during the April-May months and both observations (USAF/ETAC and station measurements (NC)) are very similar.

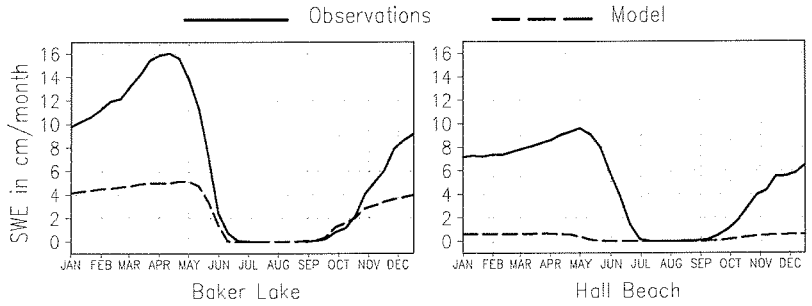

Figure 3.25: Monthly climatology mean (1979-1993) snow water equivalent (SWE) in $cm\,month^{-1}$ for two stations in Northern Canada (NC). Observed snow depth in *cm* has been converted in SWE by using *Verseghy* (1991) and the model SWE has been interpolated to the station grid.

3.7 Surface albedo

The surface albedo, describing the fraction of incident solar energy reflected back to the space is an important parameter for determining the Earth's climate. The surface energy budget is strongly determined by the surface albedo, which depends on land cover, soil moisture, cloud cover, solar angle. Snow and ice surfaces absorb a small fraction of incident solar energy due to their high albedo property. However if snow or ice starts to melt, the albedo decreases due to changes in the physical properties of snow and ice. The decreased albedo allows more solar energy to be absorbed by snow and ice and there exists a positive feedback mechanism, which rapidly melt the snow and ice. Wet soil does have less albedo than dry soil and allows more soil moisture evaporation and hence more cloud formation. Albedo depends also on the vegetation type and the season. So, any type of mismatch or error in the model albedo can alter the surface energy balance.

Figure 3.26 shows the monthly climatology mean, domain averaged surface albedo from APP (Advance Very High Resolution (AVHRR) Polar Pathfinder) observation and HIRHAM4 simulation for the same time period (1981-1993, April through

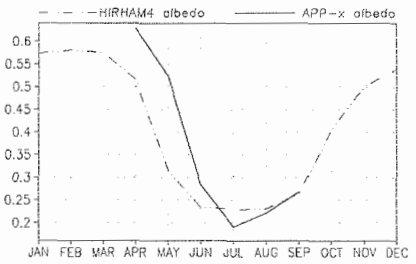

Figure 3.26: Monthly climatology mean, domain averaged (excluding glacier and ocean points) HIRHAM4 and APP albedo.

September). Glacier and sea albedo are excluded from the domain average, as we are focusing on land-surface processes. Starting from the month April to June, the model underestimates albedo by a maximum of 0.2, which is quite large (about 40 $W\,m^{-2}$) in terms of solar short wave radiation. During July the model slightly overestimates the observed albedo. The summer months (JJA) look very close to the observation.

Figure 3.27 shows the difference between HIRHAM4 and APP climatology monthly mean albedo. The positive values indicate that the model underestimates the albedo. During May, at the coastal part of the Arctic APP albedo differs very much from the HIRHAM4 albedo and the model underestimates the observed albedo by about 0.5.

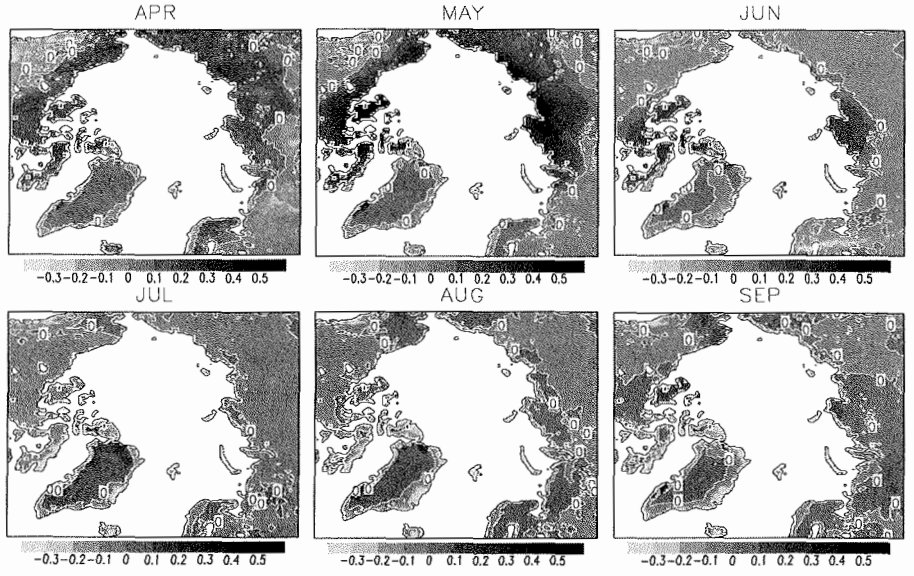

Figure 3.27: APP - HIRHAM4 monthly climatology mean surface albedo (1981-1993).

3.8 Summary

The model $2\,m$ air temperatures are in very good agreement with the measurements at all stations. Also, the large scale spatial patterns in Willmottt-Rawlins climatology are well captured by the model. However during summer, the model shows a warming of maximum 8 °C at the Northern coastal part of Canada, Siberia and Alaska. During winter, the model $2\,m$ air is warmer than Willmotts climatology in Eastern Siberia and Alaska.

The surface albedo is not effected during winter (because there is no incoming solar radiation). During April, May and June, the model underestimates the surface albedo in the Northern coastal part of Siberia, Canada and Alaska by a maximum of 50% compared to the APP climatology. This bias in the surface albedo may have contributed to the summer $2\,m$ air temperature warming in the model compared to the Willmott-Rawlins climatology.

Except for the Lena Delta, soil temperatures at all stations have shown that the model soil has a large cold bias during winter. The largest winter bias occurred in Eastern Siberia, where the model $2\,m$ air temperature has shown a strong warm bias compared to the Willmottt-Rawlins climatology. The magnitude of the winter air temperature signal has not been damped sufficiently when it penetrated down the soil. This damping phenomenon is largely influenced by the freezing action of soil moisture and the amount of snow on the ground surface. Since the HIRHAM4 does not take into account the soil moisture freezing during winter, the model soil rapidly goes down below 0 °C. The model underestimates the observed winter precipitation everywhere in the domain by a large magnitude. Also the comparisons with the station measurements and satellite observation have shown a large deficiency in the model SWE. Therefore the rapid cooling of soil is not prevented by the snow cover. Snow supposes to act as a blanket on ground surface.

Therefore the HIRHAM4 needs a more advanced soil scheme which will allow the freezing and melting of moisture. Presently there is no description of soil moisture at each soil layer. The model winter precipitation i.e. SWE has to be increased from the present values and the snow processes may need more complex treatment. Currently, the model snow density, snow optical and thermal properties do not change with time but this is not the case in reality. Snow depth as well as its thermal properties are important for the net ground heat flux. There is a need to improve the model snow albedo during the months April, May and June. It is also not clear that how the changes in soil thermal properties (i.e. heat conductivity, heat capacity) and snow depth will influence the soil temperature. Therefore we did sensitivity studies with the HIRHAM4 (in section 4) and introduced new soil scheme into the HIRHAM4 (in section 5 and 6).

4 Sensitivity studies with HIRHAM4

4.1 Introduction

After detecting a large winter soil temperature bias in HIRHAM4, it is necessary to find out the key processes in the model which influence the soil temperature evolution. There exist complex nonlinear feedback mechanisms between the land surface and the atmosphere. They interact with each other by several climate variables and the couplings between variables are not isolated. A change in one variable influences the other variables, each in a different way and itself by the others. The Arctic soil processes in the permafrost regions are poorly understood. Often the numerical models are not able to describe these processes. Therefore after perturbing one variable in such a model, it may not represent the right kind of feedback mechanism. The Arctic is a region with many unique climate features. The seasonal freezing and thawing of active layer, strong low-level temperature inversion in the PBL, large seasonal variation in the surface albedo etc. are a few of the unique Arctic climate features. The temperature in the permafrost layer i.e. the stability of permafrost is closely connected with these Arctic climate features. The model parameterizations may need further improvement to capture such unique processes. The strong winter cold bias in the model soil temperature may be due to missing key soil processes or due to inappropriate soil parameterizations. The seasonal freezing and thawing of soil account for a large amount of surface heat budget. Also the seasonal variations of soil thermal properties and snow density are equally important for the surface energy budget. But many GCMs as well as the RCM HIRHAM4 do not treat these processes in a realistic way. We are interested to know the reasons of model winter soil temperature bias. To understand the importance of different processes in the soil in a more systematic way the following sensitivity experiments with the HIRHAM4 have been performed.

4.2 Planetary boundary layer

The atmospheric planetary boundary layer (PBL) provides the physical link between the atmosphere and the Earth surface for exchange of heat, moisture and momentum. Nearly half of the frictional dissipation of the Earth-atmosphere takes place within the PBL. Wind speed increases from the bottom of PBL (which is a highly non geostrophic motion) to the top of PBL. Within the PBL, small-scale turbulent

motion induced by small scale objects like tree, buildings, rough sea surface, extracts energy from the vertical shear of the horizontal flow and dissipates it through the energy cascade mechanism. The atmospheric boundary layer consists of three horizontal layers. The lowest layer, which is in contact with the Earth surface is called *laminar sublayer*. Within this layer, the energy flux is regulated by the molecular motions. Most of the numerical models as well as HIRHAM4 do not treat this layer explicitly. The vertical extent of the *laminar sublayer* is up to few millimeters and mean wind speed is assumed to vanish at the top of this layer, also known as roughness height(z_o). Above the roughness height, there exists a layer with a vertical extent from about 20 to 100 meters called *Prandtl layer* (surface layer). within the *Prandtl layer*, the small scale turbulent motions develop and the wind flow is highly non-geostrophic. Starting from highly non-geostrophic wind flow at the bottom of the *Prandtl layer*, it reaches close to the geostrophic motion at the top of PBL. Above the *Prandtl layer* the *Ekman layer* exists with a typical vertical extent up to 1000 meter height, depending on the stability of the atmosphere.

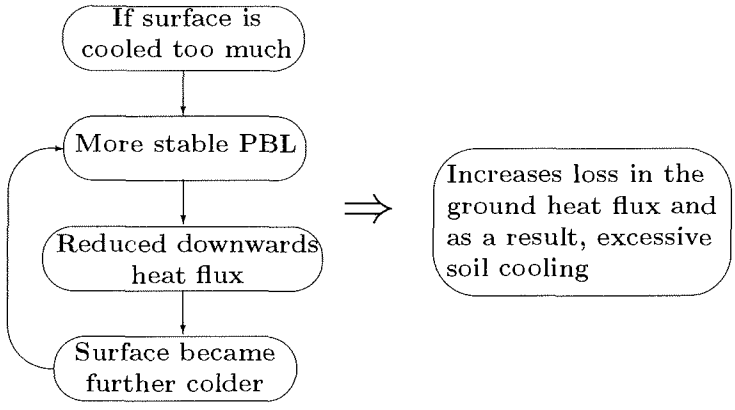

Figure 4.1: Surface temperature and PBL feedback.

There are three regimes (*unstable, near neutral and stable*), which correspond to the energy flux between the Earth and atmosphere. The occurrence of *stable regimes* in the East Siberian region is most frequent (more than 95%) during winter with a deepest surface temperature inversion of $1200\,m$ (*Serreze et al.*, 1992). During polar night, Arctic land surface does not get solar radiation but continuously emits long wave radiation and temperature is maintained by atmospheric energy transport from mid latitude and energy flux from the ocean. Warm air flow over relatively cold surfaces, causes the diabatic cooling of the air just above the colder surface. Turbulent eddies are generated by the flow of air over a rough surface,

which maintain a relatively cold thin mixed layer at the surface. Since these eddies are not strong enough, they are not able to penetrate much in upward direction due to a rapid loss of its kinetic energy by the work done against gravity. The depth of the PBL increases with the increase of wind speed and roughness of the surface. In the Arctic the low-level temperature inversion is not only due to radiative cooling and warm air advection but also due to radiative property of ice crystal, surface melt, subsidence (*Curry*, 1983; *Kahl*, 1990; *Serreze et al.*, 1992). There are also *stable regimes* during summer and spring seasons with reduced inversion height and reduced frequency of occurrence (*Serreze et al.*, 1992).

A stable stratified thin PBL dominates the heat exchange between the land-surface and the atmosphere. There exists a positive feedback between land-surface temperature and the PBL stratification. If the stratification is stable enough, so that it allows a very small vertical mixing with the atmosphere and hence a small amount of heat is transported to the soil. Then the soil will become colder in addition of long wave radiation. This will further enhance the stable stratification of the PBL (Figure 4.1). The use of different PBL parameterizations in HIRHAM4 lead to different energy fluxes from the surface to the atmosphere and these differences are of the same order as those due to synoptic-scale changes (*Dethloff et al.*, 2001).

A revised stability function by *Louis et al.* (1982) increased the turbulent heat flux downwards by the atmosphere during stable condition and improved the winter soil temperature bias in the ECMWF model (*Viterbo et al.*, 1999). The empirical formulation of stability parameter under stable condition was similar to section 2.3.6, but with different constant values:

$$f_m = \frac{1}{1 + (2 \cdot b \cdot R_i)/(\sqrt{1 + d \cdot R_i})} \quad \text{and} \tag{4.1}$$

$$f_h = \frac{1}{1 + (3 \cdot b \cdot R_i)/(\sqrt{1 + d \cdot R_i})}, \tag{4.2}$$

with $b = 5, d = 1$.

This formulation has very little impact on the surface momentum flux over land and therefore little effect on the large scale circulation. The ratio of momentum and heat diffusion is reduced, which increases the heat flux towards the surface (*Viterbo et al.*, 1999). Using this revised stability function, 5 years (1979-1983) HIRHAM4 simulations have been performed. Hereafter this simulation will be referred as PBL sensitivity. The monthly climatology mean of the above years control and the PBL sensitivity simulations are used to investigate the influences of the new stability function on the model climate, specially on the ground heat flux and the soil temperature.

Figure 4.2 shows the PBL sensitivity run *minus* control HIRHAM4, summer (JJA) and winter (DJF) average of monthly climatology mean (1979-1983) $2\,m$ air temperature. In most of the places above the land-surface, the winter $2\,m$ air temperature has been warmed up by a maximum of 2 °C. But parts of West Russia and Siberia have been cooled down by a maximum of 1 °C. The 850 hPa winter air temperature (Figure 4.3) shows a cooling over most of its land part by a maximum of 0.5 to 1.0 °C. This is indicating a net heat loss by this layer to the downward

direction, but the cooling in $2\,m$ air temperature over some part of the land surface is not explained by this. There are also minor summer cooling and warming over land parts in both $2\,m$ and 850 hPa air temperatures.

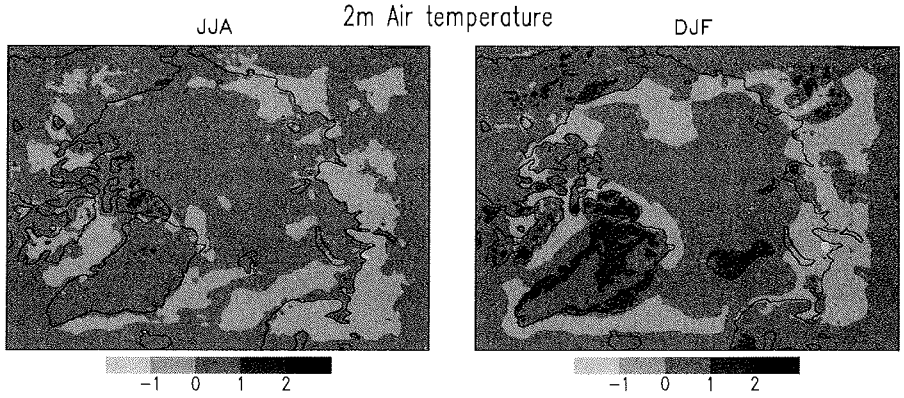

Figure 4.2: PBL sensitivity run *minus* control HIRHAM4, summer (JJA) and winter (DJF) averaged monthly mean $2\,m$ air temperature in °C. This is the average over 5 years (1979-1983) simulations. Positive values indicate warming of $2\,m$ air temperature in the PBL sensitivity experiment.

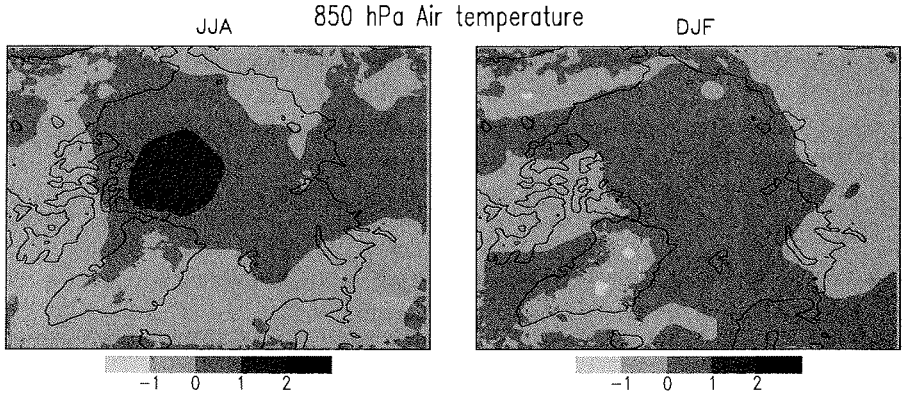

Figure 4.3: PBL sensitivity run *minus* control HIRHAM4, summer (JJA) and winter (DJF) averaged monthly mean 850 hPa air temperature in °C. This is the average over 5 years (1979-1983) simulations. Positive values indicate warming of 850 hPa air temperature in the PBL sensitivity experiment.

Monthly climatology mean, PBL sensitivity run *minus* control HIRHAM4 mean sea level pressure (MSLP) for all months is shown in Figure 4.4. Mean sea level pressure has been increased by a maximum of about 7 hPa and decreased by a maximum of $5\,hPa$. The maxima of pressure changes are mainly situated over the Arctic oceans. Above land, the MSLP did not show a significant change. The monthly mean sea level pressure changes differ very much from year to year. The standard deviations of monthly MSLP in both control and PBL sensitivity HIRHAM4 are found a maximum of 14 hPa from October through April (not shown here). The other months did not show such large variability.

The winter cooling in HIRHAM4 $2\,m$ air temperature due to the revised stability function is not in agreement with *Viterbo et al.* (1999). After introducing this revised stability function in the ECMWF model, *Viterbo et al.* (1999) found an increased January $2\,m$ air temperature by a maximum of 3-5 °C over the Arctic land-surface. *Viterbo et al.* (1999) did the simulation for one winter season but we have done HIRHAM4 simulation for 5 years using the same revised stability function. In our five years simulation, none of the winter months (DJF) have shown warming in $2\,m$ air temperature everywhere above the land-surface. The change in mean sea level pressure in the PBL sensitivity experiment indicates the change in horizonal advection of air masses. During December, the increase in mean sea level pressure centered over the Kara sea (Figure 4.4) indicates the advection of cold air mass to this region in the PBL sensitivity experiment. Therefore this region has become colder in the PBL sensitivity run compared to the control HIRHAM4.

In the PBL sensitivity experiment, the surface sensible heat fluxes during winter have been increased (Figure 4.5) compared to the control HIRHAM4 simulation by a maximum of $6\,\mathrm{W\,m^{-2}}$ over most of the land parts. The latent heat flux show only minor changes, within $\pm 1\,\mathrm{W\,m^{-2}}$. The net surface short wave (SW) radiation also does not show a significant change, it is only within $\pm 0.5\,\mathrm{W\,m^{-2}}$. The net surface long wave (LW) radiation has been increased by a maximum of $4\,\mathrm{W\,m^{-2}}$. The net surface SW radiation is very small and the model shows a maximum of $20\,\mathrm{W\,m^{-2}}$ averaged over winter months. However the LW cooling during winter is large, in the order of $50\,\mathrm{W\,m^{-2}}$. Therefore the revised stability function has increased the downward sensible heat flux. This increased sensible heat flux has increased the surface temperature and the increased surface temperature has increased the LW cooling. The net gain or loss of heat energy due to above two fluxes can be realized in the net ground heat flux also. The latent heat and SW radiation fluxes seem to be not so important in this sensitivity experiment.

The net ground heat flux which is positive (gain by the soil) during summer and negative (loss by the soil) during winter are shown in Figure 4.6 for both PBL sensitivity and control HIRHAM4 simulation. The North Canadian Arctic and the central Siberian regions show the largest winter ground heat loss (except Greenland) of maximum $15\,\mathrm{W\,m^{-2}}$. The revised PBL scheme has increased the heat gain by the soil in most part of the domain. However a loss of maximum $1\,\mathrm{W\,m^{-2}}$ is seen in the part of West Russia, Siberia and North Canada. Figure 4.7 represents the PBL sensitivity minus control winter (DJF) and summer (JJA) monthly mean first soil layer ($3.25\,cm\ depth$) temperatures, averaged over 5 years. The revised stability

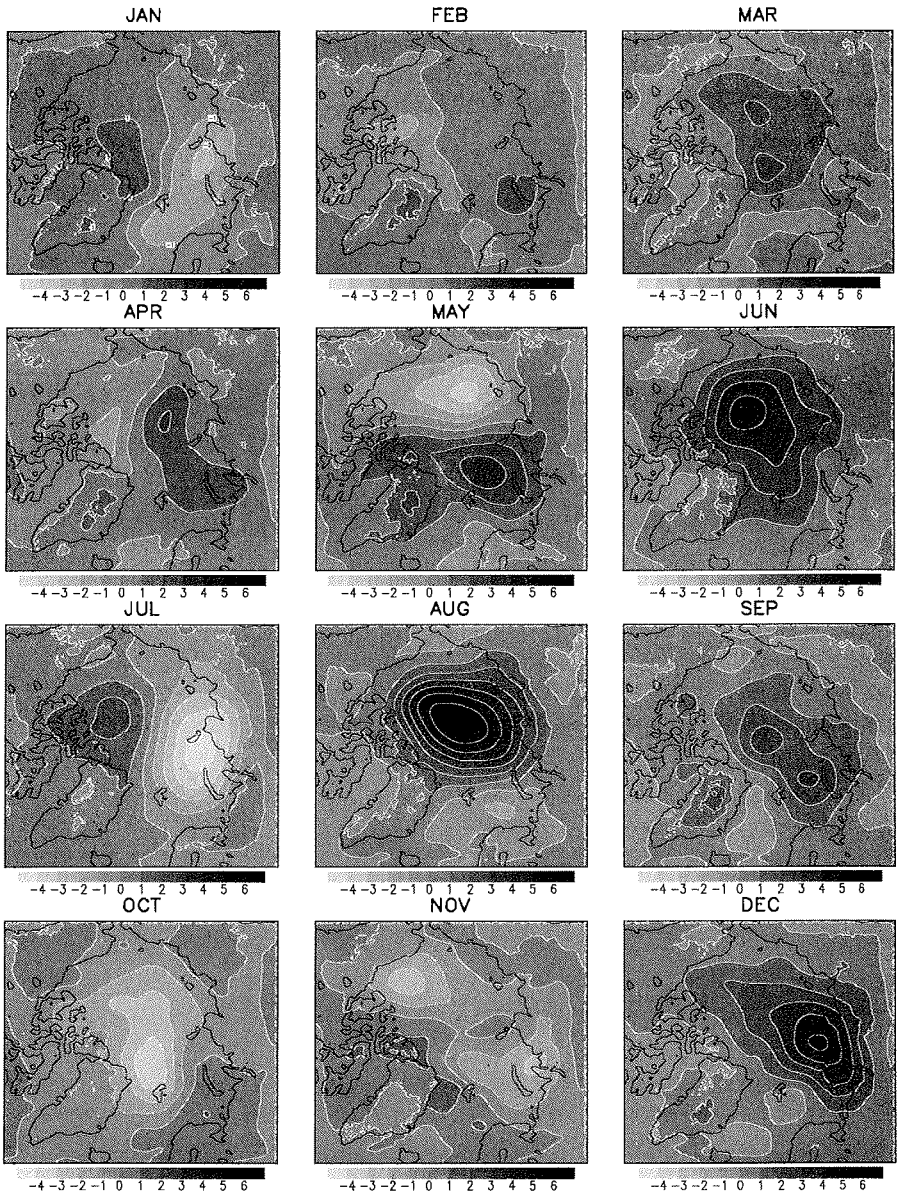

Figure 4.4: Monthly climatology mean (1979-1983), PBL sensitivity run *minus* control HIRHAM4 mean sea level pressure in hPa. The positive values show the increase in mean sea level pressure in the PBL sensitivity experiment.

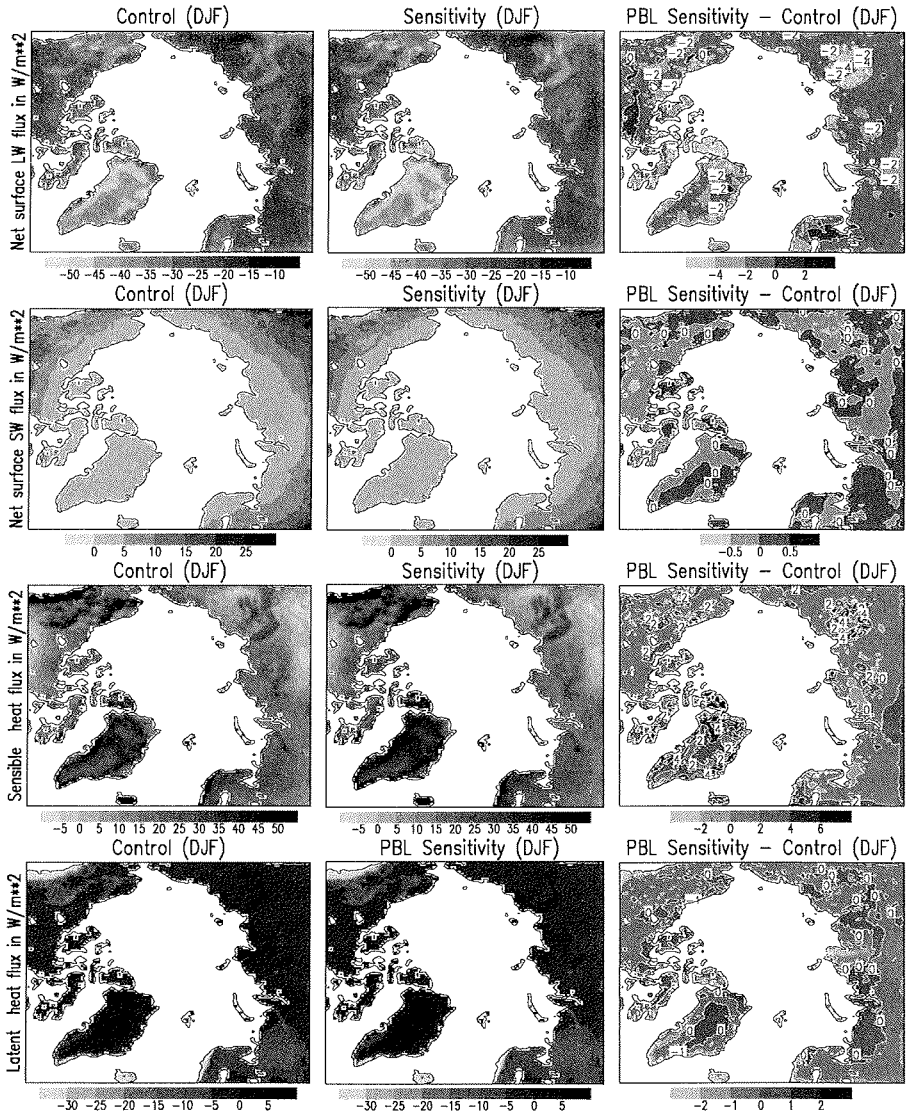

Figure 4.5: Monthly climatology mean (1979-1983) winter (DJF) averaged net surface LW, SW, sensible and Latent heat fluxes for the control and the PBL sensitivity simulations and their differences in $\mathrm{W\,m^{-2}}$.

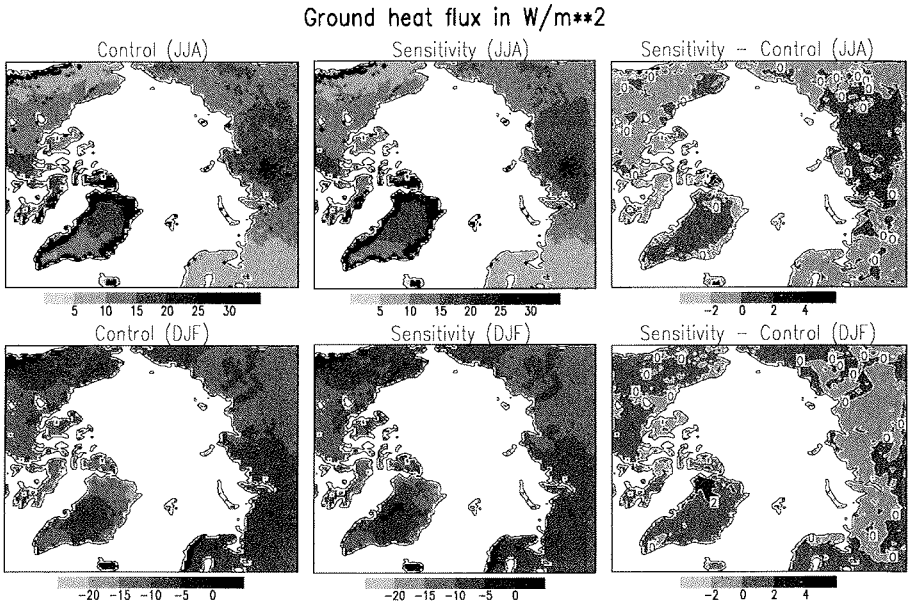

Figure 4.6: The summer (JJA) and winter (DJF) average of monthly climatology mean (1979-83) ground heat flux (in $W\,m^{-2}$) in the PBL sensitivity run and the control HIRHAM4 simulations. The right hand side of upper and lower panel shows the difference between these two simulations for summer and winter respectively.

functions have warmed up the winter soil in Alaska, North Canada, Greenland, Scandinavia and part of the far East Siberia by a maximum of about 2 °C. The soil temperature has not been increased everywhere, but in some parts of Siberia it shows a cooling of about 1 °C. The warming and cooling regions in the first soil layer are the regions of ground heat gain and loss respectively. So it is clear from the Figures 4.5 and 4.7 that, an increased downward net heat flux has increased the soil temperature. During summer, the model soil temperature shows a mixed response, but not so strong signal as in winter. The maximum cooling and warming are about 1 °C. Figure 4.8 shows the PBL sensitivity minus control monthly climatology mean (1979-1983) vertical soil temperature profile. During winter a warm signal have been penetrated down sufficiently in the soil but with a small magnitude. An enhanced downward turbulent heat flux was responsible for the winter soil temperature warming.

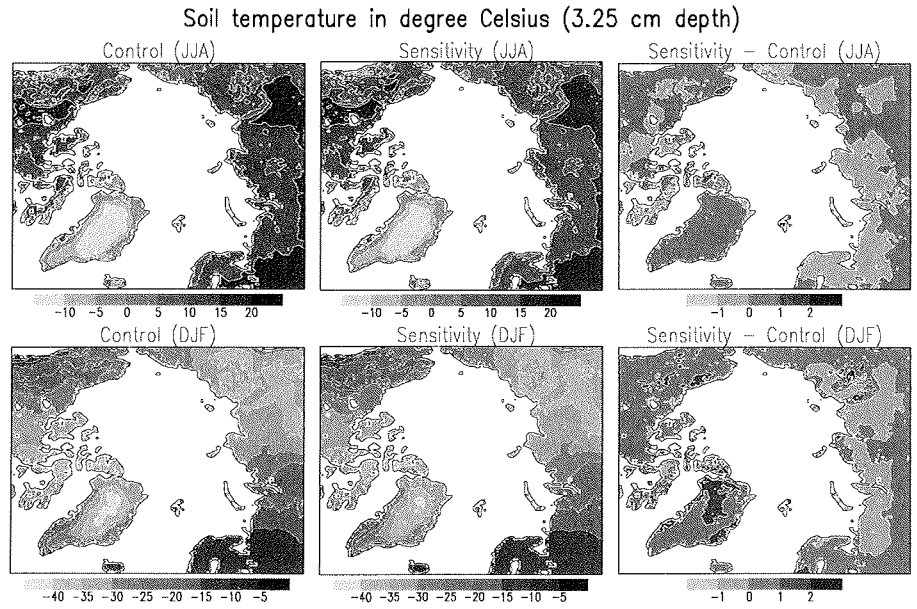

Figure 4.7: The summer (JJA) and winter (DJF) average of monthly climatology mean (1979-83) soil temperature at 3.25 *cm* depth (in °C) in the PBL sensitivity run and the control HIRHAM4 simulations. The right hand side of upper and lower panel show the difference between these two simulations for summer and winter respectively.

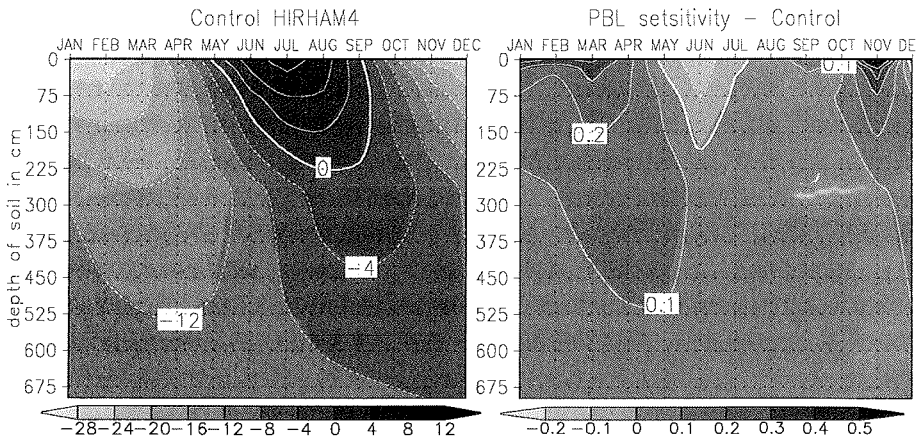

Figure 4.8: The domain averaged (excluding 10 grid points at the boundary and the glacier part) monthly climatology mean (1979-83) control HIRHAM4 and PBL sensitivity run *minus* control HIRHAM4 vertical soil temperature profile in °C.

4.3 Soil thermal heat conductivity

The main and basic mechanism of heat transfer within the soil is heat conduction and heat conduction is performed by the atomic and molecular vibrations in the crystal lattice. Stationary conductive heat transfer is represented by the Fourier's law

$$Q = -k\frac{\partial T}{\partial x}, \tag{4.3}$$

where Q is the heat flux per unit area, k is the thermal conductivity of the soil and $\frac{\partial T}{\partial x}$ is the temperature gradient between two interfaces of the soil layer. In reality, heat conduction in the soil is a three dimensional process, i.e. heat can be transferred in both horizontal and vertical directions. Also it is a non-stationary process and changes in different time scales like day, season, year and decade. Due to the large horizontal scale of the model ($50 \times 50\,km$), it does not make sense to represent horizontal soil heat conduction. The horizontal temperature gradient will be so small, that the horizontal heat flux along the grid boxes can be neglected. So, the model treats only the temporal development of the vertical soil temperature. In this case, a one dimensional non-stationary Fourier heat conduction equation is

$$C_{vol}(z)\frac{\partial T}{\partial t} = \frac{\partial}{\partial z}\left(k(z)\frac{\partial T}{\partial z}\right) + L\frac{\partial v_I}{\partial t}, \tag{4.4}$$

where L is the volumetric latent heat, v_I is the volumetric ice water content, $C_{vol}(z)$ is the volumetric heat capacity and $k(z)$ is the thermal heat conductivity of soil. The vertical distribution of soil heat capacity, heat conductivity and soil water content are not homogeneous in reality. Soil thermal heat conductivity depends on various factors like amount of moisture in the soil, organic materials, percentage of sand and clay etc. For example a Glacier has a different heat conductivity than wetlands or soil rocks. So it is important to describe the appropriate thermal properties of the soil in the model. Otherwise the model will not be able to simulate the right magnitude of temperature at the right place. A decrease in soil thermal heat conductivity will decrease the heat flux into the soil during summer, when the land surface mainly is heated up by the solar radiation and transfers heat towards deeper layers. Therefore the summer soil will be colder. During winter, most part of the Arctic does not get solar radiation and soil looses heat to the atmosphere by long wave cooling, sensible and latent heat fluxes. Therefore a decreased thermal heat conductivity will reduce the ground heat loss during winter. Therefore the winter soil is expected to warm up whereas in summer it is expected to cool down due to reduction in soil thermal heat conductivity.

The HIRHAM4 prescribes the soil thermal conductivity and volumetric heat capacity (Figure 4.9) vertically homogenous and does not take into account the latent heat of soil moisture freezing and thawing. So for the HIRHAM4, the Fourier's heat conduction equation takes the final form

$$C_v \frac{\partial T}{\partial t} = k \frac{\partial^2 T}{\partial z^2}. \tag{4.5}$$

The HIRHAM4 does not take into account the seasonal change in thermal heat conductivity and volumetric heat capacity. In reality heat conductivity depends on soil moisture and the physical state of soil moisture. The volumetric soil moisture content and the volumetric ice content change with seasons.

Considering these drawbacks, the soil thermal heat conductivity is sharply reduced to $\frac{1}{3}$ of its present value. For this experiment, the change in soil temperature by magnitude was more important than the choice of real thermal heat conductivity. The HIRHAM4 simulations are performed for 5 years (1979 – 1983) with $\frac{1}{3}$ soil thermal heat conductivity. Hereafter this simulation will be referred as conductivity sensitivity simulation.

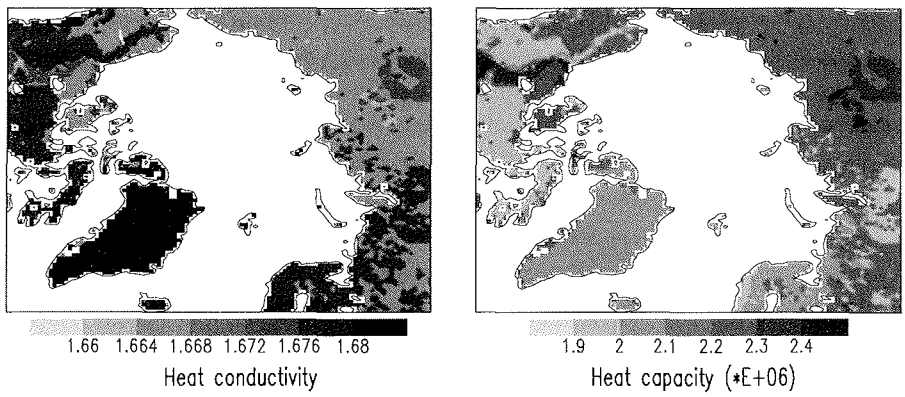

Figure 4.9: HIRHAM4 soil heat capacity (in $\mathrm{J\,m^{-3}\,K^{-1}}$) and heat conductivity (in $\mathrm{W\,m^{-1}\,K^{-1}}$).

Figure 4.10 shows the conductivity sensitivity minus control summer (JJA) and winter (DJF) monthly mean first soil layer (3.25 *cm*) temperature and the ground heat flux, averaged over 5 *years*. During winter, most of the land areas have been cooled down by a maximum of 3 °C. During summer, a small part of North Canada and Siberia have been warmed up by a maximum of 1 °C, but the remaining land parts show cooling of a maximum 1 °C. This magnitude of soil temperature change in winter due to a drastic reduction in the soil heat conductivity is not comparable to the winter model bias. Though the winter ground heat loss has been decreased everywhere in the domain, the first soil layer does not show warming. Similarly, the reduction in summer ground heat gain does not have cooling effect everywhere in the domain. The surface cooling due to LW radiation loss during winter is compensated by the downward turbulent heat flux and the conductive ground heat flux from the deeper soil layers. The winter reduction in ground heat loss due to decreased soil heat conductivity has cooled down the surface temperature and eventually the upper

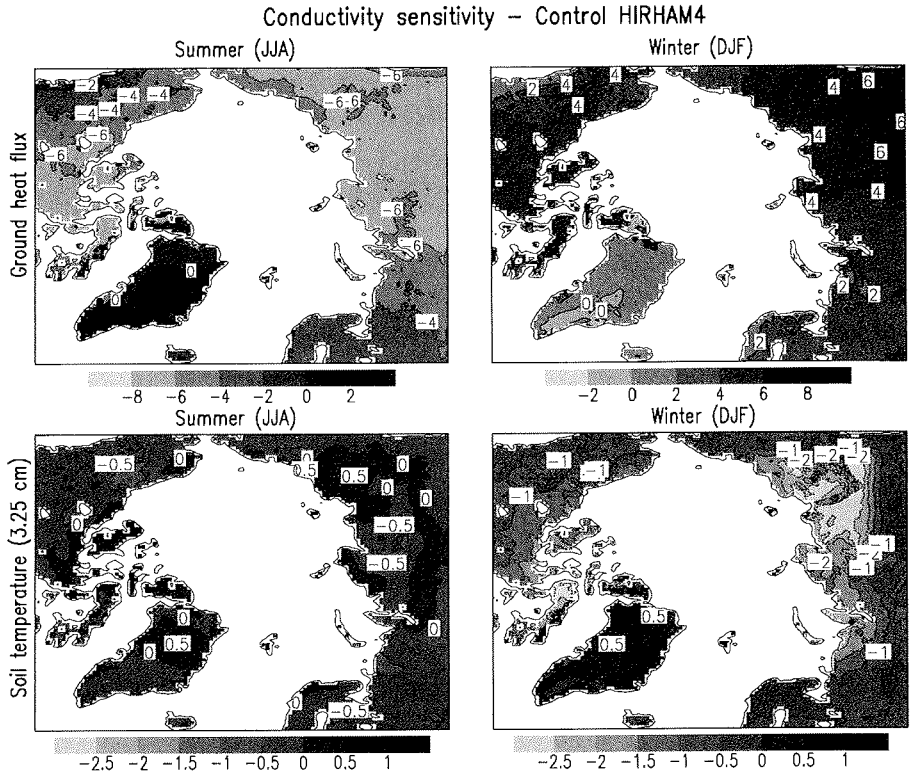

Figure 4.10: The conductivity sensitivity run *minus* control HIRHAM4, summer (JJA) and winter (DJF) monthly mean net ground heat flux (in $\mathrm{W\,m^{-2}}$) and the first soil layer (3.25 *cm. depth*) temperature (in °C), averaged over 5 years(1979-1983). The positive values represent the increase and negative values represent the decrease in the variables during sensitivity experiment.

soil layer. Since the HIRHAM4 soil thermal inertia is small (due to the absence of moisture freezing process) and the amount of snow over ground is also small, the upper soil layer has been reached quickly very close to the cold surface temperature.

The domain averaged (excluding 10 grid points at the boundary, ocean and glacier part) net ground heat flux is shown in Figure 4.11. The magnitude of net ground heat flux is reduced in both winter and summer seasons. The reduction of the soil thermal heat conductivity has reduced the winter heat loss by the ground to the atmosphere by about $5\,W\,m^{-2}$. However, the decrease in summer heat gain by the ground is larger than the decrease in winter heat loss. Figure 4.12 shows the domain averaged monthly climatology mean conductivity sensitivity minus control vertical soil temperature profile. At below 75 *cm* depth, the winter warming and summer cooling of soil temperatures are very clear. The deeper soil layers have

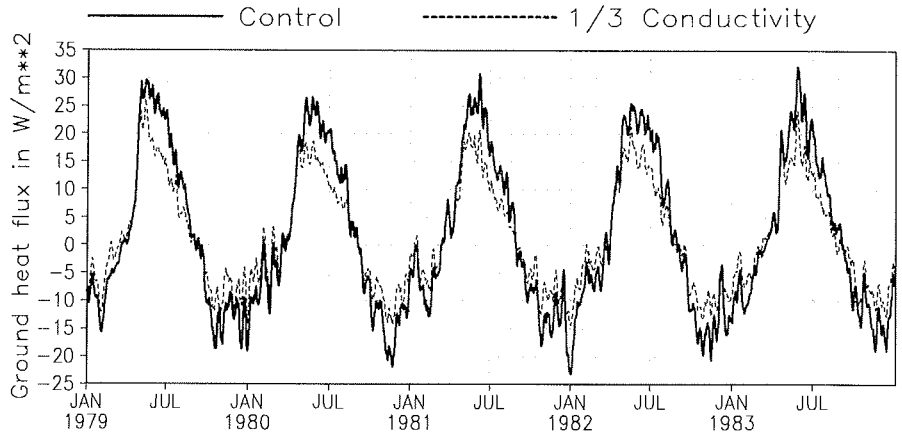

Figure 4.11: Land area averaged (excluding 10 grid points at the boundary and glacier part) ground net heat flux in $W\,m^{-2}$. The positive and negative values represent the gain and loss of soil heat flux respectively.

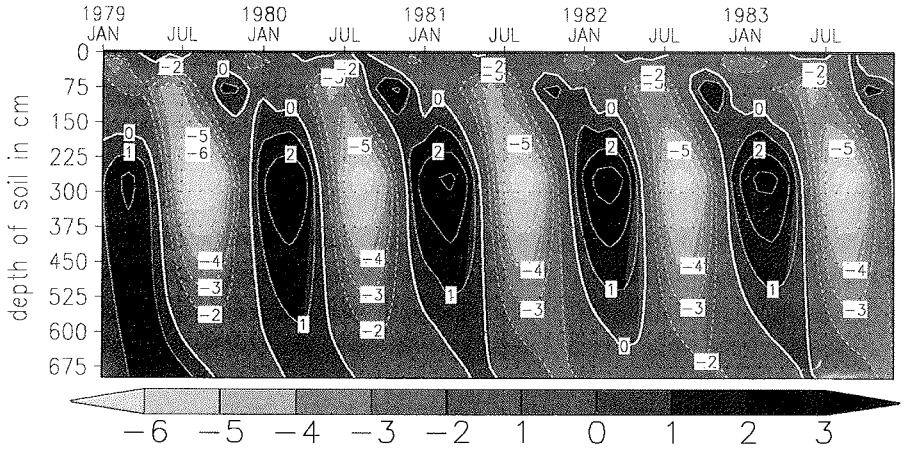

Figure 4.12: The monthly climatology mean (1979-83) land area averaged (excluding 10 grid points at the boundary and glacier part) Conductivity sensitivity run *minus* control HIRHAM4 vertical soil temperature profile in °C.

been warmed up by a maximum of 3 °C during winter, whereas during summer the same have been cooled down by a maximum of 6 °C. The summer cooling is about 2 times stronger than the winter warming and this is mainly due to the large summer net surface SW radiation.

4.4 Snow density

Fresh or new snow is lighter and contains a large amount of air within the snow pack. Due to the presence of large amount of air within the fresh snow pack, the snow thermal heat conductivity is less as compared to the old packed snow. The thermal conductivity of snow varies from 0.02 to 1.0 $W\,m^{-1}\,K^{-1}$ (*Sturm et al.*, 1997). The amount of snow also influences the soil temperature evolution. Thicker snow during winter keeps the soil isolated from the cold air and hence warms up the soil. Too early or late autumn snowfall can make a big difference in soil temperature (*Ling and Zhang*, 2003).

The snow density varies much from place to place and depends on the age of snow but the HIRHAM4 uses a fixed snow density ($\rho = 300\,kg\,m^{-3}$). In the Canadian Arctic the snow density ranges from about 125 to $500 kg\,m^{-3}$ (http://www.socc.ca/nsisw/atlas/index.cfm). Snow density directly does not effect the model soil temperature. It is used to calculate the snow depth only, since the model produces the snow water equivalent. If the model snow depth is increased, there should be a warming effect in soil during winter.

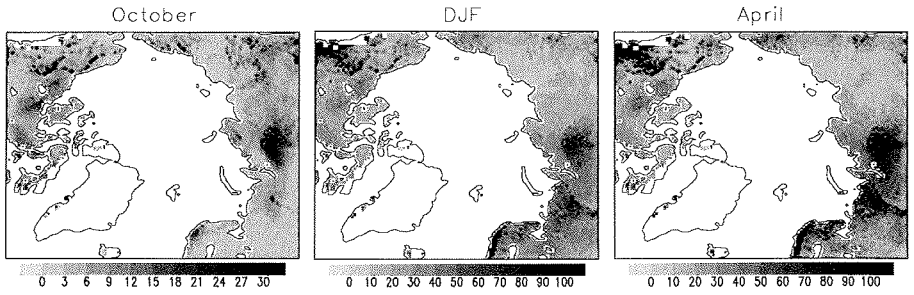

Figure 4.13: Increase in snow depth in cm, due to a decrease in snow density in the model. The left and right panels are the October and April monthly climatology mean (1979-1983) increased snow depth respectively. The middle panel is the winter (DJF) averaged increase in snow depth.

To imply this idea, the model snow density has been reduced from fixed 300 $kg\,m^{-3}$ to 100 $kg\,m^{-3}$. Though the snow depth will increase due to the decreased snow density, it will not alter the thermal properties (thermal heat conductivity, volumetric heat capacity) of snow. In the beginning of winter or in the late autumn, the snow remains light and less conductive and the deficiency of snow in the model can be reduced by decreasing the snow density. Since the thermal properties of snow remain unchanged, it is expected that the temperature gradient between snow surface and the land-surface will decrease. The increased snow depth will decrease the heat flux through it and hence the temperature at the bottom of snow layer will increase. Therefore the soil will not loose sensible heat rapidly to the colder atmosphere.

HIRHAM4 simulation is performed for 5 $years(1979 - 1983)$ using the changed snow density setup. Hereafter this simulation will be referred as the snow density

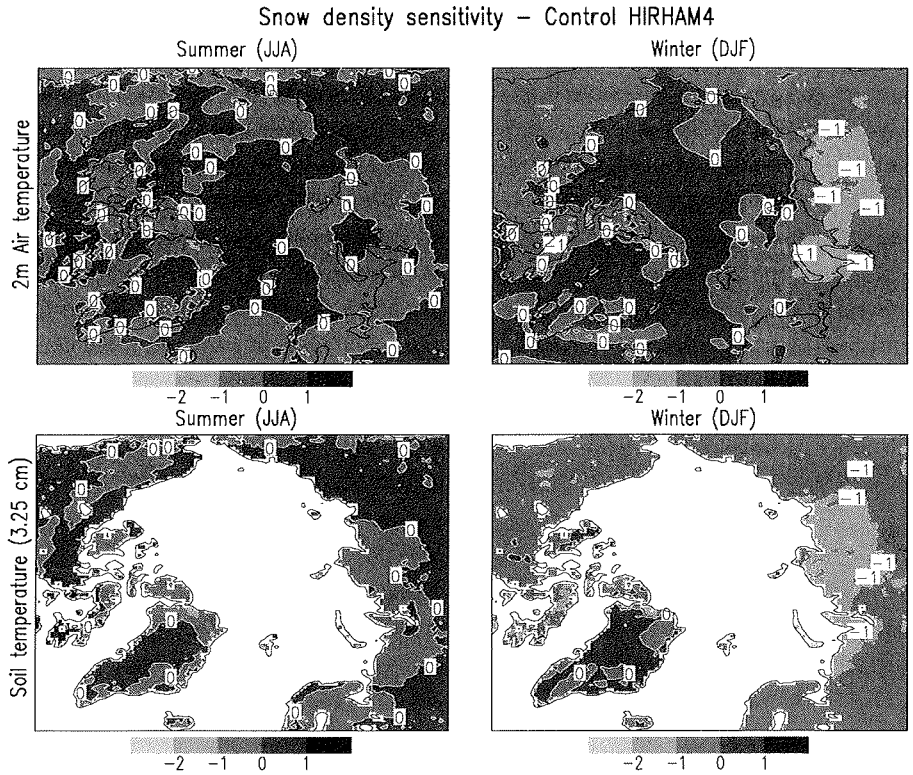

Figure 4.14: The snow density sensitivity run *minus* control HIRHAM4, summer (JJA) and winter (DJF) monthly mean, averaged over 5 years(1979-1983) $2\,m$ air temperature and first soil layer ($3.25\,cm$ *depth*) temperature in °C. Positive values represent warming of soil due to the increase in snow depth. Whereas negative values show cooling of soil.

sensitivity. Figure 4.13 shows the distribution of increased snow depth in centimeter, during the months October, April and the winter months (DJF) average. The change in snow density has increased the model snow depth by about 10 to $100\,cm$. The regions with large model winter precipitation show the largest increase in snow depth. In the West Russia, Scandinavia, North Canada and part of Alaska, the snow depth increase has a maximum value, whereas in the low winter precipitation region e.g. East Siberia, the increase in snow depth has a minimum value. Figure 4.14 shows the snow density sensitivity minus control winter (DJF) and summer (JJA) monthly mean first soil layer temperatures, averaged over 5 years. Due to the increase in snow depth, there is a cooling in most of the land parts during winter. During summer, the changes show mixed behavior, including both cooling and warming. During summer, the model does not have snow over ground except in

the mountain regions. A change in ground heat flux during winter is influencing the soil temperature during summer. This behavior is clearly due to the non-linearity in the system. The magnitude of winter soil cooling is up to a maximum of 2 °C. During summer, the soil warming is maximum up to 1 °C. Large insulation by snow could not change the soil temperature, probably because of the small temperature gradient between air and the first soil layer. The difference between 2 *meter* air and first layer soil temperature was maximum up to 1 °C. During winter, increase in snow depth has decreased the ground heat loss by a maximum of 5 $W\,m^{-2}$ as shown in Figure 4.15. The decrease in heat loss by the ground surface can warm up the soil, but the opposite is seen in the first soil layer.

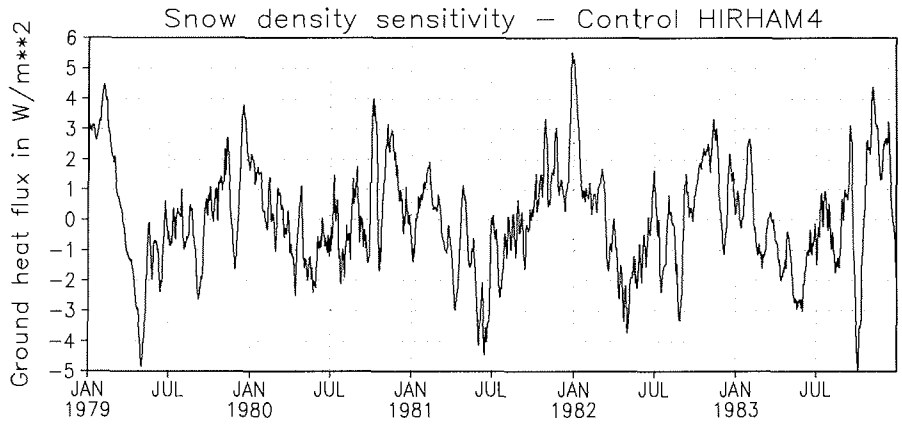

Figure 4.15: Land area averaged (excluding 10 grid points at the boundary and glacier part) ground net heat flux. The positive and negative values represent the gain and loss of soil heat flux respectively. Increase in snow depth decreases soil heat loss during winter by an average of about 2 $W\,m^{-2}$.

However the domain averaged soil temperature (Figure 4.16) shows that, there are warming and cooling in the deeper soil layers during winter and summer respectively. Very similar seasonal changes in the vertical soil temperature profile like in the conductivity sensitivity experiments are seen. The summer cooling is attributed to the increase in snow depth during normal snow melt time (spring). The net ground heat flux (which is positive at that time) has been decreased due to the increase snow insulation. The winter warming in the deeper soil layers is due to a reduction in heat loss by the ground. The ground heat loss has been reduced by the increased snow insulation. The changes in the upper soil layers are small. This may be due to the combined result of inappropriate soil thermal property and the absence of seasonal freezing and thawing processes.

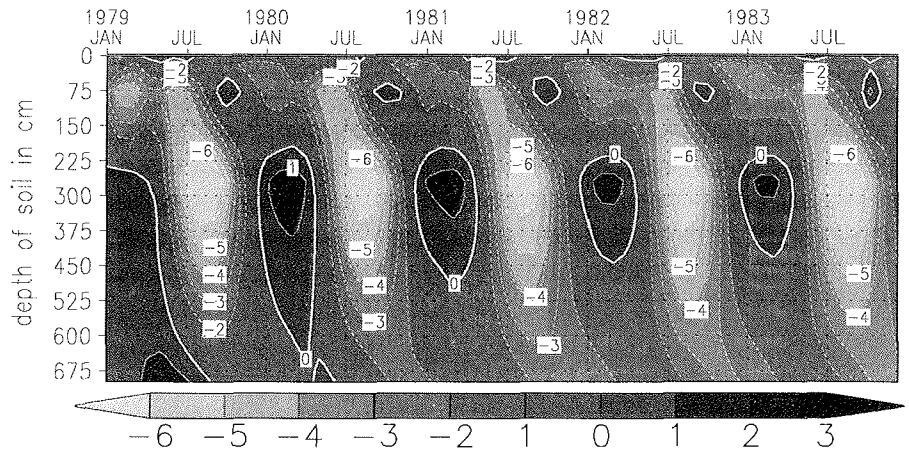

Figure 4.16: The monthly climatology mean (1979-83) land area averaged (excluding 10 grid points at the boundary and the glacier part) snow density sensitivity run - control HIRHAM4 vertical soil temperature profile in °C.

4.5 Snow albedo

It was shown in section 3.7 that, during spring time the model underestimates the surface albedo in most of the land areas. *Box and Rinke* (2003) showed that HIRHAM4 underestimates the surface albedo of Greenland ice sheet. *Køltzow and Eastwood* (2003) have shown that HIRHAM4 largely underestimates the surface albedo in non-forested areas but has a good agreement for forested areas with AVHRR data. Also low albedo in the model during spring time could enhance the snow melt and hence the $2\,m$ air temperature. Additionally, an underestimation of snow albedo at the beginning of winter can lead to a overestimation of surface net heat flux. A polynomial temperature dependent scheme, suggested by *Roesch* (2000) was found to be good for non-forested areas. *Roesch* (2000) suggested the following temperature dependency for the surface albedo over bare land

$$\alpha = 0.5 + a_1 \cdot T_S + a_2 \cdot T_S^2 + a_3 \cdot T_S^3 + a_4 \cdot T_S^4, \tag{4.6}$$

where

$$\begin{aligned} a_1 &= -0.07582627, \\ a_2 &= -5.5360168 \times 10^{-3}, \\ a_3 &= -5.2966269 \times 10^{-5}, \\ a_4 &= 4.2372742 \times 10^{-6}, \\ T_S &= \text{surface temperature in } °C \end{aligned}$$

and

$$\begin{aligned} \alpha &= 0.8 \qquad T_S \leq -10\,°C, \\ \alpha &= 0.5 \qquad T_S \geq 0\,°C. \end{aligned}$$

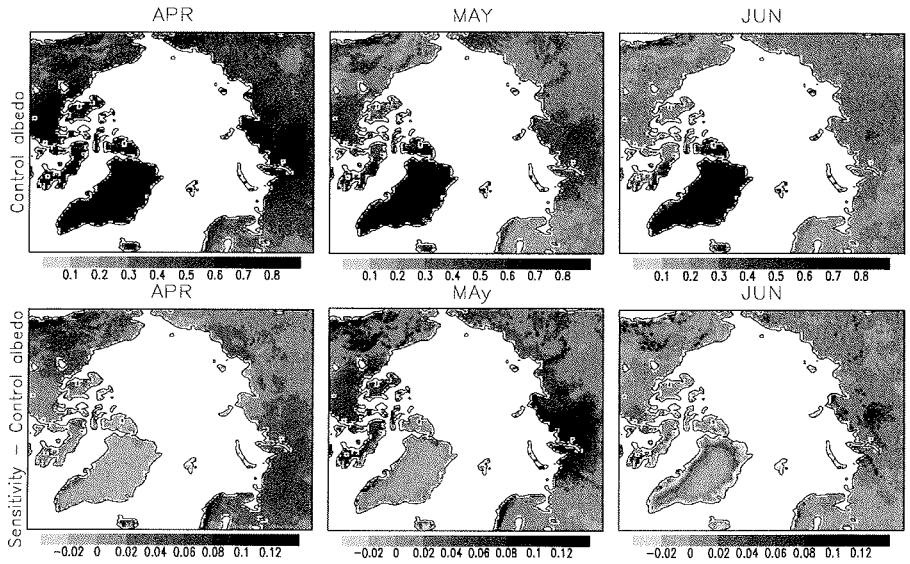

Figure 4.17: Surface albedo in control HIRHAM4 and new snow albedo scheme run *minus* control HIRHAM4 albedo.

The original HIRHAM4 albedo for the forested areas and the polynomial approach suggested by *Roesch* (2000) for the non-forested areas are adapted into the model. Using this changed surface albedo parameterizations, a 5 *years* HIRHAM4 simulation has been performed. Hereafter this simulation will be referred as snow albedo sensitivity. Figure 4.17 shows the monthly climatology mean (1979-83) control HIRHAM4 albedo for the months April, May and June and the differences between the albedo sensitivity and the control simulations. In the model validation (in section 3.7) it was shown that, the model underestimates (by a maximum of 50%) surface albedo at the coast of Siberia, North Canada and Alaska during the months April through June. The new snow albedo scheme has increased the surface albedo during the months April through June by a maximum of 0.12. Therefore the snow albedo sensitivity run has improved the surface albedo.

The model overestimates the summer observed $2\,m$ air temperature at the coast of Siberia, North Canada and Alaska (Figure 3.4). The snow albedo sensitivity run has decreased the summer $2\,m$ air temperature by a maximum of $2\,°C$ at the coast of North Canada and partly at the coast of Siberia (Figure 4.18). Therefore, the summer $2\,m$ air temperature has also improved in the snow albedo sensitivity run. The first soil layer temperature shows a minor warming and cooling of up to 1 °C in the snow albedo sensitivity run compared to the control HIRHAM4.

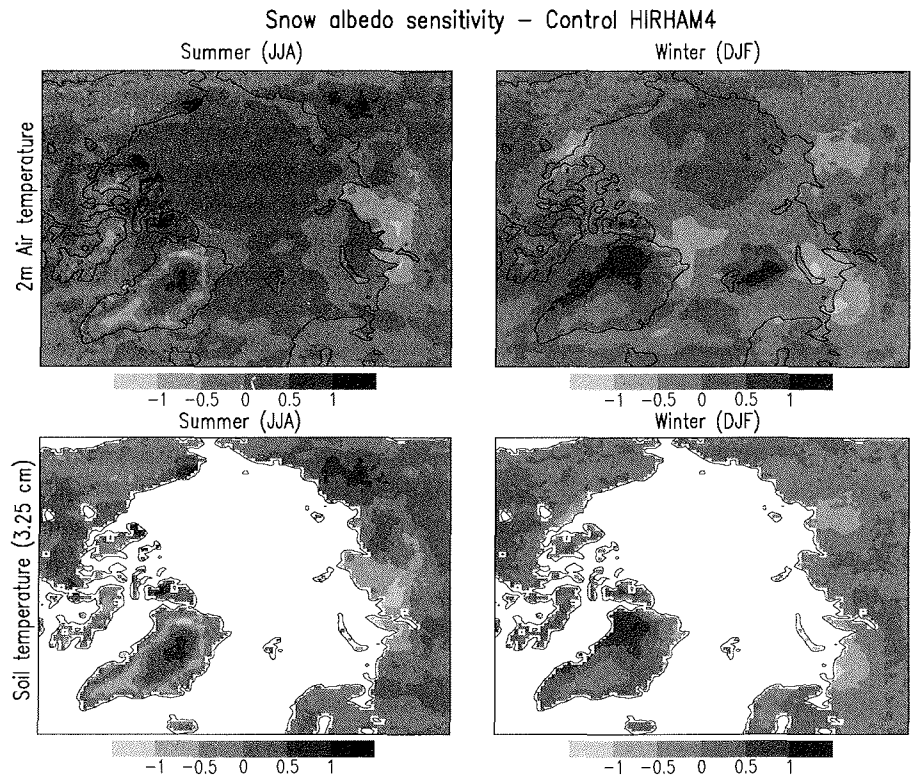

Figure 4.18: New albedo run *minus* control HIRHAM4 summer (JJA) and winter (DJF) monthly mean, averaged over 5 years(1979-1983) $2\,m$ air temperature and first soil layer ($3.25\,cm$ *depth*) temperature in °C. Positive values indicate the warming of soil in sensitivity experiment, whereas negative values represent the cooling of soil.

4.6 Summary

In all sensitivity experiments, the magnitude of soil temperature change was within $\pm 6\,°C$. The change in one model parameter was not able to improve the winter soil temperature and to reduce the cold winter bias which is up to 15 to 20 °C colder than the observations. The revised stability function under stable condition increased the downward sensible heat flux and a warming in the winter soil was detected. The domain averaged warming in the winter soil was by a maximum of $0.5\,°C$. This increased sensible heat flux has increased the surface temperature and the increase in surface temperature has increased the long wave (LW) cooling. The sum of these above changed fluxes was not positive everywhere. The latent heat and the short wave (SW) radiation fluxes seem to be not so important in planetary boundary layer sensitivity experiment.

A decrease in soil thermal conductivity was able to decrease the ground heat loss to the atmosphere during winter by 6 $W\,m^{-2}$. During summer the ground heat gain decreased by a maximum of 6 $W\,m^{-2}$. Warming and cooling signals due to the gain and loss of ground heat flux during winter and summer respectively were found in the deeper layers. The upper soil layer's thermal inertia seems to be small and therefore it was able to reach very quickly close to the near surface air temperature.

During the snow density sensitivity run, the soil temperature behaved in a same way as in the conductivity sensitivity experiment. This sensitivity experiment increased the soil temperature at the deeper layer by 1 °C during winter whereas during summer a decrease of maximum 6 °C was found at the same depth.

The new snow albedo scheme was able to increase the surface albedo during the months April, May and Jun by a maximum of 0.12, which was underestimated by the model by a maximum of 0.5. Though the increase in surface albedo due to the new snow albedo scheme was small compared to the model bias, it was able to decrease the summer model bias in $2\,m$ air temperature by a maximum of 1.5 °C in some places. The effects on the soil temperature due to the new snow albedo scheme were not so large but the improvement in surface albedo and summer $2\,m$ air temperature was in the right direction.

The mean sea level pressure was very sensitive to the change in model parameters. The influences on mean sea level pressure over land surface were not high. A changes in mean sea level pressure in the order of ± 6 hPa compared to the control HIRHAM4 simulation were found in all sensitivity experiments. A small change in the surface net heat flux due to the model parameter change caused atmospheric stability change. The change in the atmospheric stability caused the change in the vertical mixing of heat and momentum and hence a change in atmospheric circulation. Therefore a change in mean sea level pressure during the sensitivity experiment compared to the control was expected. All sensitivity experiments failed to reduce the cold winter bias in soil temperature. Therefore, in the next step an advanced land surface model has been applied in the HIRHAM4 domain. The land surface model description and model results are described in the following chapter.

5 NCAR LSM (version 1.0) Land Surface Processes & results

5.1 Introduction

The National Center for Atmospheric Research (NCAR) Land Surface Model (LSM version 1.0), developed by *Bonan* (1996a) is used here to simulate the soil processes in the current HIRHAM4 model domain. The land surface model is a one-dimensional model of energy, momentum, water and CO_2 exchange between the atmosphere and the land. In contrast to HIRHAM4, LSM calculates soil moisture for each soil layers and takes into account the soil moisture freezing and thawing. Additionally wetlands are represented in LSM, which are important for the Arctic climate and not treated explicitly in HIRHAM4. Though the LSM's soil textures are assumed vertically uniform, the soil thermal properties (i.e. heat capacity and heat conductivity) are now variable according to its moisture content, texture and the physical state of the moisture. In a first step, atmospheric variables from HIRHAM4 are used to drive the LSM in each time step (30 minutes) and a 15 *years* simulation (1979 – 1993) has been performed with this *stand alone* setup. The required LSM input variables for each grid box are listed in the Table 5.1.

5.2 Model description

The land surface model uses complex and sophisticated vegetation and soil schemes. Plants are characterized by 12 types, depending on leaf and stem areas, root profile, height, leaf dimension, optical properties, stomatal physiology, roughness length, displacement height and biomass. There are 28 types of land cover (vegetation, glacier, desert, wetland) and each of them is described as a combination of maximum 3 plant types. The model soil colors are divided into 9 classes and each of these classes prescribes dry and saturated soil albedos for visible and near infrared bands. Each grid box in the domain prescribes fraction of wetland, fraction of lake, soil texture (percentage of sand, clay, silt) and land cover type. The seasonal variations of leaf and stem area, optical properties of plant types, snow and water are prescribed.

	Variable name	unit
1	reference height	m
2	temperature at reference height	K
3	zonal wind at reference height	$m\,s^{-1}$
4	meridional wind at reference height	$m\,s^{-1}$
5	specific humidity at reference height	$kg\,kg^{-1}$
6	pressure at reference height	Pa
7	surface pressure	Pa
8	convective precipitation	$mm\,H_2O\,s^{-1}$
9	large-scale precipitation	$mm\,H_2O\,s^{-1}$
10	partial pressure O_2 at reference height (0.209)	$mol\,mol^{-1}$
11	partial pressure CO_2 at reference height (355×10^{-6})	$mol\,mol^{-1}$
12	incident direct beam solar radiation $< 0.7\,\mu m$ SW $\downarrow^{\mu}_{vis}$	$W\,m^{-2}$
13	incident direct beam solar radiation $\geq 0.7\,\mu m$ SW $\downarrow^{\mu}_{nir}$	$W\,m^{-2}$
14	incident diffuse solar radiation $< 0.7\,\mu m$ SW $\downarrow_{vis}$	$W\,m^{-2}$
15	incident diffuse solar radiation $\geq 0.7\,\mu m$ SW $\downarrow_{nir}$	$W\,m^{-2}$
16	incident long wave radiation LW $\downarrow$	$W\,m^{-2}$

Table 5.1: The atmospheric input variables to the LSM.

5.3 Soil temperature

The model soil column of total depth 6.3 meter is divided into six layers with a thickness of 0.1, 0.2, 0.4, 0.8, 1.6 and 3,2 meter (shown in the Figure 5.1). The thermal properties of the soil are defined at the center of each soil layer. The heat conduction equation is solved using the Crank-Nicholson method. The boundary conditions of lower and upper soil layers are the same as in the HIRHAM4, i.e. zero heat flux at the bottom of deepest soil layer and a net atmospheric heat flux at the top of first soil layer.

The soil heat capacity and heat conductivity at each soil layer are calculated in each time step. During the phase transition of soil moisture, the latent heat of freezing/thawing is added to the heat capacity. Phase transition is assumed to take place within $T_f \pm 0.5$K (*Lunardini*, 1981), where $T_f = 273.16$K. So the soil heat capacity for the i^{th} layer is

$$c_i = \begin{cases} c_u & \text{for } T_i > T_f + \Delta T \\ \frac{c_f + c_u}{2} + \frac{L_i}{2\Delta T} & \text{for } T_f - \Delta T \leq T_i \leq T_f + \Delta T \\ c_f & \text{for } T_i < T_f - \Delta T\ , \end{cases}$$

where $\Delta T = 0.5\,\mathrm{K}$, c_f and c_u are frozen and unfrozen volumetric heat capacity respectively. Volumetric latent heat for the i^{th} layer is given by

$$L_i = W_i h_{fus} \rho_w, \tag{5.1}$$

$\Delta z_1 = 0.10\,m$	T_1, k_1, c_1
$\Delta z_2 = 0.20\,m$	T_2, k_2, c_2
$\Delta z_3 = 0.40\,m$	T_3, k_3, c_3
$\Delta z_4 = 0.80\,m$	T_4, k_4, c_4
$\Delta z_5 = 1.60\,m$	T_5, k_5, c_5
$\Delta z_6 = 3.20\,m$	T_6, k_6, c_6

Figure 5.1: Schematic diagram of LSM soil layers and soil profile. Temperature T_i, heat capacity c_i and conductivity k_i are defined at the center of each layer with thickness Δz_i.

where W_i is the volumetric water content of i^{th} soil layer, h_{fus} is the latent heat of fusion of water and ρ_w is the density of water. The frozen and unfrozen soil heat capacities depend on the soil water content and are expressed as

$$c_u = (1 - W_{sat})c_s + c_w W_i \quad \text{and} \tag{5.2}$$

$$c_f = (1 - W_{sat})c_s + c_I W_i, \tag{5.3}$$

where c_w ($4.188\times10^6\,\mathrm{J\,m^{-3}\,K^{-1}}$) and c_I ($4.188\times10^6\,\mathrm{J\,m^{-3}\,K^{-1}}$) are the volumetric heat capacity of water and ice respectively, c_s is the heat capacity of soil solids and W_{sat} is the saturation volumetric water content. For glacier and wetland, $W_i = W_{sat} = 1$, so that $c_u = c_w$ and $c_f = c_I$. Frozen and unfrozen thermal conductivity are parameterized using soil texture and soil moisture. For the temperature range $T_f \pm 0.5\,\mathrm{K}$, blending of frozen and unfrozen thermal conductivity as recommended by *Lunardini* (1981) is used

$$k_i = \begin{cases} k_u & \text{for } T_i > T_f + \Delta T \\ k_f + \frac{k_u - k_f}{2\Delta T}\left(T_i - T_f + \Delta T\right) & \text{for } T_f - \Delta T \le T_i \le T_f + \Delta T \\ k_f & \text{for } T_i < T_f - \Delta T\ , \end{cases}$$

with $\Delta T = 0.5\mathrm{K}$. The frozen k_f and unfrozen k_u thermal conductivities are calculated from *Farouki* (1981)

$$k_u = \left(k_s^{(1-W_{sat})} k_w^{W_i} - 0.15\right)\frac{W_i}{W_{sat}} + 0.15 \quad \text{and} \tag{5.4}$$

$$k_f = \left(k_s^{(1-W_{sat})} k_I^{W_i} - 0.15\right)\frac{W_i}{W_{sat}} + 0.15, \tag{5.5}$$

where k_I ($0.6\,\mathrm{W\,m^{-1}\,K^{-1}}$) and k_w ($2.2\,\mathrm{W\,m^{-1}\,K^{-1}}$) are the thermal conductivity of ice and water respectively, k_s is the thermal conductivity of solid soil. For glaciers and wetland, $W_i = W_{sat} = 1$, therefore $k_u = k_w$ and $k_f = k_I$. The heat capacity and thermal conductivity of solid soil depend on the soil textures only.

$$c_s = \left(\frac{2.128\,\%\mathrm{sand} + 2.385\,\%\mathrm{clay}}{\%\mathrm{sand} + \%\mathrm{clay}}\right) \times 10^6\ \mathrm{J\,m^{-3}\,K^{-1}}, \tag{5.6}$$

$$k_s = \left(\frac{8.80\,\%\mathrm{sand} + 2.92\,\%\mathrm{clay}}{\%\mathrm{sand} + \%\mathrm{clay}}\right). \tag{5.7}$$

In the presence of snow over ground surface, the LSM does not calculate heat flux through snow independently like in the HIRHAM4 but the thermal properties of first soil layer are blended with the snow thermal properties to create a snow-soil layer. The thermal conductivity and heat capacity of this snow-soil layer are given by

$$k_1 = \frac{k_{sn}\,k_i(i=1)(\Delta z_1 + S_n)}{k_{sn}\,\Delta z_1 + k_i(i=1)S_n} \quad \text{and} \tag{5.8}$$

$$c_1 = \frac{c_{sn}\,c_i(i=1)(\Delta z_1 + S_n)}{c_{sn}\,\Delta z_1 + c_i(i=1)S_n}, \tag{5.9}$$

where S_n is the snow depth, k_{sn} ($0.34\,\mathrm{W\,m^{-1}}$) and $k_i(i=1)$ are the heat conductivity of snow and first soil layer respectively, c_{sn} ($0.525\times10^6\,\mathrm{J\,m^{-3}\,K^{-1}}$) and $c_i(i=1)$ are the heat capacity of snow and first soil layer respectively.

5.4 Soil hydrology

The volumetric soil moisture is described at each of the LSM soil layers. The LSM parameterizes interception, throughfall, snow accumulation, infiltration, surface runoff, subsurface drainage and redistribution of moisture within the soil column. For the non-irrigated soil, the water budget equation is

$$\Delta W_{can} + \Delta W_{sn} + \sum_i \Delta W_i \Delta z_i = \left(P_{prl} + P_{prc} - E_v - E_g - R_R - q_{drai}\right)\Delta t, \tag{5.10}$$

where

ΔW_{can}	canopy water,
ΔW_{sn}	snow water equivalent,
$\sum_i \Delta W_i \Delta z_i$	total soil water content,
P_{prl}	large scale precipitation,
P_{prc}	convective precipitation,
E_v	vegetation evaporation,
E_g	ground evaporation,
R_R	surface runoff and
q_{drai}	sub-surface drainage.

Here, all fluxes directed upwards (in the direction away from the Earth's center) are considered positive (it is just opposite as in HIRHAM4 where all fluxes directed towards the Earth's center are positive). The canopy water is a mass balance determined by gain from interception (intercepted precipitation by leaf and steam), dew and loss from evaporation. After interception, precipitation falls to the ground as rain if the atmospheric temperature $T_{atm} > 2.2\,°\mathrm{C}$ or as snow if $T_{atm} \leq 2.2\,°\mathrm{C}$. The snow mass balance is determined by the flux of snow at the surface, surface dew and losses from snow melt and sublimation. A fixed snow density ($\rho_{sn} = 250\,kg\,m^{-3}$) is used to calculate the snow depth and if the snow depth $S_n \geq 5\,cm$, then ground is 100% covered by the snow. Ground evaporation is partitioned into soil evaporation and surface dew. Vegetation evaporation is partitioned into canopy evaporation, transpiration and canopy dew. Water at the ground surface either infiltrates into the soil or losses as surface runoff depending on water content within the first soil layer relative to the saturation level.

5.4.1 Soil water

Soil water is calculated from the conservation equation

$$\frac{\Delta W \Delta z}{\Delta t} = -q_i + q_o - e, \tag{5.11}$$

where

W is the volumetric soil water content ($\mathrm{mm^3\,mm^{-3}}$),
q_i water flux into the soil ($\mathrm{mm\,s^{-1}}$),
q_o water flux out of the soil ($\mathrm{mm\,s^{-1}}$),
e evapotranspiration from soil ($\mathrm{mm\,s^{-1}}$),
Δt time step in seconds.

The vertical water flow in an unsaturated porous media is described by the Darcy's law

$$q = -k\left(\frac{\partial(\psi + z)}{\partial z}\right) = -k\left(\frac{\partial \psi}{\partial z} + 1\right) = -k\left(\frac{\partial W}{\partial z}\frac{\partial \psi}{\partial W} + 1\right), \tag{5.12}$$

where

k hydraulic conductivity of soil and
ψ soil matrix potential.

The hydraulic conductivity and soil matrix potential vary with soil moisture and soil texture based on work of *Clapp and Hornberger* (1978) and *Cosby et al.* (1984). The hydraulic conductivity and soil matrix potential for the i^{th} layer are

$$k_i = k_{sat}\, s_i^{2b+3}, \tag{5.13}$$
$$\psi_i = \psi_{sat}\, s_i^{-b}, \tag{5.14}$$

where $s_i = \frac{W_i}{W_{sat}}$, k_{sat} and ψ_{sat} are the soil hydraulic conductivity and matrix potential respectively at saturation. k_{sat}, ψ_{sat} and b are empirically related to $\%sand$ and $\%clay$

$$k_{sat} = 0.0070556 \times 10^{-0.884+0.0153(\%sand)}, \quad (5.15)$$
$$\psi_{sat} = -10.0 \times 10^{1.88-0.0131(\%sand)}, \quad (5.16)$$
$$W_{sat} = 0.489 - 0.00126(\%sand), \quad (5.17)$$
$$b = 2.91 + 0.159(\%clay). \quad (5.18)$$

Setting $e = 0$ in equation 5.11 , $\frac{\Delta W}{\Delta t} = -\left(\frac{q_i - q_o}{\Delta z}\right)$, i.e. $\frac{\partial W}{\partial t} = -\frac{\partial q}{\partial z}$ and using equation 5.12 takes the form of Richards equation

$$\frac{\partial W}{\partial t} = \frac{\partial}{\partial z}\Big[k\Big(\frac{\partial W}{\partial z}\frac{\partial \psi}{\partial W} + 1\Big)\Big]. \quad (5.19)$$

The upper and lower boundary conditions are the influx of water into soil (q_{infl}) and the gravitational drainage ($q_{drai} = k$) respectively. Using these two boundary conditions and including the evapotranspiration term, soil water is calculated for six layers. For irrigated crop, soil layers to a depth of $1\,m$ are kept saturated during the growing season and the soil water is conserved only for non-irrigated soils

$$\sum_i \Delta W_i \Delta z_i = (q_{infl} - e - q_{drai})\Delta t. \quad (5.20)$$

5.5 Stand alone LSM

The main objective of this setup was to validate the LSM soil processes in the Arctic region, driven by validated HIRHAM4 atmospheric variables. A 15 years (1979-1993) LSM simulation was performed by using arbitrary initializations of the soil variables (*snow water equivalent, intercepted water, vegetation temperature, ground temperature, soil moisture and soil temperature*). It was investigated (not shown here) that 10 years spin up time was enough for the LSM and also suggested by *Dickinson et al.* (1993). The last 5 years (1989-1993) monthly climatology mean January soil variables are used to initialized the LSM. Using this initialization another 15 years (1979-1993) simulation has been performed and analyzed.

5.5.1 Surface and input data

The LSM grid was exactly the same as for the HIRHAM4. At the center of each grid box, latitude and longitude were provided for calculating solar zenith angle. Land cover data (vegetation types) were from USGS (version 1.2). Sand, silt and clay data were from *Webb et al.* (1993) 1.0 °by 1.0 °data. Inland data were from *Cogley* (1991) 1.0 °by 1.0 °data for perennial freshwater lakes and swamps/marshes.

Lakes are assumed of $50\,m$ depth. Soil colors were taken from BATS T42 data set (*Dickinson et al.*, 1993).

The LSM driving atmospheric variables are listed in the Table 5.1. In the standard HIRHAM4 version, the incident solar radiations are calculated in two spectral bands ($0.28 - 0.68$ *and* $0.68 - 4.0\,\mu m$). However the HIRHAM4 final output of incident solar radiation is the sum of above two components. The incident solar radiation can be divided into direct and diffuse components. The solar radiation that directly reaches to the Earth surface is called direct solar radiation and the radiation that scatters out of direct beam and reaches to the Earth surface is called diffuse short wave radiation. A ratio of total incident diffuse solar radiation to the total incident solar radiation is called *diffuse ratio*. For the clear sky condition the diffuse ratio is mainly determined by the solar angle, since the effect of atmospheric water vapor, aerosol are small. During noon, the clear sky diffuse ratio is about $10 - 15\%$ and increases to 100% before sunset. The formula for the clear sky diffuse ratio given by *Goudriaan* (1977) is

$$r_d = \frac{5}{\beta} + \frac{exp(\frac{\beta}{60})}{100}, \tag{5.21}$$

where β is the solar angle in degree. *Roesch* (2000) found that the above formula agrees quite well with the observations for solar angles above $10\,°$. However for the cloudy sky the description of diffuse ratio is quite complex. The following assumptions are made for calculating the diffuse ratio in the presence of cloud (personal communication with A. C. Roesch).

When the model grid box fractional cloud cover reaches 1.0, then the diffuse ratio is assumed to be 1. Otherwise for the solar angle greater than $5\,°$and for the fractional cloud cover, the diffuse ratio is

$$r_{dcloud} = r_d(1 - c_f) + c_f, \tag{5.22}$$

where c_f is the fractional cloud cover ($0.0 \leq c_f \leq 1.0$). Within the model the diffuse ratio is calculated and saved as an output. Using this diffuse ratio, the incident solar radiation in two spectral bands (i.e. visible ($0.28 - 0.68\,\mu m$) and near infrared ($0.68 - 4.0\,\mu m$)) are split into direct and diffuse components.

$$I_d^{VIS} = r_{dcloud} \cdot I_{tot}^{VIS}, \tag{5.23}$$

$$I_{di}^{VIS} = I_{tot}^{VIS} - I_d^{VIS}, \tag{5.24}$$

$$I_d^{NIR} = r_{dcloud} \cdot I_{tot}^{NIR}, \tag{5.25}$$

$$I_{di}^{NIR} = I_{tot}^{NIR} - I_d^{NIR}, \tag{5.26}$$

where I_d^{VIS}, I_{di}^{VIS} are the incident diffuse and direct visible solar radiations respectively, I_d^{NIR}, I_{di}^{NIR} are the diffuse and direct near infrared solar radiations respectively and I_{tot}^{VIS}, I_{tot}^{NIR} are the total visible and near infrared incident solar radiations respectively.

5.6 Results and discussions

As earlier done with HIRHAM4, the stand alone LSM soil temperatures are linearly interpolated to 10, 20, 40, 80, 160 and 320 *cm* depths. The monthly climatology mean winter (DJF) and summer (JJA) averaged soil temperatures at 10 *cm* depth for HIRHAM4, LSM and the differences among these two models are shown in Figure 5.2. During winter, the large scale soil temperature patterns in the LSM are similar to the HIRHAM4 but the LSM shows a warming over the whole domain in the order of about 5 °C. In Scandinavia, West Siberia, part of North Canada, Alaska and Greenland, the LSM shows a warming. It has been shown in section 3.1 that, the HIRHAM4 has a strong winter cold bias in the East Siberian part and now the LSM indicates a slight reduction of that cold bias. During summer, the large scale patterns have not changed in the LSM except at the wetland regions, where it shows a strong cooling compared to the HIRHAM4. Since LSM does treat wetlands explicitly, these regions become colder during summer due to the release of latent heat of moisture evaporation. Over Greenland, the LSM is warmer compared to the HIRHAM4 by about 4 °C. The prescribed thermal and optical properties of glaciers in the two models are different. These differences are the reason for the temperature difference between the two models over glaciers.

The winter soil warming is partly attributed to the SWE increase in the LSM due to the different hydrology schemes. Figure 5.3 shows the winter (DJF) monthly climatology mean (1979-1993) LSM and HIRHAM4 snow water equivalent and their difference. The LSM maximum and minimum SWE spatial patterns are similar to HIRHAM4, since LSM is driven by the HIRHAM4 total (large scale plus convective) precipitation. However, LSM has more SWE in Scandinavia, West Russia, part of the Eastern Siberia and mountain ranges of Alaska by about 5 *cm*. The LSM soil temperature scheme is partly different from HIRHAM4 and may contribute to this warming. In the presence of snow, LSM blends the thermal properties of the first soil layer with the snow thermal properties. The latent heat of freezing/thawing is added to the heat capacity of soil. Therefore, the soil cooling during winter at around 0 °C will be a very slow process depending on the soil moisture content. A calculation shows that 1 *g* of soil with 20% moisture content will release heat energy of about 70 J due to the phase transition of soil moisture. That amount of heat can warm up 1 *g* of rock by about 40 °C. The active soil layer with seasonal changes e.g. freezing during winter and thawing during summer, has a big potential in terms of heat energy absorbed or released during the phase transition.

The deeper LSM soil layers also show the winter warming in most land part compared to HIRHAM4. Figure 5.4 shows the summer (JJA) and winter (DJF) monthly climatology mean LSM and HIRHAM4 soil temperatures and their differences at 320 *cm* depth in °C. During winter, the LSM soil is warmer in most of the

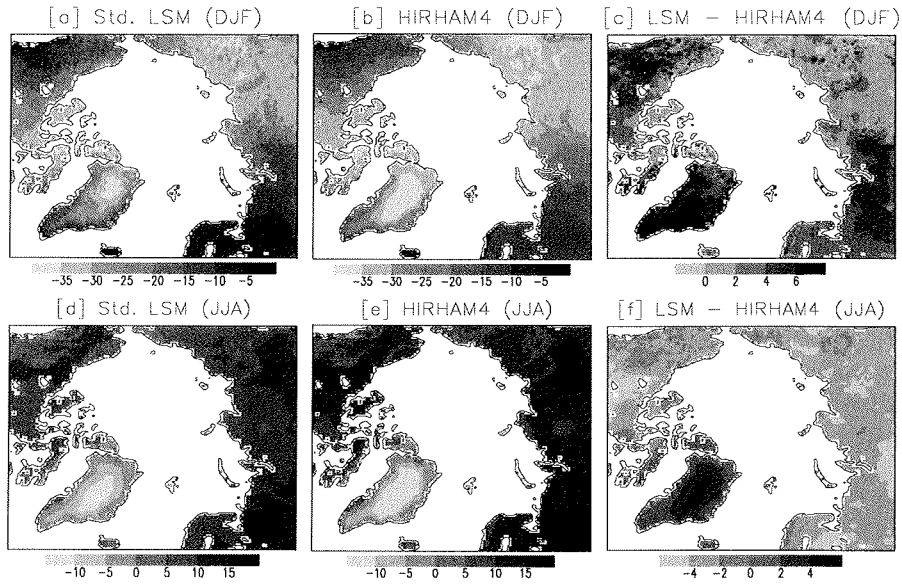

Figure 5.2: 10 cm soil temperature in °C, [a] is the stand alone LSM winter (DJF) monthly climatology mean (1979-1993), [b] is the same as [a] but for HIRHAM4, [c] is the LSM run minus HIRHAM4 winter monthly climatology mean soil temperature. The lower panels i.e. [d], [e], [f] are same as in the upper panels but for the summer (JJA) months.

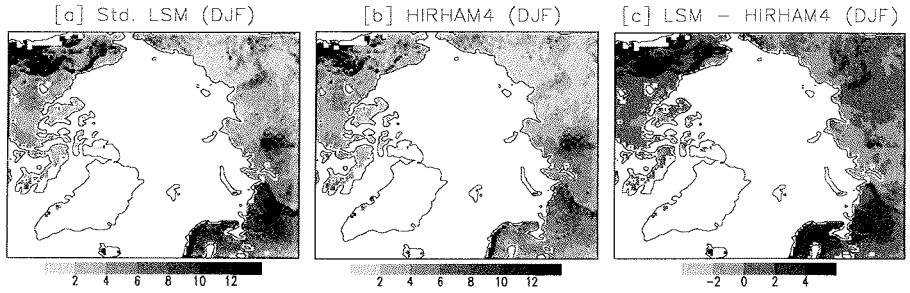

Figure 5.3: [a] is the winter (DJF) monthly climatology mean LSM snow water equivalent (SWE) in centimeter, [b] is the same as in [a] but for HIRHAM4, [c] is the LSM run minus HIRHAM4 snow water equivalent.

land parts compared to HIRHAM4 by about 10 °C and hence reducing the cold winter bias. However during summer it shows a mixed behavior, cooling and warming both in the order of about 6 °C. The spatial warming patterns at 320 *cm* depth are

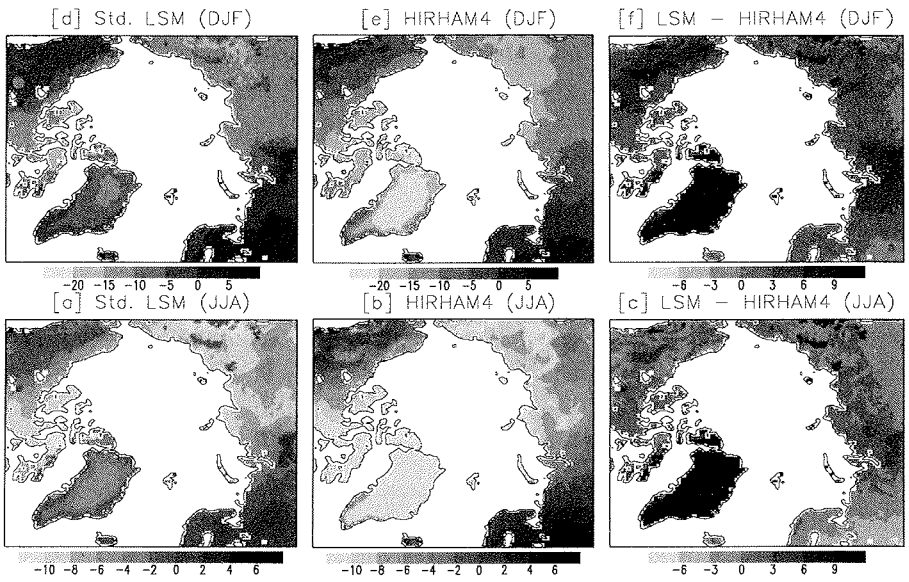

Figure 5.4: 320 cm soil temperature in °C, [a] is the stand alone LSM winter (DJF) monthly climatology mean (1979-1993), [b] is the same as [a] but for HIRHAM4, [c] is the LSM run minus HIRHAM4 winter monthly climatology mean soil temperature. The lower panels i.e. [d], [e], [f] are same as in the upper panels but for the summer(JJA) months.

quite similar to the patterns at 10 *cm* depth, but the magnitude has been reduced at the deeper layer. Due to the time lag between successive soil layer's heat flow, the deeper soil temperature maximum and minimum will not coincide with the top soil layer. Therefore at 320 *cm* depth, the winter and summer soil temperatures may not represent the minimum and maximum values respectively.

Figure 5.5 shows the station averaged monthly climatology mean (1979-1990) soil temperatures at 5 different depths from West Russian (WR) station measurements, HIRHAM4 simulation and stand alone LSM simulation. Clearly, the LSM shows improvement in the soil temperature compared to the HIRHAM4 during winter. At 20 *cm* depth, the LSM soil has been warmed up compared to the HIRHAM4 by a maximum of 5 °C, whereas the same has been cooled down by a maximum of 5 °C during summer. The summer cooling in LSM soil is partly due to the latent heat of soil moisture thawing. The HIRHAM4 soil can warm up immediately after snow melt and becomes warmer but LSM needs extra heat energy to melt the frozen soil. However the HIRHAM4 results are close to the observed summer soil temperature but it may be due to the wrong reasons.

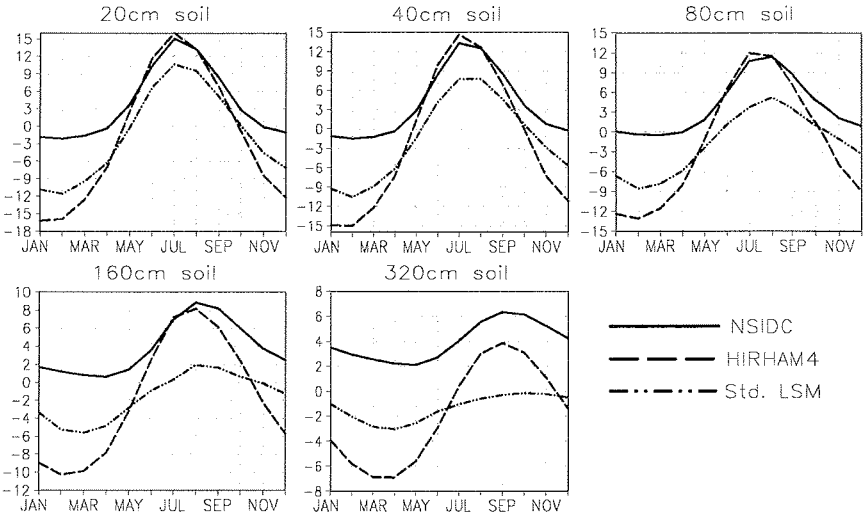

Figure 5.5: West Russian (WR) station averaged monthly climatology mean (1979-1990) soil temperatures in °C at 5 different depths. The solid lines are from observations, archived from NSIDC, the dot-dashed lines are from stand alone LSM and the dashed lines are from HIRHAM4.

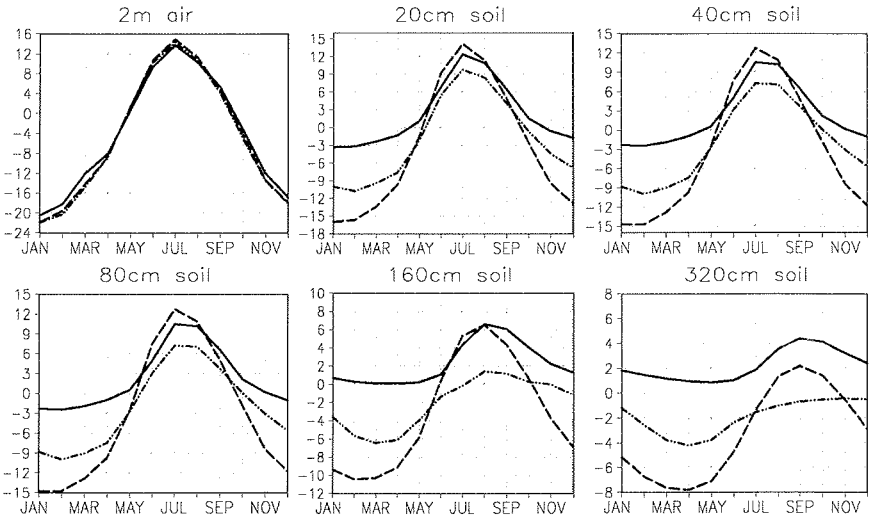

Figure 5.6: West Russian (WRII) station averaged monthly climatology mean (1979-1993) $2m$ air and soil temperatures in °C at 5 different depths. The solid lines are from observations, the dot-dashed lines are from stand alone LSM and the dashed lines are from HIRHAM4.

The West Russian (WRII) station averaged observed and the LSM simulated 2 m air and soil temperatures at 5 different depths are shown in Figure 5.6. Here the $2m$ air temperature of LSM is very close to the observations. However the winter improvements and summer biases in the LSM soil temperatures compared to these observations are very similar to the comparison at West Russian (WR) stations (Figure 5.5). The LSM has reduced the winter cold bias compared to HIRHAM4 but still remains a winter cold bias of about 6 °C compared to both observed data sets (WR, WRII).

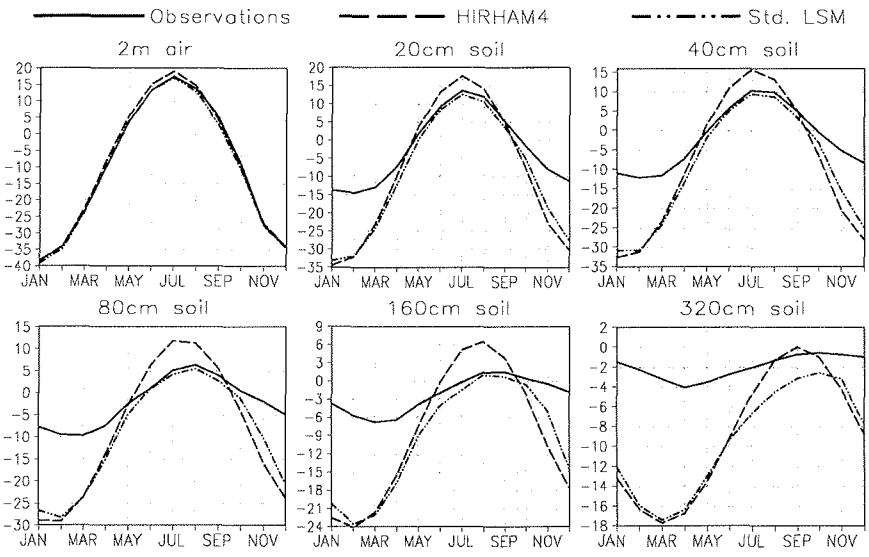

Figure 5.7: East Siberian (ES) stations averaged monthly climatology mean (1979-1993) 2m air and soil temperatures in °C at 5 different depths. The solid lines are from observations, the dot-dashed lines are from LSM and dashed lines are from HIRHAM4.

The cloud radiative forcing is very important for the Arctic surface energy budget. It plays a role in the surface energy budget in two opposite ways: the cloud radiates LW back to the Earth surface and reflects SW back to the space. However there are large differences in the cloud parametrization among different GCMs (*Tao et al.*, 1996; *Chen et al.*, 1995). An increase in the net surface radiative flux may reduce the present LSM soil temperature bias. It has been shown in section 3.1, that HIRHAM4 has large SWE deficiency everywhere in the domain. Therefore an increased snow depth (due to increased precipitation) also could increase the winter soil temperature.

The LSM soil temperatures were also compared with the East Siberian (ES) observed data set and are shown in Figure 5.7. An average over all 31 stations monthly

climatology mean for the years 1979-1993 is used here. The LSM $2\,m$ air temperature has a good agreement with this observations. It has especially improved during summer compared to HIRHAM4. The soil temperatures during summer at 20, 40, 80 and 160 cm depth have been improved considerably compared to the HIRHAM4 simulation and the values are very close to the observations. The winter soil temperature simulations are slightly improved compared to HIRHAM4. It has been shown in the section 3.1 that in Siberia, HIRHAM4 largely underestimates winter precipitation everywhere and summer precipitation except at the mountain ranges. Therefore the lack of soil moisture and snow over ground also may accelerate the winter soil cooling. The snow water equivalent for these stations are compared with HIRHAM4 in section 3.6 and showed large differences. The HIRHAM4 underestimates SWE by about $6\,cm\,month^{-1}$ during winter months. The LSM shows slightly higher SWE (Figure 5.8) compared to the HIRHAM4 runs, due to different hydrological schemes.

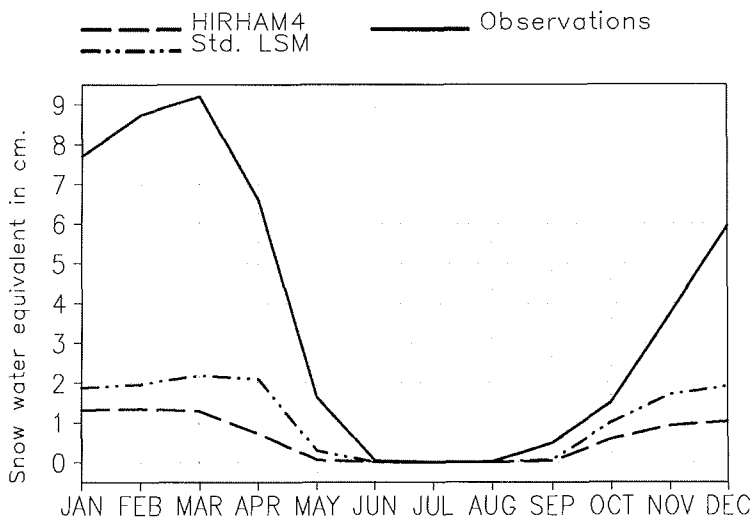

Figure 5.8: East Siberian (ES) stations averaged snow water equivalent (SWE) in cm. The solid lines are from observations, the dot-dashed lines are from LSM and dashed lines are from HIRHAM4.

The domain averaged (except 10 grid points at the boundary, glacier part) monthly climatology mean vertical soil temperatures from stand alone LSM, HIRHAM4 and the difference between these two models are shown in Figure 5.9. The stand alone version of LSM shows a seasonal cycle in soil temperature which is very similar to the HIRHAM4. The LSM soil is warmer than the HIRHAM4 by a maximum of 3 °C during winter, whereas the same is colder by a maximum of 4 °C during

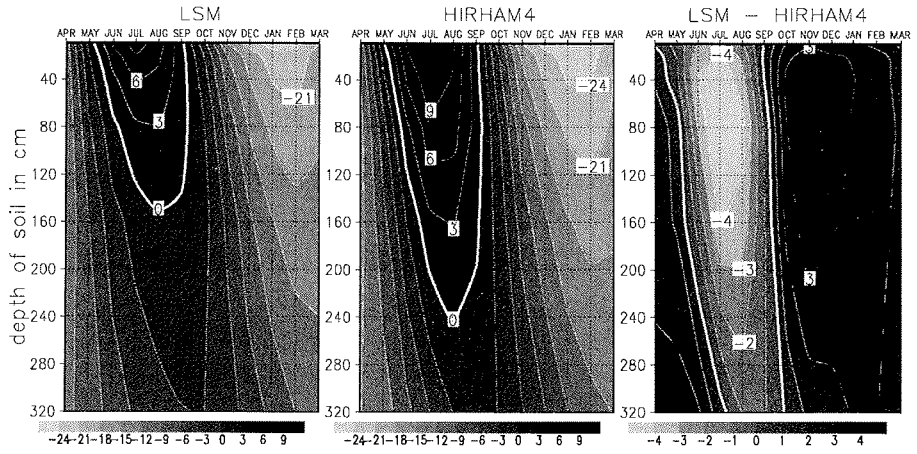

Figure 5.9: Monthly climatology mean (1979-1993) domain averaged (except 10 grid points at the boundary and glacier part) stand alone LSM run and HIRHAM4 vertical soil temperatures profile and their difference in °C.

summer. Winter soil warming in LSM starts from September and stays warmer up to April. The thermal inertia of soil in LSM is supposed to be larger compared to HIRHAM4. Therefore the penetration depth of colder soil temperature during winter and warmer soil temperature during summer have been reduced in LSM compared to HIRHAM4. The 0 °C temperature contour has a deeper extent in the HIRHAM4 compared to the LSM. Similarly during winter the -21 °C contour in the HIRHAM4 soil has deeper extent compared to the LSM.

The monthly climatology mean volumetric soil moisture content (in $mm^3\,mm^{-3}$) at the 6 LSM soil layers are shown in Figure 5.10. The volumetric moisture content of $1\,mm^3\,mm^{-3}$ indicates the saturation level. The glacier part and the wet-land regions are representing the regions with maximum moisture content. The West Russian (WR, WRII) regions, where LSM showed large improvement in winter soil temperature, contain large amount of soil moisture. The East Siberia (ES) region has a relatively small amount of soil moisture for the whole year. The first soil layer shows that it is dryer during summer compared to the winter. Also the first soil layer is dryer compared to the deeper soil layers. A large amount of ground evaporation takes place during summer through evapotranspiration by vegetation and by the direct evaporation from ground surface to the atmosphere. Therefore, the relatively dry first soil layer during summer seems to be realistic.

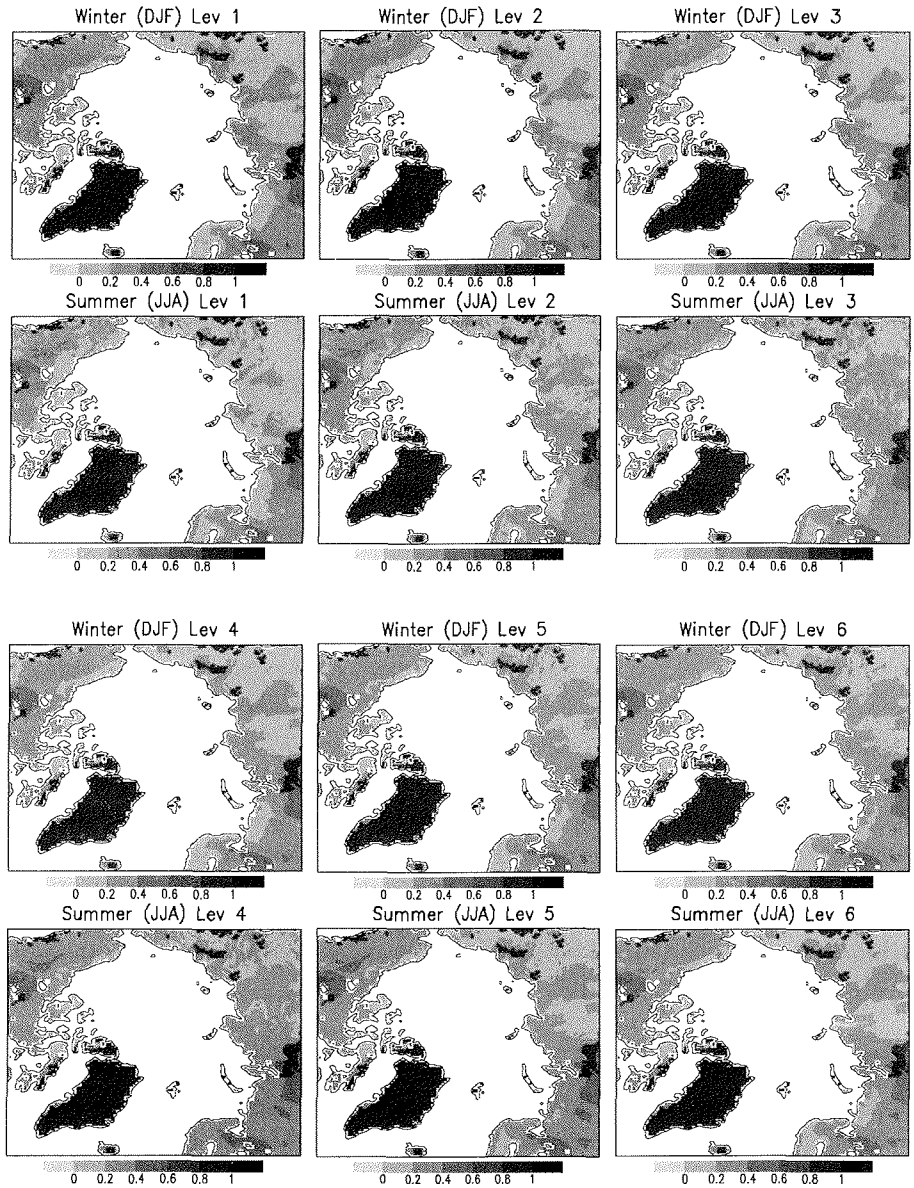

Figure 5.10: Monthly climatology mean (1979-93) summer (JJA) and winter (DJF) averaged volumetric moisture content (in $mm^3\,mm^{-3}$) of 6 soil layers in the stand alone LSM. Here Lev 1, ...,Lev 6 are indicating the soil layers 1,...,6 respectively.

5.7 Summary

The new land surface model has improved the winter soil temperature everywhere in the domain compared to the HIRHAM4 and reduced the cold winter bias. At 10 cm depth during winter, the LSM was warmer by a maximum of 5 °C compared to HIRHAM4. At 320 cm depth, the winter cooling reduced by a maximum of 10 °C. At the East Siberian (ES) stations, the LSM was not able to improve the winter cold bias in soil temperature. There was also an increase in SWE which is believed to be largely underestimated by the HIRHAM4. At the East Siberian (ES) stations, LSM soil temperatures were very similar to the HIRHAM4. The reasons, why LSM improved the winter soil temperature at the West Russian stations and not at the East Siberian stations can be summaries as following:

1) During winter there was a relatively large amount of snow at West Russian stations compared to the East Siberian stations. Therefore the insulation by the snow during winter could prevent the ground heat loss to the colder atmosphere. Missing insulation of snow is responsible for cold winter bias.

2) There were a large amount of soil moisture content at West Russian stations compared to the East Siberian stations. Since the HIRHAM4 does not have soil moisture freezing and thawing schemes, the soil became quickly colder during winter. In LSM, around 0 °C the soil moisture was allowed to freeze first and only after that soil temperature starts to fall down further. A similar process was involved during spring time, when soil starts to warm up and melting of soil moisture takes place. Therefore, the heat release due to the soil moisture freezing process during winter was able to reduce the amplitude of winter soil temperature.

Concluding, the soil processes in LSM are more realistic compared to HIRHAM4 soil processes. In the stand alone version of LSM, the model got the driving fields from the HIRHAM4 but the improved processes could not influence the HIRHAM4 results. Improved land-surface processes in the HIRHAM4 may influence the HIRHAM4 climate regionally and perhaps at the large scale. Also the feedback processes between land-surface and the atmosphere will be addressed in a more realistic way. So we decided to couple the LSM with the atmospheric model HIRHAM4 to improve the present interaction between the land-surface and the atmosphere. A detailed description of the LSM coupling with HIRHAM4 will be given in the next chapter.

6 Coupling of HIRHAM4 & LSM

6.1 Introduction

The land-surface is known to be an important part of the climate model. It controls the surface radiative heat budget, which partly depends on the optical properties of the land cover (i.e. emissivity, reflectivity). Partitioning of the surface available energy into sensible and latent heat, available water into evaporation and runoff are also performed by the land-surface. There exist nonlinear feedback processes between the land-surface and the atmosphere. Large scale or regional scale changes in the key land-surface characteristics (albedo, soil temperature, moisture etc.) can lead to a change in the regional or even large scale atmospheric part of the climate and vice versa. Figure 6.1 shows the complex nature of positive and negative feedback loops between different components of land and atmosphere. The land-surface characteristics like albedo and soil moisture are formulated by very complex biological, chemical and physical processes of vegetation, soil type, snow and other components of the land-surface. Therefore, a two-way interaction between a complex land surface model and an atmospheric model will address the real feedback processes. The soil and vegetation scheme of the NCAR LSM should respond differently compared to the current HIRHAM4 soil and vegetation scheme under the same atmospheric forcing. Until now we used a one-way coupling between the atmospheric model HIRHAM4 and the complex land-surface model LSM. In each time step of LSM, it was forced by the HIRHAM4 output atmospheric variables but the output of LSM was not given back to the HIRHAM4. In this chapter, the interactive two-way coupling between HIRHAM4 and LSM is described.

6.2 Coupling technique

The strategy of the coupling was not to remove the land-surface processes completely in HIRHAM4 but to update some of the key surface variables in it by LSM output in each time step. The main objective was to reduce the cold biases in winter soil temperature using the advanced LSM soil scheme in a coupled way. In the coupled model, soil moisture, skin moisture, surface temperature and snow water equivalent are updated in HIRHAM4 by the LSM output in every time step. A schematic diagram of this coupling is shown in Figure 6.2. The surface energy budget of the HIRHAM4 is expected to change due to the coupling with the LSM. An update of the surface latent and sensible heat fluxes in HIRHAM4 by LSM fluxes was avoided because this was the first step towards an adaption of the advanced soil-vegetation scheme into HIRHAM4 in a consistent way. The first priority was to improve the soil

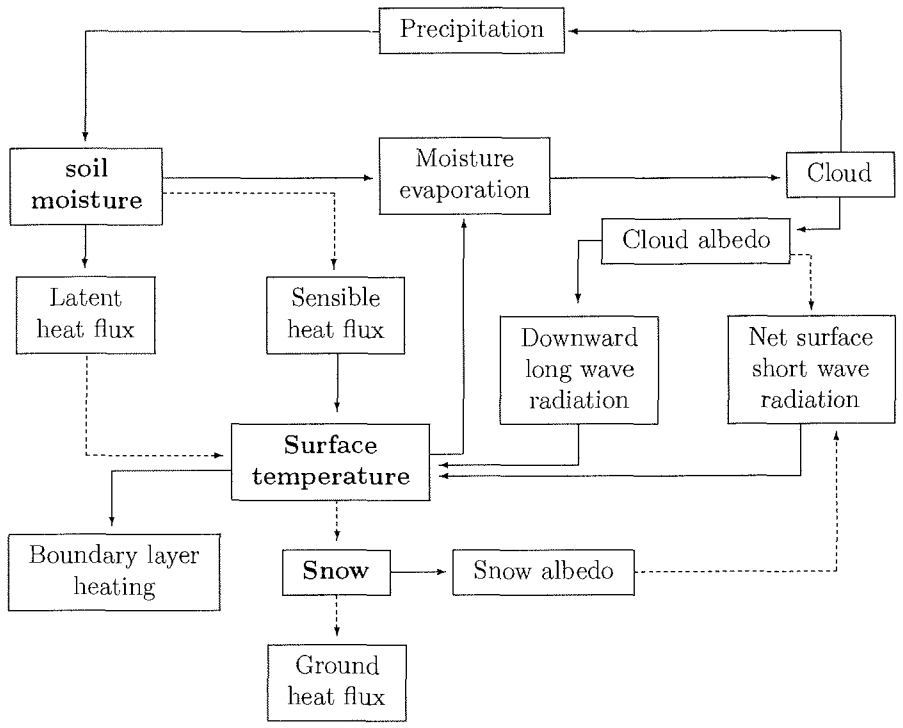

Figure 6.1: Feedback loop. Solid and dashed lines are describing positive and negative feedbacks respectively. If the direction of change in output signal is the same as the direction of change in input signal, then the feedback is called positive. Otherwise it is called a negative feedback.

temperature simulation without changing the PBL scheme and fluxes associated with it. Hereafter the model HIRHAM4 coupled with the NCAR LSM will be referred as HIR-LSM.

The HIRHAM4 soil moisture calculation is based on a bucket model (*Dümenil and Todini*, 1992) and the available soil moisture controls the ground evaporation, which later is used for the cloud water formulation. On the other hand in LSM, the soil moisture is described at each layer and the moisture holding capacity of each layer is explicitly determined by the soil texture. In contrast to HIRHAM4, the LSM moisture infiltration is calculated in a realistic way. Each layer has its own hydraulic properties and the soil moisture infiltrates through the next deeper layer. Wet-lands are not treated explicitly in HIRHAM4 but are present in LSM with its saturation soil moisture level. Therefore the spatial distribution of the soil moisture was very different from HIRHAM4. The priority was set to force HIRHAM4 by a comparable magnitude of LSM soil moisture. A sum of the first 3 LSM soil layer moisture

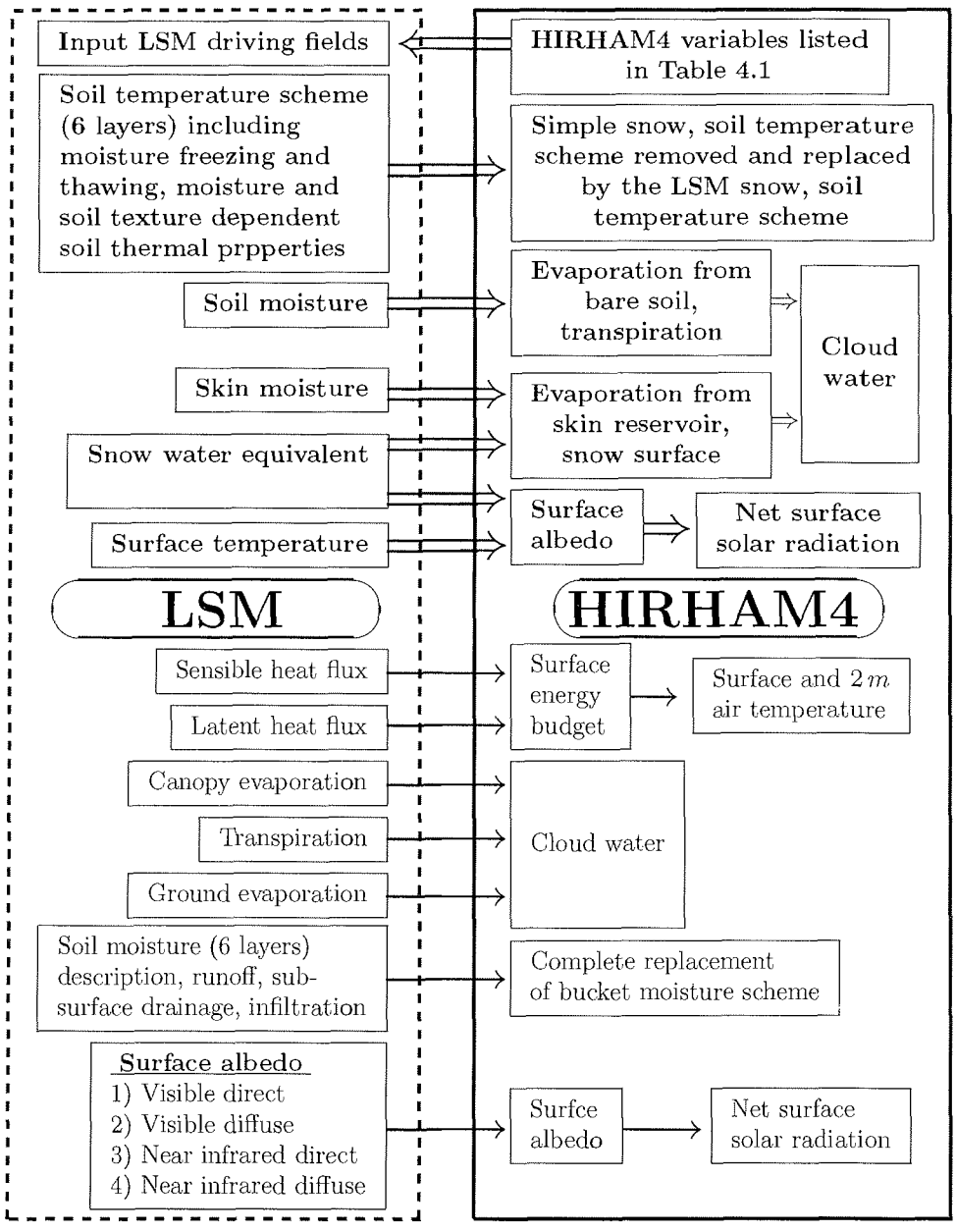

Figure 6.2: Schematic diagram of the coupling between the atmospheric model HIRHAM4 and the land surface model. Bold text within boxes and thick arrows indicate the present coupling. Thin text within boxes and thin arrows indicate possible future coupling options.

content was found very close to the present HIRHAM4 soil moisture content. The domain average of HIRHAM4 soil water content was 17 to 19 cm through out the year, whereas for the first 3 and first 4 LSM soil layers, the moisture content was 19 to 22 cm and 41 to 46 cm, respectively. The presence of wet-lands in the LSM showed a higher soil moisture content on the basis of the domain area average. A part of precipitation (rain or snow fall) is captured by the vegetation depending on the capacity of the skin reservoir and the rest of the precipitation falls on the ground surface. This skin reservoir also contributes to the land surface moisture evaporation and hence to the cloud water.

Ground/snow surface temperature acts as an interface between the atmosphere and the land-surface. The existence of snow, the long wave upward radiation and the surface albedo parametrization depend on the surface temperature. The surface temperature is also closely connected to the vegetation and soil schemes. Since there is no description of moisture at each soil layer in the HIRHAM4, it is difficult to calculate the active layer temperature in the Arctic. Melting or freezing of soil moisture accounts for a large part of surface heat budget during the seasonal transition period. Therefore, a large winter cold bias in the HIRHAM4 soil is expected. The amplitude of seasonal temperature swing from positive to negative in the active layer or vice versa is largely determined by the presence of moisture in it. An increase in soil moisture in the active layer of a region makes the layer relatively colder during summer and relatively warmer during winter. Therefore such an advanced soil scheme will also influence the temperature on its top of the surface, i.e. the surface temperature.

The snow amount determines the surface short wave radiation and long wave radiation due to its high albedo and emissivity respectively. Thick snow over ground prevents the excess cooling of the soil to the colder atmosphere, which acts as a blanket over ground. The amount of snow does not only depend on the amount of winter precipitation but also on the vegetation type. For example, a region with Arctic shrub type of vegetation can have more snow than the bare ground. HIRHAM4 underestimates snow in most of the Arctic region whereas LSM, driven by HIRHAM4 output (precipitation etc.) showed an increase in snow. Therefore the snow update in HIRHAM4 from LSM will improve the HIR-LSM snow albedo scheme.

6.3 Results and discussions

Figure 6.3 shows the HIR-LSM *minus* HIRHAM4, monthly climatology mean of summer (JJA) and winter (DJF) averaged $2m$ air temperature. The influence of LSM is clearly seen on the land parts of the HIR-LSM model. The ocean parts show only minor change. During summer, the coastal part of East and West Russia have been cooled down in the HIR-LSM model compared to the HIRHAM4 by a maximum of 5 °C. The other parts of the domain, except Greenland, show a moderate cooling of about 1 to 2 °C. Different ice thermal conductivity, emissivity and albedo schemes are used in HIRHAM4 and LSM (in HIRHAM4 ice thermal conductivity $k_i = 2.508\,\mathrm{W\,m^{-1}\,K^{-1}}$, volumetric heat capacity $c_i = 2.09 \times 10^6\,\mathrm{J\,m^{-3}\,K^{-1}}$,

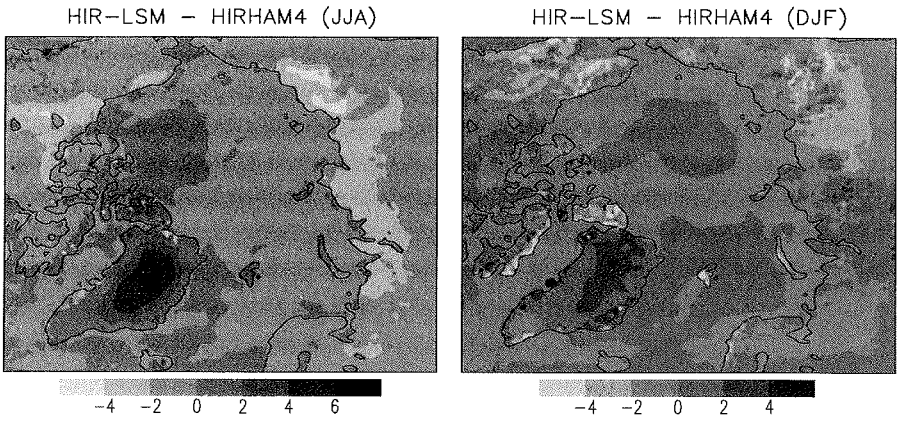

Figure 6.3: Monthly climatology (1979-1993) summer (JJA) and winter (DJF) averaged HIR-LSM *minus* HIRHAM4 2m air temperature. Positive values indicate the warming in HIR-LSM model whereas negative values indicate the cooling in the HIR-LSM model.

emissivity $\epsilon = 0.996$; in LSM $k_i = 2.2\,\mathrm{W\,m^{-1}\,k^{-1}}$, $c_i = 2.094 \times 10^6\,\mathrm{J\,m^{-3}\,K^{-1}}$, $\epsilon = 0.97$). Also for glacier, the LSM albedo for direct and diffuse solar radiation are fixed to 0.80 and 0.55 respectively, whereas for HIRHAM4, the albedo is a function of surface temperature (section 2.3.5). As a combined effect of the above described differences, the LSM air temperature became warmer compared to the HIRHAM4 air temperature over the Greenland area.

It has been shown in the section 5.6 that during summer, the soil temperature at $10\,cm$ depth was colder in stand alone LSM compared to the HIRHAM4. Therefore in the HIR-LSM model, the $2\,m$ air temperature has the same trend as in the stand alone version of LSM.

The HIR-LSM model shows a winter warming of 1 to 2 °C in the parts of North Canada, West Russia and Scandinavia. A winter cooling of maximum 4 °C can be seen over Alaska and East Siberia. Over Greenland, the warming is not very high compared to the summer time. During winter, the Arctic does not get much solar radiation and hence the albedo seems not to be important in this season. But, different albedo schemes might be largely responsible for the summer $2\,m$ air temperature increase over Greenland. The winter warming signal in the $2\,m$ air temperature is not so strong as seen in the stand alone soil temperature. This is probably because of the unchanged sensible, latent and radiative heat flux schemes in the HIR-LSM model. However in the HIR-LSM model, the LSM surface temperature and snow water equivalent influence the HIRHAM4 albedo and hence indirectly the solar net radiation at the surface of the model HIR-LSM.

Since the direct exchange of surface sensible and latent heat fluxes were not introduced during the coupling, the soil is expected to evolve in a similar way as in the stand alone version of LSM. Figure 6.4 shows the monthly climatology mean summer

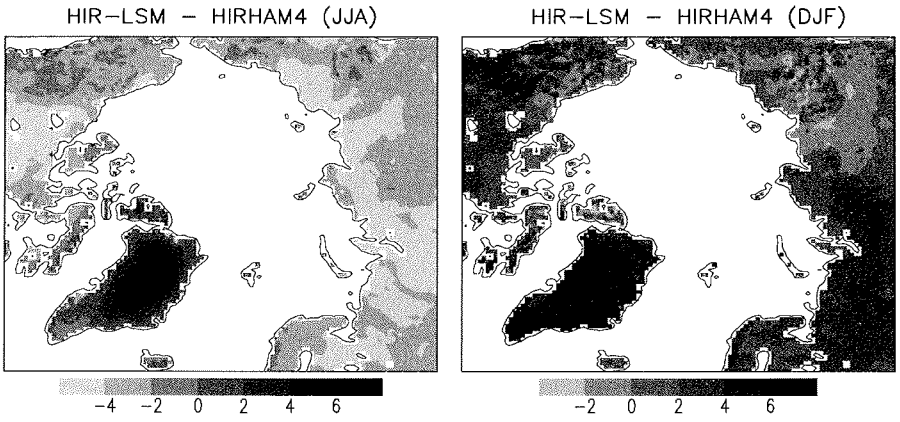

Figure 6.4: Monthly climatology (1979-1993) summer (JJA) and winter (DJF) averaged HIR-LSM *minus* HIRHAM4 10 *cm* soil temperature. Both HIRHAM4 and HIR-LSM soil temperatures are linearly interpolated to 10 *cm* soil layer.

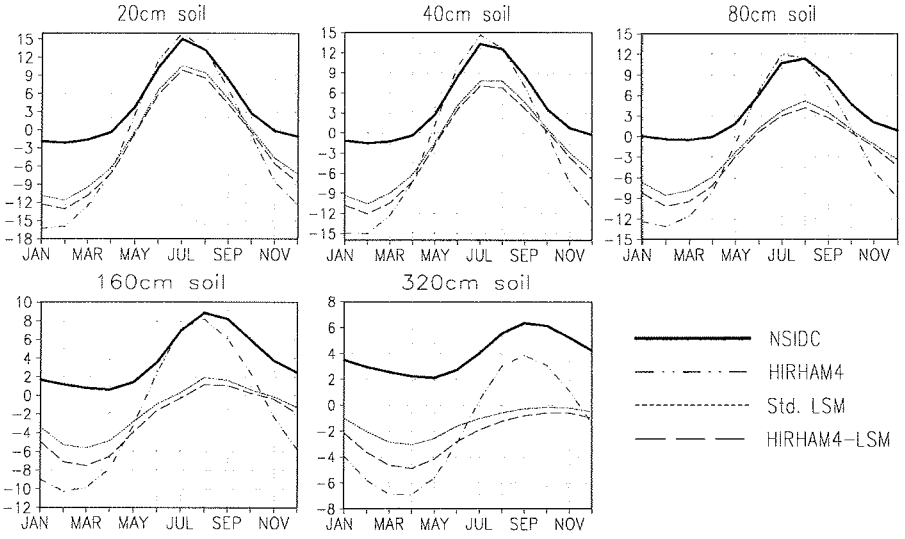

Figure 6.5: West Russian (WR) stations averaged monthly climatology mean (1979-1990) soil temperature (in °C) at five different depths.

and winter averaged HIR-LSM *minus* HIRHAM4 soil temperature at 10 *cm* depth. Summer cooling in its land part (except Greenland) is much higher in soil than in the air. In some places during summer, the soil is colder in the HIR-LSM model

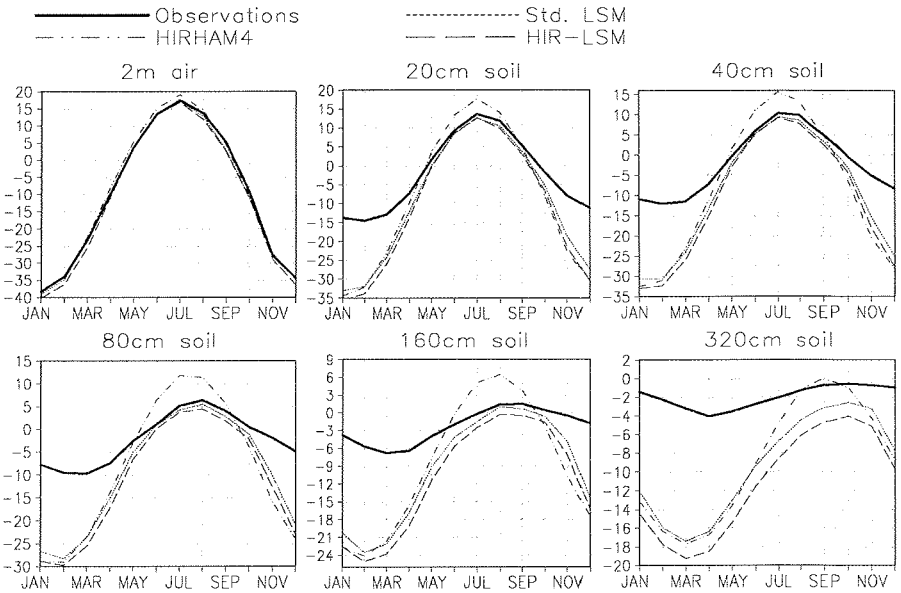

Figure 6.6: East Siberian (ES) stations averaged monthly climatology mean (1979-1993) $2\,m$ air and soil temperature (in °C) at five different depths.

compared to the HIRHAM4 by more than 5 °C. In West Russia, Scandinavia, major part of Alaska and North Canada, the HIR-LSM model shows a winter warming in the order of 6 °C at $10\,cm$ depth soil compared to HIRHAM4 and reduces the cold winter bias. In the East Siberian part, the HIR-LSM model shows a mixed response of warming and cooling by a maximum of ± 2 °C compared to the HIRHAM4. The HIR-LSM model shows a overall cooling during both winter and summer seasons by a maximum of about 1 to 2 °C compared to the stand alone LSM. Beside this cooling, the HIR-LSM model is however promising in soil temperature simulation.

The soil temperatures at West Russian (WR) stations, simulated by the HIR-LSM model are very similar to the stand alone LSM simulation(Figure 5.5). The HIR-LSM model soil temperatures during winter have been improved much compared to the HIRHAM4 simulation. Figure 6.5 shows the soil temperatures at the West Russian (WR) stations from observations and the model simulations (HIRHAM4, stand alone LSM and HIR-LSM model). At each of the five soil layers, the HIR-LSM model temperature profiles are very close to the stand alone LSM. There is a maximum of 2 °C cooling during both summer and winter seasons compared to the stand alone LSM simulation. Also for the East Siberian stations (Figure 6.6), the HIR-LSM model shows that the soil and air temperature profiles are very similar to the stand alone LSM simulation. Summer soil temperatures have been improved but the winter soil temperatures have not changed.

Figure 6.7 shows the summer and winter averaged monthly climatology mean (1979-1993), sensible and latent heat fluxes simulated by HIR-LSM, HIRHAM4 and the differences between both models. In the HIR-LSM model wetland regions experience a strong increase in latent heat flux and a decrease in sensible heat flux during summer. Therefore an increase in convective cloud formation and hence an increase in small scale precipitation is seen during summer (Figure 6.8). There is a decrease in summer precipitation by a maximum of $30\,mm\,month^{-1}$ mainly over mountain regions. Land parts only experience a large summer precipitation deficit, which are very local in nature. During winter, the precipitation shows a change over the North Atlantic, North and North-east coastal part of Scandinavia by a maximum of $10\,mm\,month^{-1}$ and these regions get precipitation mainly due to the storm track over the North Atlantic. A decrease in precipitation is directly associated with the cloud formation and the net surface short wave, long wave radiations depend on the cloud cover. Since the HIRHAM4 surface albedo does not depend on the moisture level of soil explicitly, the surface albedo does not influence directly the summer net surface short wave radiation. Therefore a relatively dry soil (in reality dry soil albedo is larger than wet soil albedo), with decreased clouds gets more short wave radiation (Figure 6.9). On the other hand, the downward long wave radiation has been decreased in most of the regions due to decreased cloud. During winter the HIR-LSM model does not show a big change in radiative fluxes as in the summer. An increase in snow decreases the net surface solar radiation in Alaska, East Siberia (Figure 6.9,6.8). Therefore a reduction in the net short wave radiation and hence a reduction in surface temperature leads to the reduction in long wave radiation loss. During all sensitivity experiments, a change in the mean sea level pressure by more than 5 hPa have been found, but in the HIR-LSM model winter changes are by a maximum of 3 hPa. The summer changes are by a maximum of 2 hPa. Over Greenland, a large pressure difference occurred due to the warmer LSM surface temperature over this region (Figure 6.3).

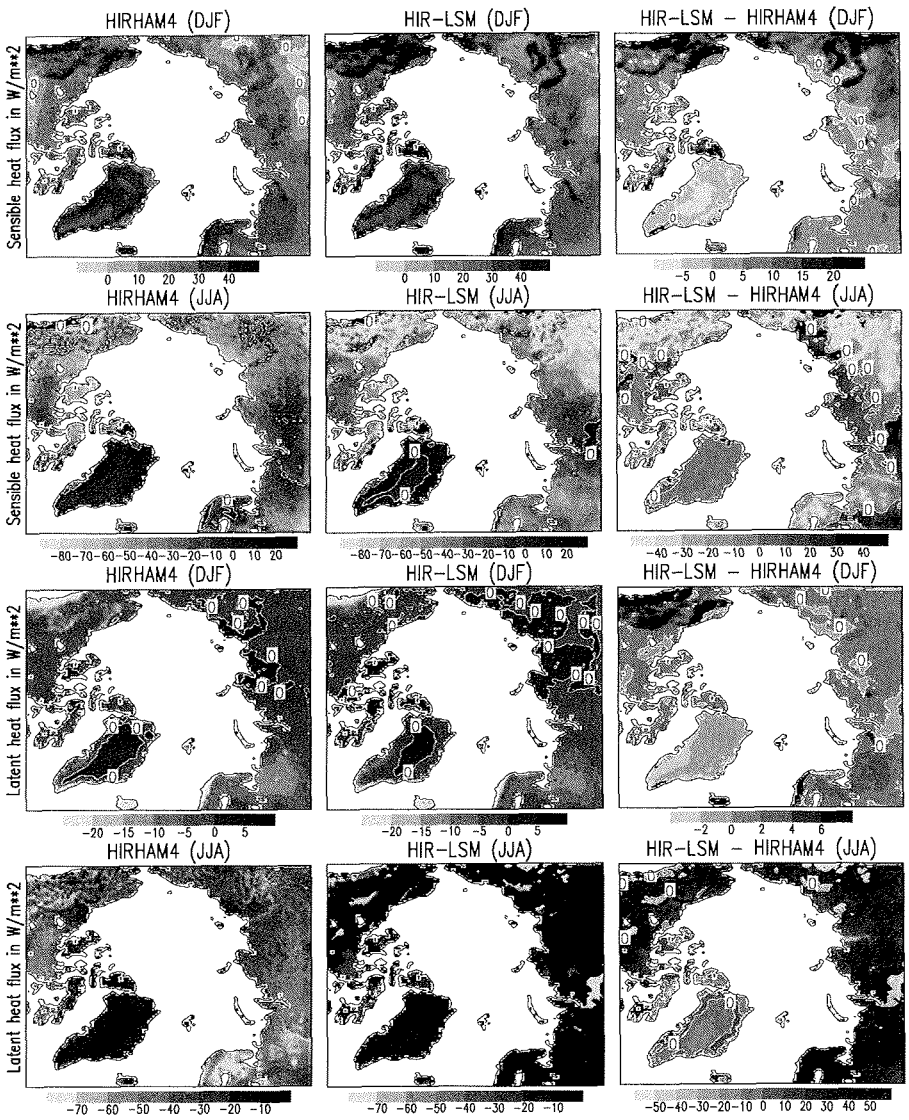

Figure 6.7: Monthly climatology mean (1979-1993) summer and winter averaged, surface latent heat flux (in $\mathrm{W\,m^{-2}}$) and surface sensible heat flux (in $\mathrm{W\,m^{-2}}$) from HIR-LSM and HIRHAM4 simulations and their differences.

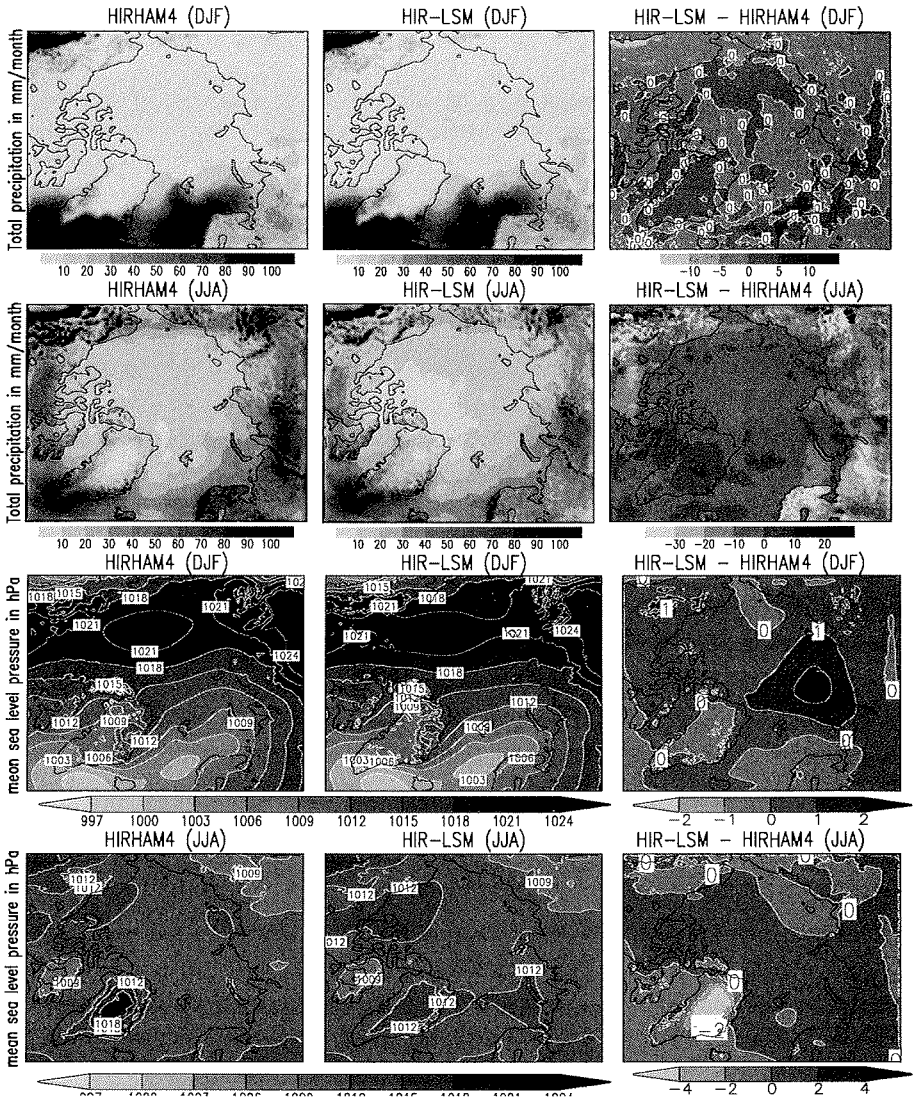

Figure 6.8: Monthly climatology mean (1979-1993) summer and winter averaged, total precipitation (in mm month^{-1}) and mean sea level pressure (in hPa) from HIR-LSM and HIRHAM4 simulations and their differences.

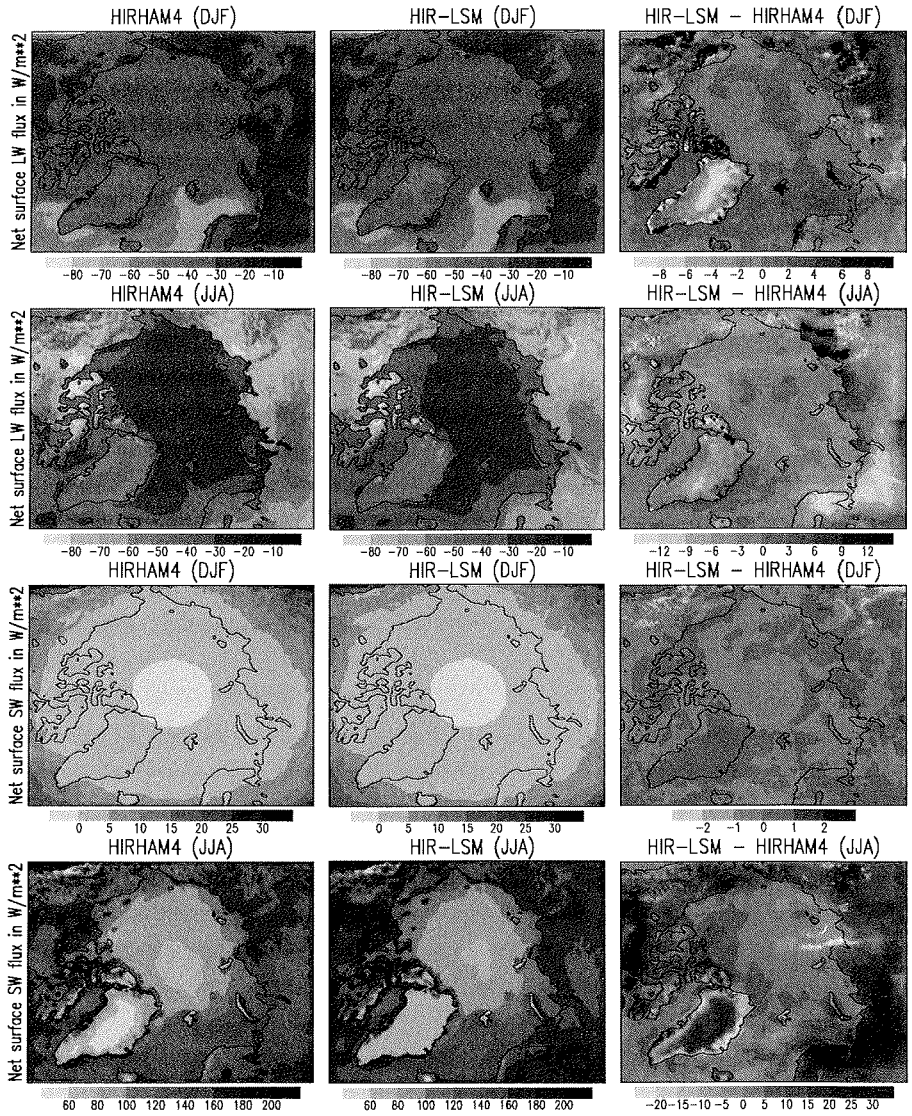

Figure 6.9: Monthly climatology mean (1979-1993) summer and winter averaged, net surface long wave radiation (in $W\,m^{-2}$) and net surface short wave radiation (in $W\,m^{-2}$) from HIR-LSM and HIRHAM4 simulations and their differences.

6.4 Summary

A significant change in the surface energy budget of the HIR-LSM model was found during summer season compared to HIRHAM4. During winter the HIR-LSM model was not much different from the control HIRHAM4. The nature of feedback processes in the climate, partly shown in Figure 6.1 is very complex. A decrease or increase in soil moisture at two different places by the same magnitude does not necessarily mean the same change in partitioning of latent and sensible heat flux neither in net surface long wave radiation nor in short wave radiation. Apart from available soil moisture, moisture flux from the land surface to the atmosphere depends on various factors like land cover, near surface relative humidity, wind speed, available energy etc. Also the Arctic soil moisture distribution is not known accurately or not available directly by their absolute values.

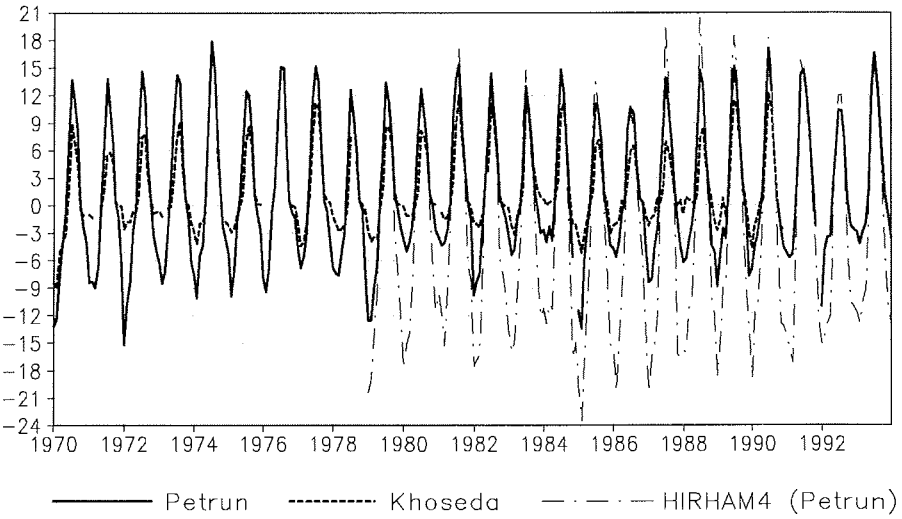

Figure 6.10: Monthly mean soil temperature at 20 *cm* depth from stations Petrun, Khoseda and the HIRHAM4 simulation at Petrun station in °C. The solid line is for soil temperature at Petrun, dashed line is for Khoseda and the dot-dashed line is for HIRHAM4 simulated soil temperature at Petrun.

During winter, the HIR-LSM model soil temperatures have been improved at West Russian stations compared to HIRHAM4 and the cold winter bias has been reduced. The station averaged winter soil at West Russia is now warmer than the HIRHAM4 simulation by about 3-5 °C. At 10 *cm* depth, the soil in West Russia, Alaska and Scandinavia has been warmed up by a order of 6 °C. There are still remains a winter biases in the coupled model soil temperature compared to the station measurements at West Russia (WR) by about 7-10 °C. The East Siberian (ES) stations do not show any improvement in winter soil temperature biases. During

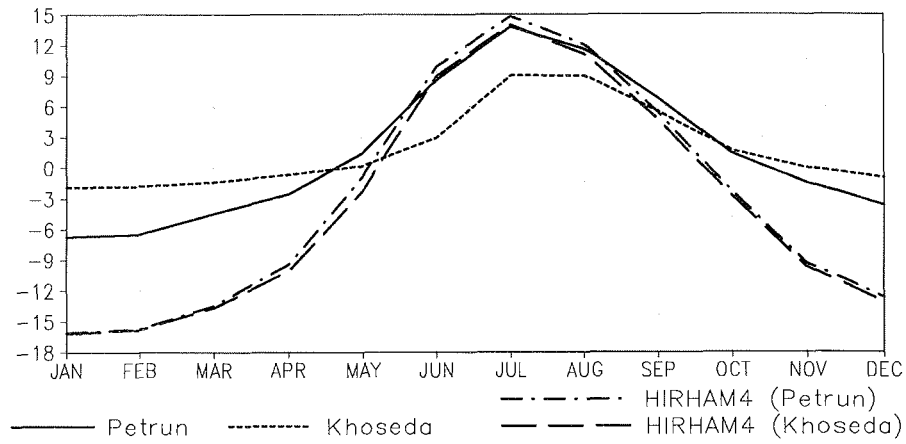

Figure 6.11: Monthly climatology mean (1979-1993) soil temperature at 20 cm depth in °C. The solid line is for soil temperature at Petrun, short dashed line is for Khoseda. The dot-dashed and long dashed lines are HIRHAM4 simulated soil temperature at station Petrun and Khoseda respectively.

summer the HIR-LSM model soil temperatures have been cooled down everywhere in the land areas and at West Russian (WR) stations, it is colder than the observations by a maximum of 5 °C. However the summer cooling has brought the HIR-LSM model soil temperature at East Siberian (ES) stations very close to the observations.

There are also difficulties in comparing station data with the model simulation of 50 × 50 km horizontal resolution. Within the 50 × 50 km area, a large variations in soil temperature can not be ruled out. Figure 6.10 shows the monthly mean soil temperatures at 20 cm depth from two nearby West Russian stations, Petrun (60.49E, 66.26N) and Khoseda (59.23E, 67.05N). The station Petrun has an altitude of 61 m and situated ovear a flat forested tundra region. The station Khoseda has an altitude of 84 m and situated over upper river terrace, which is also a tundra region. Although these two stations are not far awy from each othere, there are large differences between these two station's soil temperatures. At the station Petrun, winter soil is colder than at the station Khoseda in the order of 12 °C. The summer differences are also of the order of 6 °C. The monthly climatology mean (1979-1993) of the two stations observed and HIRHAM4 simulated soil temperatures are shown in Figure 6.11. Here the two observations differ from each other by about 5 °C during both summer and winter seasons. The HIRHAM4 simulation is very close to the Petrun station during summer, but during winter, at both stations, the HIRHAM4 soil is colder than the observations by about 9 °C.

More extensive monitoring of ground temperatures and active layer started near the Canadian station Baker Lake (90.05W, 64.18N) in the late 1990s. While the record is short, it includes a nice sensitivity study. One of the four monitored sites

has artificially thick snow cover (close to a fence). The effect (damping) on ground temperatures was found in the order of 10 °C at 3 m depth (*Smith et al.*, 2001; *Smith*, 2003).

As discussed before, the winter soil temperature evolution has been improved in major part of the domain. In the next step the HIR-LSM model need to improve the winter precipitation. The winter precipitation in the HIR-LSM model is very similar to the HIRHAM4 and it has been shown in the section 3.1 that the snow water equivalent in HIRHAM4 largely underestimates the observations. Therefore the HIR-LSM model need to increase the precipitation by improving the storm track over East Siberia, cloud parametrization and by increasing the model horizontal resolution. The increase in model horizontal resolution will enhance the orographic precipitation.

However this was the first step towards the coupling of the atmospheric model HIRHAM4 with the advanced NCAR land surface model. There are other options in future to couple the HIRHAM4 with LSM through other variables indicated in Figure 6.2. The coupled model's performance in soil temperature simulation was very similar to the stand alone LSM. In future a further improvement in the soil temperature will involve the improvement in model precipitation (both winter and summer) and a treatment of a more complex snow scheme.

7 IPCC B2 Scenario by HIRHAM4 and HIRHAM-LSM Coupled Model

7.1 Introduction

Natural climate variability along with the anthropogenic changes in the climate system leads to the change in future states of the climate. Demographic, socio-economic and the technological developments contribute to the GreenHouse Gas (GHG) emission, aerosol and land use changes. Scenarios are the plausible states of the future climate, based on the plausible changes in the climate. It does not mean the probable future development but a plausible development and to guide policy makers as well as the public, so that the decision and action can be taken. Four emission scenarios based on the plausible future GHG emission, aerosol, land use changes with consistent assumptions of future demographic, socio-economic and technological developments are prepared by a group of economists and social scientist in SRES (IPCC Special Report on Emission Scenario):

(A1) *a world of rapid economic growth and rapid introduction of new and more efficient technology,*

(A2) *a very heterogeneous world with a emphasis on family values and local traditions,*

(B1) *a world of "dematerialization" and introduction of clean technologies and*

(B2) *a world with an emphasis on local solutions to economic and environmental sustainability.*

Global coupled Atmosphere-Ocean General Circulation Models (AOGCMs), based on the physical laws and numerical techniques are widely used for the climate scenarios. The third assessment report, prepared by the Intergovernmental Panel on Climate Change (IPCC) based on a set of AOGCM projections and provided the following information. For the last three decades of the 21^{st} century (2071-2100), a change of 3.0 °C (with a range of 1.3 to 4.5 °C between the nine models used by IPCC) in globally averaged surface air temperature relative to the period 1961-1990 for the A2 scenario and 2.2 °C (with a range of 0.9 to 3.4 °C) for the B2 scenario have been simulated. It is likely that the land area will warm up more rapidly than the global average, particularly in the high latitude Northern Hemisphere. A decrease in diurnal air temperature range, with night-time low increase more than the day-time high is seen in AOGCM scenarios. In the Northern Hemisphere land areas, the daily variability of winter surface air temperature is decreased while the summer air

temperature variability is increased in many AOGCMs. The Northern Hemisphere snow cover and sea-ice extent are projected to decrease and the glaciers and ice caps will continue their retreat in the 21^{st} century. Mean precipitation is projected to increase and will likely increase the inter-annual variability. Extremes of precipitation are projected to increase more than the mean and the intensity of precipitation events is projected to increase. Frequency of extreme precipitation events are likely to increase in everywhere. Most of the AOGCMs show a weakening of Northern Hemisphere thermohaline circulation, which contributes to the reduction of surface warming in sub-Arctic North Atlantic (*Houghton et al.*, 2001).

The coarse horizontal resolutions (300-500 km.) of the AOGCM's are unable to provide regional details of possible future developments. Currently, only very few high resolution estimates for future climate change are available from RCM studies (*Kiilsholm et al.*, 2003; *Dorn et al.*, 2000). The dynamically down-scaled model HIRHAM4 provides the high resolution scenario for a chosen limited area, here for the whole circumpolar Arctic. The large scale atmospheric phenomena enter into the model through boundary relaxation and small scale Arctic processes are evolved according to the model physics and dynamics with a higher horizontal resolution. For the current study lateral and lower boundaries are from IPCC B2 scenario runs of the global coupled Atmosphere-Ocean model ECHO-G (ECHAM4/HOPE-G). The ECHO-G model consists of the atmospheric GCM ECHAM4 (*Roeckner et al.*, 1996) at T30/L19 resolution (horizontal grid point distance approximately 3.75° and 19 vertical levels) and the global version of the Hamburg Ocean Primitive Equation GCM HOPE-G (*Wolff et al.*, 1997), which incorporates a dynamic-thermodynamic sea-ice model with snow cover.

7.2 NAO regime and period selection

The North Atlantic Oscillation (NAO) (*Exner*, 1913; *Walker*, 1924; *van Loon and Rogers*, 1978) is one of the most prominent teleconnection pattern in the Northern Hemisphere. NAO influences the climate variability from eastern seaboard of the United States to Siberia and from the Arctic to the subtropical Atlantic. Although this teleconnection pattern persists throughout the year, the amplitude is largest during winter (December-March). The NAO accounts for about 37% of the monthly time series of December, January, February 500 hPa height variability over the Atlantic (*Wallace and Gutzler*, 1981; *Kushnir and Wallace*, 1989; *Wallace et al.*, 1996) The strength and the state of NAO is defined by an index, called NAO index, which is calculated as the anomalous difference between the Icelandic low and the subtropical high during the winter season (December through March).

For the calculation of the NAO index in this study, ECHO-G (IPCC B2 scenario for 1990-2100) 111 years monthly mean data are used. According to *Hurrell* (1995), the NAO index has been calculated as the difference between the normalized winter sea level pressure anomalies at Lisbon (38°42′N, 9°10′W), Portugal and Stykkisholmur (65°4′N, 22°43′W), Iceland. The ECHO-G nearest grid points to these stations are used here for the index calculation. Figure 7.1 shows the ECHO-G based NAO index for 111 years. A positive future trend of NAO index onward 2030

	Model	
Time slice	HIRHAM4	HIR-LSM
1990-1995	HIR_90	HIRLSM_90
2024-2029	HIR_NAO$^-$	HIRLSM_NAO$^-$
2037-2042	HIR_NAO$^+$	HIRLSM_NAO$^+$

Table 7.1: The selected time slices for the HIRHAM4 and the coupled model HIR-LSM simulations and the given name of these simulations.

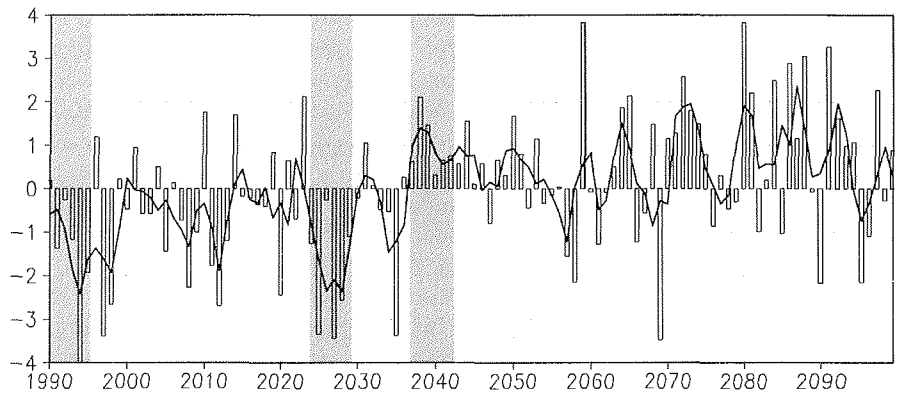

Figure 7.1: Winter (DJFM) NAO index based on the difference of ECHO-G (B2 scenario) normalized sea level pressure (SLP) anomalies between nearest point of Lisbon, Portugal and Stykkisholmur, Iceland from 1990 through 2100. The average winter SLP anomaly in each season and at both stations were normalized by the mean standard deviation (1991-2100) of SLP. The bars are representing the NAO index for the corresponding years and the curve is a 3 years running mean of NAO indices. The shaded regions represent the selected positive and negative NAO time slices.

is noticeable here. Due to the limited computer resource, the whole 111 years time period was not possible to down scale. Therefore two time slices of each 6 years duration, during positive and negative NAO were chosen. The first time slice was from 2024 to 2029 associated with a negative phase of NAO and the second time slice was from 2037 to 2042 associated with a positive NAO phase. Using the same ECHO-G IPCC B2 scenario boundary and initial forcing, HIRHAM4 and HIR-LSM were simulated for these two time slices. The HIR-LSM model is used here to realize the changes in future scenario due to the different soil-vegetation schemes. Not only the plausible GHG emission but also an improved understanding of the physical processes and their implications into the numerical model may influence the future climate estimates. As a reference climate, HIRHAM4 simulation of the time slice 1990 to 1995 with ECHO-G IPCC B2 scenario initial and lateral boundary forcing

is used. Hereafter the HIRHAM4 simulations of positive and negative NAO time slices are referred as HIR_NAO$^+$ and HIR_NAO$^-$ respectively, while the 1990-1995 HIRHAM4 simulation is referred as HIR_90. The HIR-LSM simulations for positive and negative NAO time slices are referred as HIRLSM_NAO$^+$ and HIRLSM_NAO$^-$ respectively and the 1990-1995 HIR-LSM simulation is referred as HIRLSM_90.

7.3 Influences of land-surface scheme and NAO phase on future climate

The consequences of NAO on Northern Hemisphere climate are known from many years. A positive NAO index means a stronger than usual subtropical high pressure center and a deeper than normal Icelandic low. An enhanced westerly flow across the North Atlantic during winter moves relatively warm and moist maritime air over much of Europe and far downstream across Asia, while stronger northerlies over Greenland and north-eastern Canada carry cold air southward and decrease the land surface temperature and SST over the north-west Atlantic. The negative NAO index means a weak subtropical high and a weak Icelandic low. The reduced pressure gradient causes a winter flow on a more west-east pathway and as a result warm winter in the Mediterranean and cold winter in the Northern Europe, south-west part of Greenland and at the east coast of the US.

Figure 7.2 shows the winter and summer averaged $2\,m$ air temperatures from HIR_90, HIR_NAO$^+$, HIRLSM_90 and HIRLSM_NAO$^+$ simulations and the warming/cooling signals in the future (2037-2042) with respect to the present climate (1990-1995). The winter averaged spatial patterns of $2\,m$ air temperatures simulated by HIRHAM4 and HIR-LSM are very similar to each other in both time slices. The coldest winter temperature persists over central Arctic, East Siberia and central part of Greenland. A winter warming of maximum 10 °C over central Eurasia, Western Europe and a cooling of maximum 6 °C over Eastern Alaska, Eastern Siberia are seen in HIR_NAO$^+$ simulation with respect to HIR_90 simulation. The HIRLSM_NAO$^+$ simulation also shows a warming over central Eurasia, Western Europe and cooling over Eastern Alaska, East Siberia compared to the HIRLSM_90 simulation. The winter warming over central Eurasia and Western Europe are due to both, the increased greenhouse gas and the NAO signal. Since the time slices 1990-1995 and 2037-2042 are associated with the negative and positive NAO phases respectively, HIR_NAO$^+$ *minus* HIR_90 or HIRLSM_NAO$^+$ *minus* HIRLSM_90 represents the positive NAO *minus* negative NAO signal. Therefore a winter warming over Western Europe and central Eurasia in the 2037-2042 time period compared to 1990-1995 time period is expected due to the NAO signal. The increased GHG will trap more outgoing surface long wave radiations and hence it will also contribute to the warmer climate.

The summer averaged spatial patterns of HIRHAM4 and HIR-LSM simulations over the ocean are similar to each other but over land, the HIRHAM4 simulations are warmer than the HIR-LSM simulations. During summer, the future (2037-2042) warming and cooling signals with respect to the present (1990-1995) are not so strong

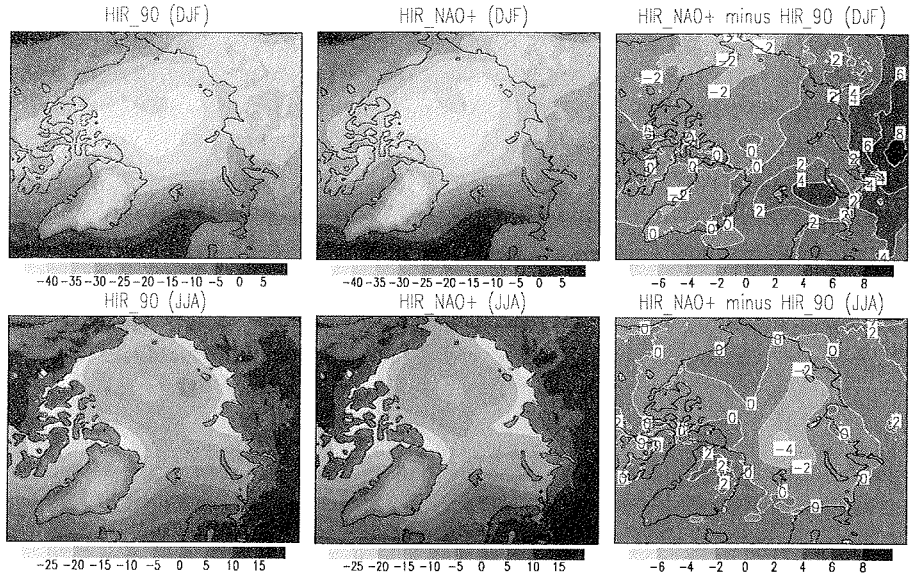

(a)

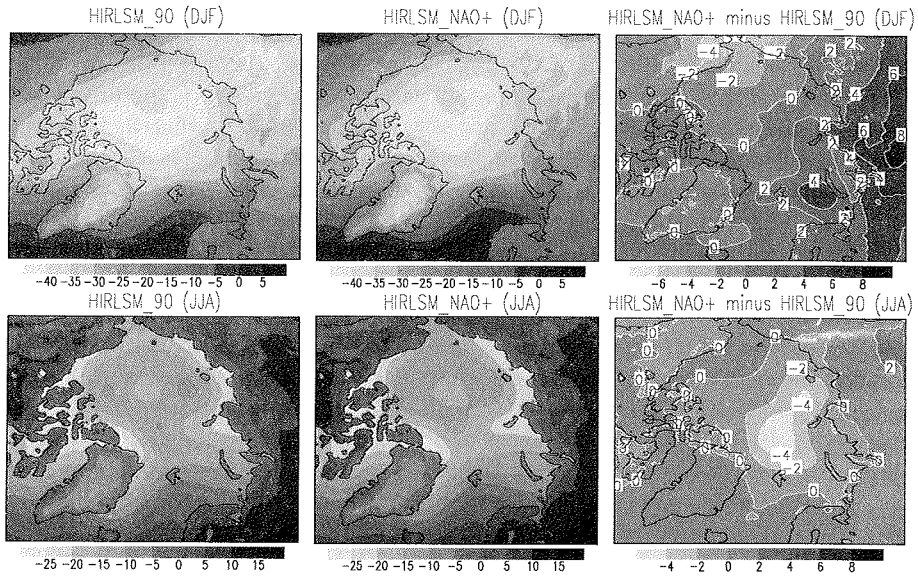

(b)

Figure 7.2: (a) Winter (DJF) and summer (JJA) averaged 2m air temperatures from HIR_90 (1990-95), HIR_NAO$^+$ (2037-2042) simulations and the differences between these two simulations. (b) is similar to (a), but a simulation by the model HIR-LSM.

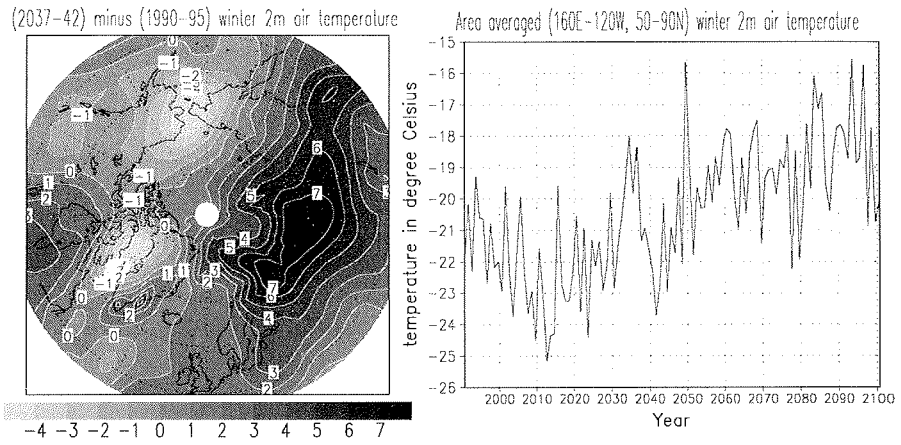

Figure 7.3: The $2\,m$ air temperature from ECHO-G IPCC B2 scenario simulation. The left panel shows the winter (DJF) averaged (2037-2042) *minus* (1990-1995) air temperature in °C. The right panel shows the temporal evolution of area averaged (160E-120W, 50-90N) mean winter (DJF) $2\,m$ air temperature in °C.

as during the winter. Except over Alaska, both of the models show a warming over land during 2037-2042 time slice compared to 1990-1995 time slice by a maximum of 4 °C.

In the IPCC B2 scenario, CO_2 and CH_4 gases are projected to increase largely in this century and they are the major contributors to the GHG global warming. Both model simulations show a winter cooling in Alaska and far-east Siberia instead of warming everywhere in the domain during 2037-2042 compared to 1990-1995. This winter cooling over Alaska and far-east Siberia in the $2\,m$ air temperature can be explained with the driving ECHO-G B2 scenario $2\,m$ air temperature. Figure 7.3 shows the winter averaged (2037-2042) *minus* (1990-1995) ECHO-G B2 scenario $2\,m$ air temperature. The ECHO-G scenario does not show the warming in $2\,m$ air temperature everywhere in the domain. There are also cooling over Alaska and far-east Siberia. *Machenhauer et al.* (1996) found that the large scale errors of driving model ECHAM4 are also present in HIRHAM4 simulation. Here we see also the large scale signal of ECHO-G in the HIRHAM4 and HIR-LSM simulations. The temporal evolution of area averaged (over the cooling region 50-90 °N, 160 °E-120 °W), winter mean $2\,m$ air temperature from ECHO-G B2 scenario simulation is shown in Figure 7.3. There is a very clear trend of warming from 2010 onward, but with a large inter-annual variability. Therefore, an area average over short time periods (like our 6 year periods 1990-1995 and 2037-2042) must not show a general warming.

The winter and summer averaged mean sea level pressure (MSLP) of HIR_NAO$^+$, HIR_90, HIRLSM_90, HIRLSM_NAO$^+$ simulations are shown in Figure 7.4. Both

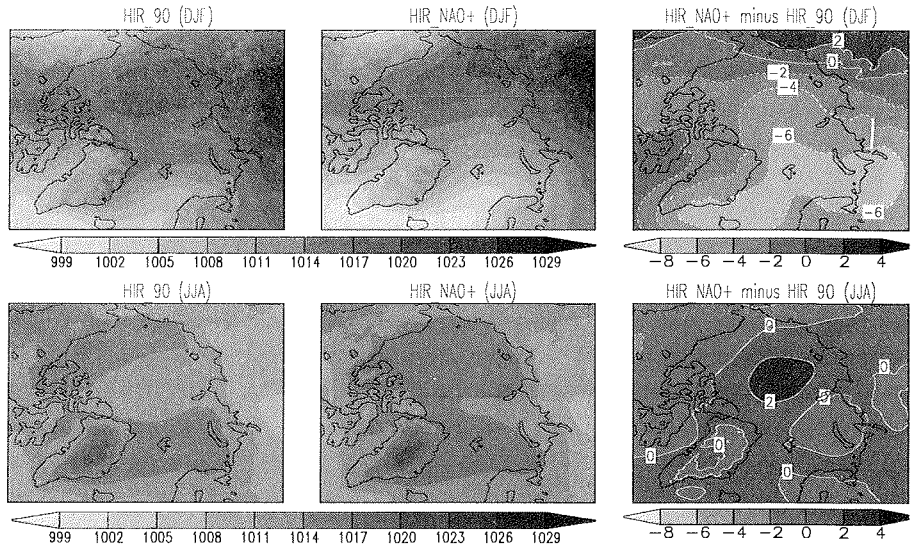

(a)

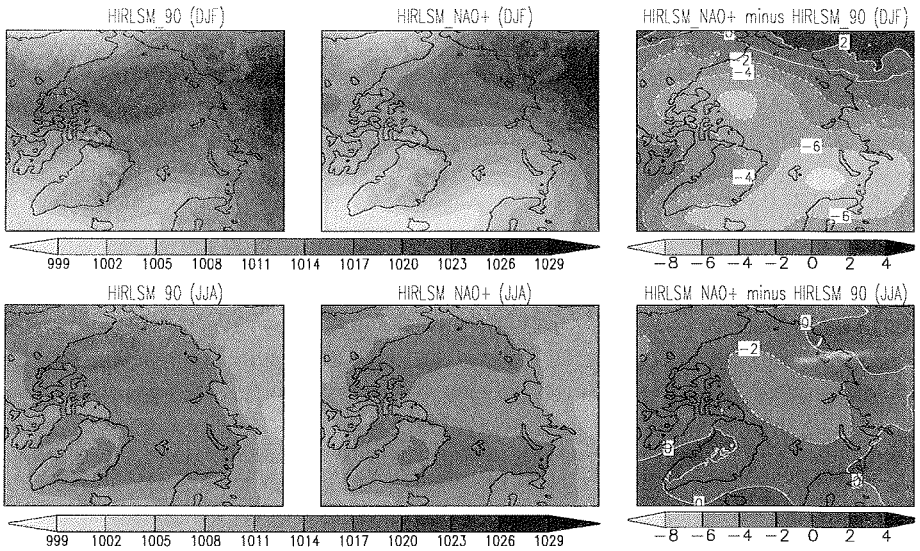

(b)

Figure 7.4: (a) Winter (DJF) and summer (JJA) averaged mean sea level pressure (in hPa) from HIR_90 (1990-1995), HIR_NAO$^+$ (2037-2042) simulations and the differences between these two simulation. (b) is similar to the (a), but a simulation by the model HIR-LSM.

of the models show that, there are changes in mean sea level pressure during 2037-2042 summer compared to 1990-1995 summer. The summer changes over the central Arctic are opposite in two models and are within ±4 hPa. The winter decrease in MSLP during 2037-2042 compared to 1990-1995 in both model simulations are by a maximum of 8-10 hPa. Except in the far-east part of Siberia, the decrease in MSLP is over the entire model domain. Since the positive NAO phase is associated with the deeper winter Icelandic low, a decrease in winter MSLP is expected. In section 6.3, it has shown that the HIR-LSM simulated summer MSLP differed from the HIRHAM4 by only within ±2 hPa. Here the difference in summer MSLP realization between two models has increased.

Figure 7.5 shows the summer and winter averaged total precipitation (large scale plus convective) in HIR_90, HIR_NAO$^+$ and HIRLSM_90, HIRLSM_NAO$^+$ simulations. During winter there is a decrease in precipitation at the south and south-east coasts of Greenland by more than 20 $mm\,month^{-1}$ in both HIRLSM_NAO$^+$ and HIR_NAO$^+$ simulations compared to HIRLSM_90 and HIR_90 simulations respectively. Also there is an increased precipitation at east coast of Greenland, over North Atlantic, Scandinavia and West Russia by more than 30 $mm\,month^{-1}$. All of these increases in precipitation are associated with the winter storm track crossing the North Atlantic during positive NAO phases. There is also increase in precipitation by more than 30 $mm\,month^{-1}$ in Southern part of Alaska. The summer precipitations are very local in nature and are largely due to the convective processes. Therefore the change in summer precipitation in HIR_NAO$^+$ compared to HIR_90 simulation or in HIRLSM_NAO$^+$ compared to HIRLSM_90 are mainly distributed over land and they are very patchy in nature. The spatial distributions of decreased or increased precipitations in both models are very similar.

Figure 7.6 shows (HIRLSM_NAO$^+$ *minus* HIRLSM_90) *minus* (HIR_NAO$^+$ *minus* HIRLSM_90) winter and summer averaged $2\,m$ air and $10\,cm$ soil temperatures in °C, precipitation in $mm\,month^{-1}$ and mean sea level pressure in hPa. This Figure shows the differences between two model's (HIRHAM4 and HIR-LSM) future (2037-2042) projected climate change. These changes are due to the new land surface scheme and the coupling of it with the HIRHAM4 model. There are cooling and warming of maximum ±2 °C in $2\,m$ air temperature over most of the land parts during both winter and summer. During winter at $10\,cm$ depth, the HIRHAM4 soil shows a warming of more than 2 °C compared to the HIR-LSM soil. During summer, the HIRHAM4 soil at $10\,cm$ is colder than the HIR-LSM soil by more than 2 °C. Therefore these two models show an uncertainty of ±2 °C in the projection of future air and soil temperature. There are increased and decreased precipitation patterns during summer and their distributions are very patchy. There are also changes in precipitation during winter but they are mainly over North Atlantic and Southern part of Alaska. The mean sea level pressure changes are mainly over oceans. During winter and summer the MSLP has been decreased in the HIR-LSM by a maximum of 2 and 4 hPa respectively.

The changes in MSLP, $2\,m$ air and soil temperatures during the positive (2037-2042) NAO phase compared to the negative (2024-2029) NAO phase, similar to *Dorn et al.* (2003) and the uncertainty due to two models are analyzed.

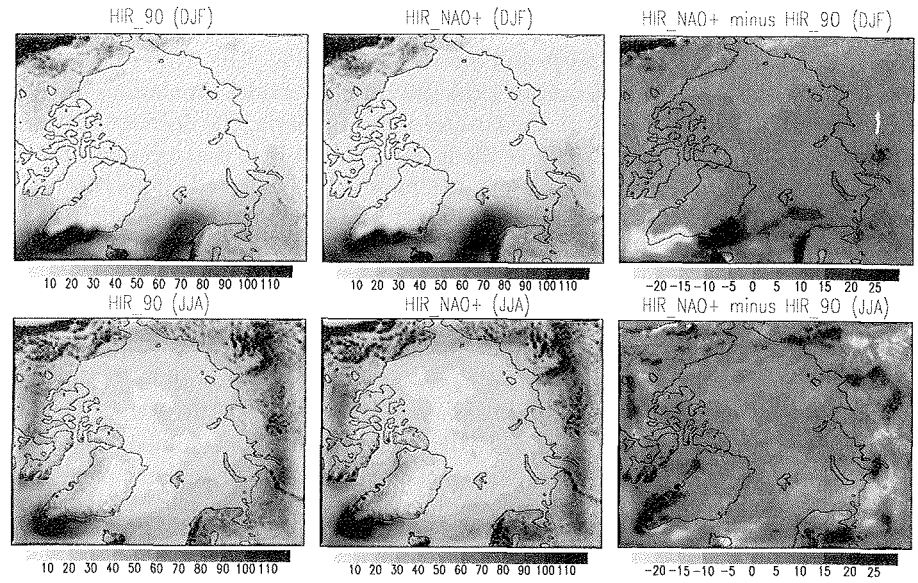

(a)

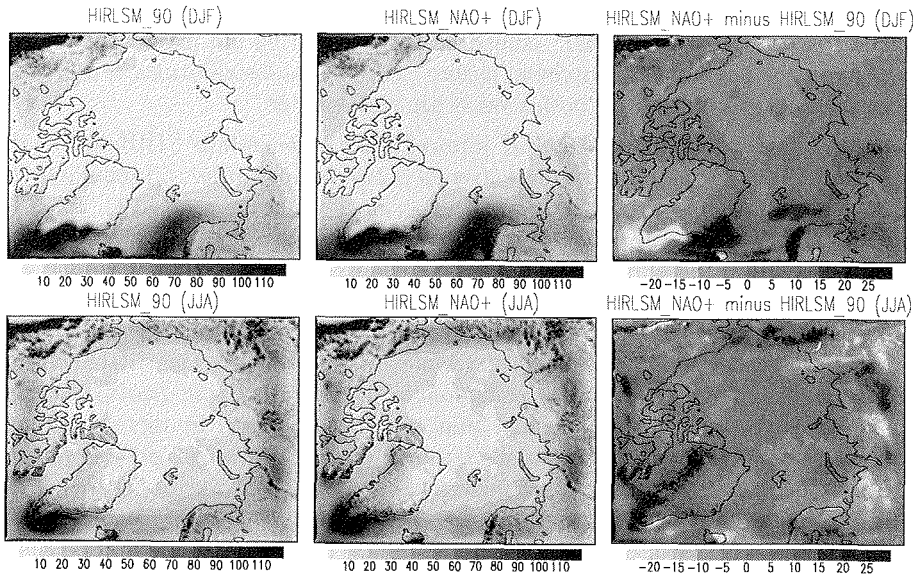

(b)

Figure 7.5: (a) Winter (DJF) and summer (JJA) averaged total precipitations (large scale plus convective in $mm\,month^{-1}$) from HIR_90 (1990-1995), HIR_NAO$^+$ (2037-2042) simulations and the differences between these two simulation. (b) is similar to (a), but a simulation by the model HIR-LSM.

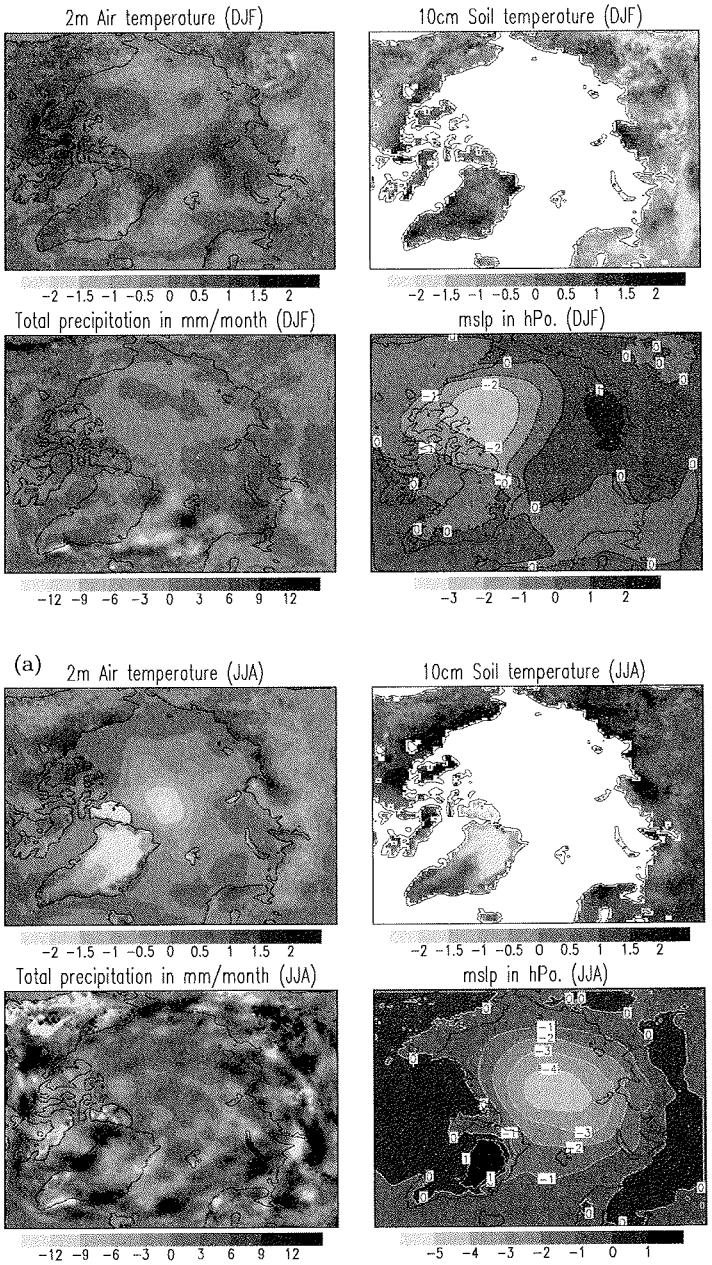

Figure 7.6: (HIRLSM_NAO$^+$ *minus* HIR-LSM) *minus* (HIR_NAO$^+$ *minus* HIR_90) winter (DJF) and summer (JJA) averaged $2\,m$ air and $10\,cm$ soil temperature in °C, precipitation in $mm\,month^{-1}$ and mean sea level pressure in hPa. **(a)** is for winter (DJF) and **(b)** is for summer.

Figure 7.7 shows the winter and summer averaged HIR_NAO$^+$ *minus* HIR_NAO$^-$ and HIRLSM_NAO$^+$ *minus* HIRLSM_NAO$^-$ mean sea level pressure and $2\,m$ air temperature. Both of the models show a decrease in winter averaged MSLP over North Atlantic during the positive NAO phase compared to the negative NAO phase (changes are similar to *Dorn et al.* (2003). However there are differences between two model's MSLP simulations by ± 3 hPa over oceans. During summer, the MSLP changes between the two NAO phases are not so pronounced like winter in both models. The HIR-LSM shows a smaller NAO$^+$ *minus* NAO$^-$ MSLP over the central Arctic by a maximum of 3 hPa compared to the HIRHAM4. The large scale warming and cooling patterns in $2\,m$ air temperature during positive NAO phase compared to the negative NAO phase are very similar in both models. There is a warming during positive NAO phase compared to negative NAO phase over Western Europe, central Eurasia and Alaska by a maximum of 4 °C. The two model's summer and winter projected changes in $2\,m$ air temperature during 2037-2042 compared to 2024-2029 are within ± 2 °C. These differences are over the costal part of Siberia, West Russia, North Canada and also these regions are known as permafrost region.

Figure 7.8 shows the winter averaged positive NAO (2037-2042) phase *minus* negative NAO (2024-2029) phase soil temperatures at $10\,cm$ and $320\,cm$ depth, simulated by both models (HIRHAM4 and HIR-LSM) and the differences between these two model's simulations. The HIRHAM4 simulation shows that soil at $10\,cm$ depth in Western Europe, central Eurasia and Alaska has been warmed up by a maximum of 4 °C, whereas there is a minor cooling of maximum 2 °C over North Canada. The soil warming and cooling spatial patterns are very similar to the spatial patterns of warming and cooling in $2\,m$ air temperature but the warming and cooling spatial patterns are slightly different in HIR-LSM. The projected changed signal at $10\,cm$ is higher than at $320\,cm$ soil in both models. The HIR-LSM differs from the HIRHAM4 by about ± 2 °C and the coastal part of Siberia is warmer in the HIR-LSM compared to the HIRHAM4. The difference between the two model's projected relative warming or cooling is larger in soil temperature compared to the $2\,m$ air temperature.

The domain averaged warming and cooling in soil, during the positive NAO phase compared to the negative NAO phase are shown in Figure 7.9. The HIRLSM_90 winter soil is warmer than the HIR_90 winter soil. During summer the 0 °C contour has a deeper extent in the HIRLSM_90 simulation compared to the HIR_90 simulation. These features (i.e. the HIR-LSM is warmer during winter and colder during summer compared to the HIRHAM4) are know already from section 6.3. Both of the models show a winter warming by a maximum of about 1 °C at $320\,cm$ depth during 2037-2042 compared to 1990-1995. There is a difference in two models projected warming (i.e. (HIRLSM_NAO$^+$ *minus* HIRLSM_90) *minus* (HIR_NAO$^+$ *minus* HIR_90)) in soil. During winter, the HIR-LSM projected soil is warmer than the HIRHAM4 projection by a maximum of 0.6 °C.

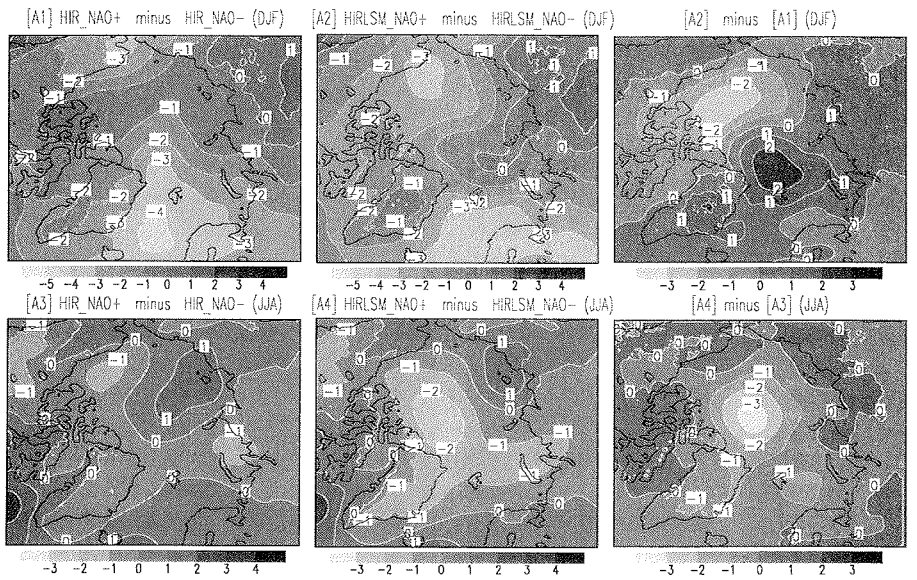

(a)

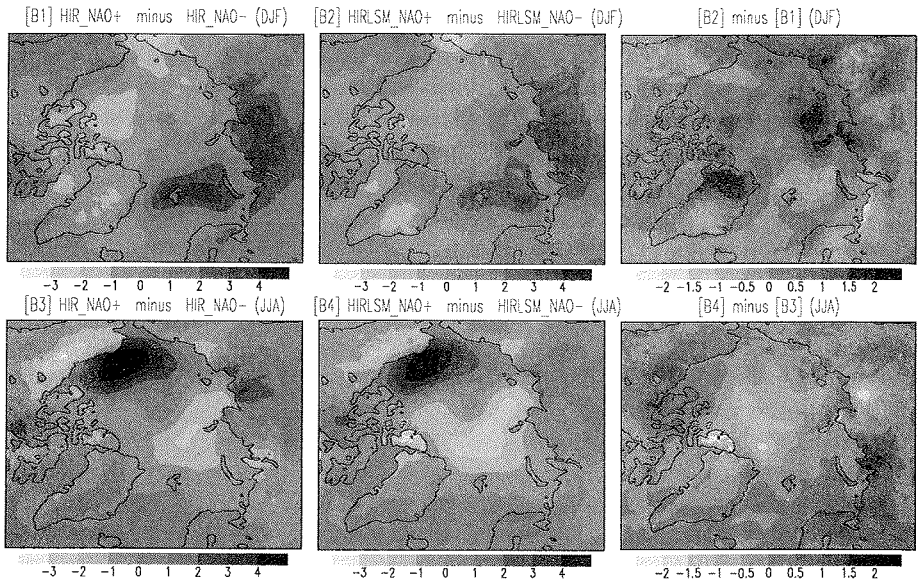

(b)

Figure 7.7: (a) winter (DJF) and summer (JJA) averaged HIR_NAO$^+$ *minus* HIR_NAO$^-$, HIRLSM_NAO$^+$ *minus* HIRLSM_NAO$^-$ and (HIRLSM_NAO$^+$ *minus* HIRLSM_NAO$^-$) *minus* (HIR_NAO$^+$ *minus* HIR_NAO$^-$) mean sea level pressure in hPa. (b) is similar to (a) but for $2\,m$ air temperature in °C.

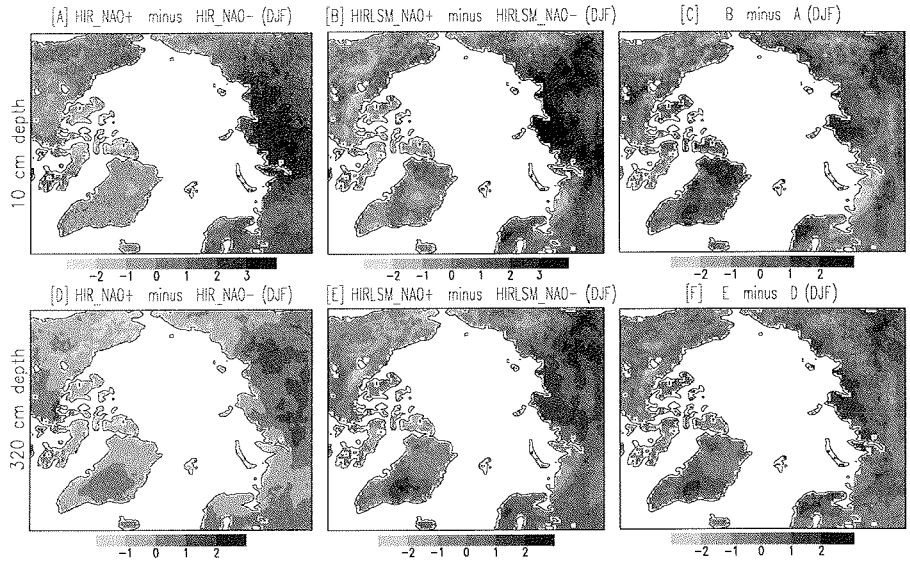

Figure 7.8: The winter (DJF) averaged soil temperature in °C. The first row is for soil temperature at 10 *cm* depth and the second row is for soil temperature at 320 *cm* depth. [**A**] is HIR_NAO$^+$ *minus* HIR_NAO$^-$ soil temperature, [**B**] is HIRLSM_NAO$^+$ *minus* HIRLSM_NAO$^-$ soil temperature and [**C**] is (HIRLSM_NAO$^+$ *minus* HIRLSM_NAO$^-$) *minus* (HIR_NAO$^+$ *minus* HIR_NAO$^-$) soil temperature. [**D**], [**E**], [**F**] are the same as [**A**], [**B**], [**C**] respectively but for soil temperature at 320 *cm* depth.

7.4 Summary

The main objective of this chapter was to find out the influences of different soil and vegetation schemes in the Arctic climate during scenario simulations. In future time slice, NAO has a large influence on the winter climate of the Arctic. Both models show a large winter warming/cooling in 2 *m* air temperature during the positive NAO phase (2037-2042) compared to the negative NAO phase (2024-2029). The Eurasia and West Europe have warmed up by a maximum of 10 °C and Alaska, far-east Siberia have cooled down by a maximum of 6 °C.

A similar warming and cooling spatial patterns are also in the global model (ECHO-G) calculated future climate scenario (e.g. 2037-2042 *minus* 1990-1995). There is also a large inter-annual variability in global model calculated 2 *m* air temperature and a clear warming trend from 2010 onward. Therefore the temperature change in every part of the domain largely depends on the choice of integration periods i.e. for specific chosen time period, cold can appear over some regions.

The new land surface scheme and its coupling with the atmospheric model have shown an influence on the future mean sea level pressure, precipitation, 2 *m* air

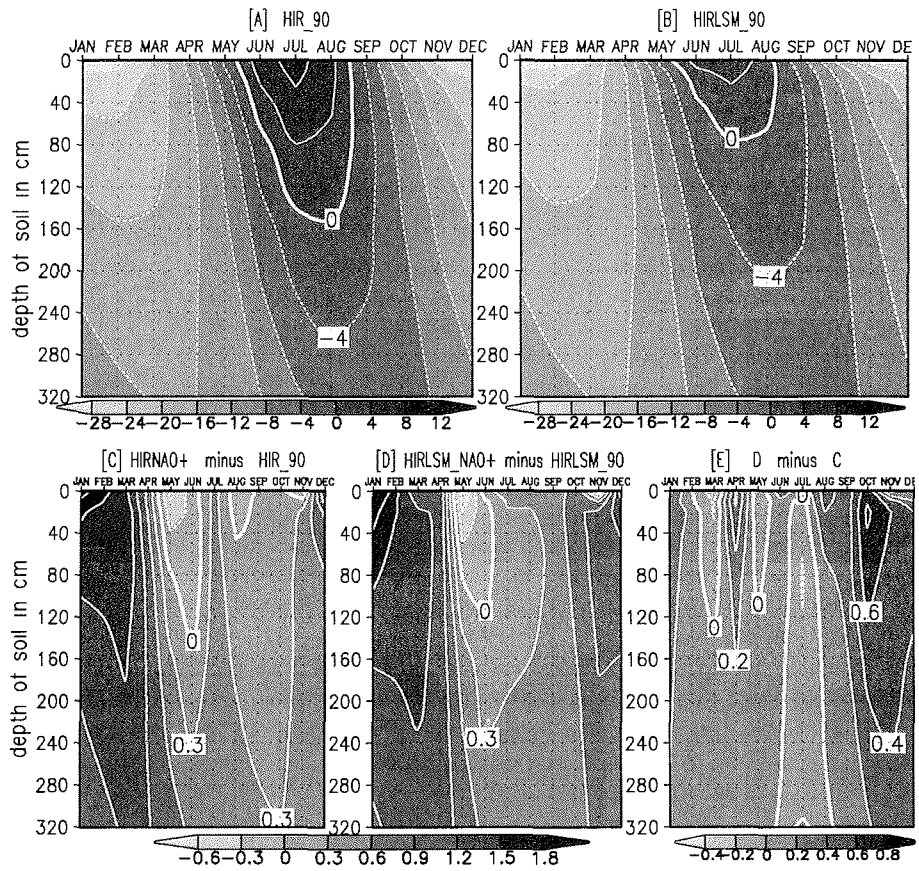

Figure 7.9: Domain averaged (except 10 grid points at the boundary and glacier) monthly climatology mean vertical soil temperature profile in °C for HIR-LSM and HIR_90 simulations and the warming and cooling during 2037-2042 compared to 1990-1995 in HIRHAM4 simulation (HIR_NAO$^+$ *minus* HIR_90) and HIR-LSM simulation (HIRLSM_NAO$^+$ *minus* HIRLSM_90)

and soil temperature. The difference between two model's projected (during 2037-2042 compared to 1990-1995) air temperature is within $\pm 2\,°C$. The soil temperature differences between HIR-LSM and HIRHAM4 are of the order of $\pm 2\,°C$ at $20\,cm$ depth. The deeper soil layer's ($320\,cm$) temperatures in both model have also differed from each other by $\pm 2\,°C$. The HIR-LSM winter projected soil temperature at the coast of Siberia is warmer than the HIRHAM4 projected soil temperature. Also there are differences in summer projected precipitation by $\pm 12\ mm\,month^{-1}$ between two models and their spatial distributions are very patchy. The projected mean sea level pressure is differed in HIR-LSM from HIRHAM4 by a maximum of 4 hPa.

8 Conclusions

The regional climate model HIRHAM4 has been simulated for the years 1979-1993 using ERA-15 lateral and lower boundary forcing. The model simulated $2\,m$ air and soil temperature, precipitation, mean sea level pressure (MSLP), snow water equivalent (SWE) and surface albedo have been compared with the available observed and ERA-15 reanalysis data sets. The station averaged $2\,m$ air temperatures, simulated by the model at all locations (West Russia, East Siberia, Lena Delta and North Canada) are very close to the observations. The summer averaged model $2\,m$ air temperature, overestimates the Willmottt-Rawlins climatology at the north coast of Canada, Alaska and Siberia by a maximum of 8 °C. Also the model surface albedo during the months April, May and Jun underestimates the satellite APP climatology at the north coast of Siberia, Canada and Alaska by a maximum of 50%. Therefore the model summer warm bias in $2\,m$ air temperature is partly due to the less surface albedo. Except for the Lena Delta, the soil temperatures at all stations have shown that the model soil has a large cold bias during winter. The largest winter cold bias occurred at East Siberian stations, the model was colder than the observations by a maximum of about 20 °C. Also the model has a large deficiency in SWE compared to the station measurements and satellite observation. The large winter cooling in the model soil is partly due to the lack of SWE and the absence of soil moisture freezing/thawing scheme. However during summer, the model soil temperature was quite good compared to the observations.

The revised stability function under the stable condition has increased the downward sensible heat flux during winter. Therefore a warming in the winter soil was found. The domain averaged warming in the winter soil was by a maximum of 0.5 °C. An increase in sensible heat flux at the surface increased the surface temperature and hence the surface long wave radiation. A decrease in soil thermal conductivity and a decrease in snow density influenced the winter soil temperature in a similar way. At the deeper soil layer, the model soil temperature increased during winter by a maximum of 3 °and decreased during summer by a maximum of 6 °C (on the basis of domain averaged soil temperature). Due to the decrease in soil thermal conductivity or decrease in snow density, the ground heat loss during winter was reduced. During summer, the ground heat gain was also reduced. Therefore, a cooling and warming at the deeper soil layer were found compared to the control HIRHAM4 simulations, during summer and winter respectively. The upper soil layer during winter was colder than the control in both, snow density and thermal conductivity sensitivity experiments. Since during winter, the soil acts as a source of heat, the lower thermal conductivity and higher snow depth reduced the ground heat flux. Therefore a relatively (compared to the control) cold surface, cooled down the up-

per soil layer further. The new snow albedo scheme was able to increase the surface albedo during the months April, May and Jun by a maximum of 0.12, which was underestimated by the model by a maximum of 0.5. Though the increase in surface albedo due to the new snow albedo scheme was small compared to the model bias, it was able to decrease the summer model bias in $2\,m$ air temperature by a maximum of 1.5 °C. The mean sea level pressure is seen very sensitive to the change in model parameters. The influences on mean sea level pressure over the land surface was smaller compared to the ocean surface. A maximum of ±6 hPa changes in mean sea level pressure compared to the control HIRHAM4 simulation were found in all sensitivity experiment.

The NCAR LSM was driven by the HIRHAM4 output at each time step and a simulation of 15 years was performed. The land surface model improved the winter soil temperature everywhere in the domain compared to the HIRHAM4. At 10 cm depth during winter, the LSM was warmer by a maximum of 5 °C compared to the HIRHAM4. However at 320 cm depth, the winter warming was by a maximum of 10 °C. There was also an increase in SWE. The LSM showed that, the soil moisture content and the amount of snow over ground are important for the winter soil temperature evolution. The warming in soil during winter reduced the winter cold bias. The overall performance of the LSM in soil temperature simulation was found encouraging. Therefore a two way interactive coupling between the HIRHAM4 and LSM was designed. The HIRHAM4 coupled LSM (HIR-LSM), was used to simulate the same ERA-15 periods climate and the simulated soil temperature was found quite good during winter compared to the HIRHAM4. Improvement in winter soil temperature was comparable to the stand alone LSM simulation. There were large changes in the HIR-LSM simulated surface sensible, latent and radiative fluxes compared to the HIRHAM4. The surface sensible and latent heat flux change were probably due to the different spatial distribution of soil moisture content in HIRHAM4 and land surface model. The surface radiative fluxes were indirectly influenced by the changed surface sensible and latent heat fluxes. The model HIR-LSM was able to reduce the winter cold bias in soil temperature. In future, there are possibility to couple the land surface model with HIRHAM4, through sensible and latent heat fluxes from LSM.

The soil temperature in the permafrost regions was found sensitive to the use of different land surface schemes during scenario simulations. The differences between the coupled HIR-LSM and the HIRHAM4 projected change (2037-42 *minus* 1990-95) in soil temperature are of the order of ±2 °C. Also there are changes in summer precipitation by ±12 $mm\,month^{-1}$ in the coupled HIR-LSM compared to the HIRHAM4 and their spatial distributions are very patchy. The mean sea level pressure was also changed in the coupled HIR-LSM by a maximum of 4 hPa.

To reduce the remaining winter soil bias there is a need to increase the model precipitation, particularly during the winter season. Ground insulation by the snow during winter is very important for maintaining the relatively warm soil temperature. Currently both models HIRHAM4 and HIR-LSM are using a simplified snow scheme. The snow scheme has to be improved by introducing more than one snow layer, time dependent snow density and thermal properties. The model also need to increase

the horizontal resolution. Increase in model resolution will capture the small scale processes in a better way and the uncertainty due to interpolation of model simulated data to a station point will decrease.

The number of stations, that measure the soil temperature are very few in the Arctic. More station data is needed for understanding the present permafrost conditions and its future evolution.

A Appendix

Data set	Station name	Longitude (°. ′)	Latitude (°. ′)	Elevation (m)
East Siberia (**ES**)	Amga	131.98	60.9	- -
	Bestyal	124.2	65.2	- -
	Borogol	131.62	62.6	- -
	Chaingl	119.51	62.17	- -
	Chumpul	116.55	64.14	- -
	Churapl	132.6	62.03	- -
	Dobrolet	127.05	60.37	- -
	Drughil	145.2	68.12	- -
	Dzhardl	124.00	68.73	- -
	Isit	125.32	60.82	- -
	Kazachie	125.32	60.82	- -
	Khatyrl	125.1	63.8	- -
	Krest_1	134.43	62.82	- -
	Namtsyl	129.67	62.73	- -
	Ohotsk	135.50	61.87	- -
	Oimyakl	143.0	63.16	- -
	Olekmil	120.42	60.4	- -
	Olenekl	112.40	68.50	- -
	Pokrovsk	134.43	61.5	- -
	Sangarl	127.47	63.97	- -
	Sanyyal	124.0	60.7	- -
	Sukhanl	117.58	68.48	- -
	Tongull	124.33	61.55	- -
	Uchurdat	130.37	58.44	- -
	Ustmaya	134.45	60.38	- -
	Ust_mol	143.14	66.27	- -
	Verhoyl	133.38	67.55	- -
	Viluisk	121.62	63.77	- -
	Yakutsl	129.80	62.10	- -
	Ytyk_kel	133.55	62.37	- -
	Zhigansk	123.4	66.77	- -
North Canada (**NC**)	Hall Beach	-81.15	68.47	8
	Baker Lake	-96.05	64.18	18

Data set	Station name	Longitude (°. ′)	Latitude (°. ′)	Elevation (m)
Lena Delta (**LD**)	Lena Delta	126.48	72.37	- -
West Russia (**WR**)	Arkhangel'sk, Solombala	40.50	64.58	3
	Eletskaya	64.17	67.17	113
	Ust'-Usa	56.92	65.97	77
	Troitsko-Pechorskoe	56.20	62.70	107
	Syktyvkar	50.85	61.67	96
	Sidorovsk	82.33	66.67	34
	Salekhard	66.53	66.53	35
	Tarko-Sale	77.82	64.92	27
	Turukhansk	87.95	65.78	32
	Kargopol'	38.95	61.50	121
	Arkhangel'sk, exp.field	40.50	64.58	4
	Velikii Ustyug	46.30	60.77	94
	Saranpaul'	60.88	64.28	28
	Berezovo	65.05	63.93	27
	Tura	100.07	64.17	186
	Syktyvkar	50.85	61.67	96
	Ust'-Un'ya	57.92	61.80	174
	Vologda, Molochnoe	39.87	59.28	118
	Berezniki	56.60	59.38	124
	Kudymkar	54.65	58.98	150
	Ivdel'	60.43	60.68	101
	Konosha	40.17	61.00	224
	Khoseda-Khard	59.38	67.08	84
	Ust'-Tsil'ma	52.17	65.45	70
	Kotkino	51.20	67.02	18
West Russia (**WRII**)	Khatanga	102.28	71.59	33
	Varandei	58.01	68.49	5
	Khorei Ver	58.04	67.25	72
	Khoseda Khard	59.23	67.05	84
	Petrun	60.49	66.26	61
	Ust Usa	56.55	65.58	77
	Pechora	57.06	65.07	59
	Ust Shugor	57.37	64.16	73
	Troitsko Pechorsk	56.12	62.42	139
	Narjan Mar	53.01	67.39	7
	Ust Tsilma	52.28	65.42	68
	Vorkuta	64.02	67.29	165
	Eletskaya	64.04	67.03	113
	Polar Urals	65.05	67.01	182
	Verkhni Shugor	59.30	64.02	290

Table A.1: The five data sets, which are used for the model validations and the corresponding name, location (longitude, latitude) and elevation (in m) of each stations.

Bibliography

Abegg, C., Parameterization of atmospheric boundary layer processes in a regional climate model of the Arctic (in German), Reports on Ploar Research 311, Alfred Wegener Inst., Bremerhaven, Germany, 1999.

Anisimov, O. A., and F. E. Nelson, Permafrost Distribution in the Northern Hemisphere under Scenarios of Climate Change, *Global Planetary Change*, *14*, 59–72, 1996.

Atlas, R., N. Wolfson, and J. Terry, The Effect of SST and Soil Moisture Anomalies on GLA Model Simulations of the 1988 U.S. Summer Drought, *J. Clim.*, *6*, 2034–2048, 1993.

Barry, R., T. Zhang, and D. Gilichinsky, Russian historical soil temperature data, National Snow and Ice Data Center, Boulder, CO, Digital media, 2001.

Beljaars, A. C. M., P. Viterbo, M. J. Miller, and A. K. Betts, The Anomalous Rainfall over the United States during July 1993: Sensitivity to Land Surface Parameterization and Soil Moisture Anomalies, *Mon. Weather Rev.*, *124*, 362–383, 1996.

Beringer, J., A. H. Lynch, F. S. C. III, M. Mack, and G. B. Bonan, The representation of Arctic Soils in the Land Surface Model, *J. Clim.*, *14*, 3324–3335, 2001.

Boike, J., and H. Becker, Thermal and hydrologic dynamics of the active layer. In: Rachold, V. and Grigoryev, M.M. (eds): Russian-German Cooperation SYSTEM LAPTEV SEA 2000: The Expedition LENA 1999, Tech. Rep. 354, Alfred Wegener Inst., Bremerhaven, Germany, 2000.

Bonan, G. B., A land surface model (LSM version 1.0) for ecological, hydrological and atmospheric studies: Technical description and user's guide, Tech. Rep. NCAR/TN-417 + STR, National Center for Atmospheric Research, NCAR, P.O. Box 3000, Boulder, Co 80307, 1996a.

Bonan, G. B., The Land Surface Climatology of the NCAR Land Surface Model Coupled to the NCAR Community Climate Model, *J. Clim.*, *11*, 1307–1326, 1998.

Box, J. E., and A. Rinke, Evaluation of Greenland Ice Sheet Surface Climate in the HIRHAM4 Regional Climate Model Using Automatic Weather Station Data, *J. Clim.*, *16*, 1302–1319, 2003.

Chen, B., D. H. Bromwich, K. M. Hines, and X. Plan, Simulations of the 1979–1988 polar climates by global climate models, *Ann. Glaciol.*, *21*, 83–90, 1995.

Christensen, J. H., O. B. Christensen, P. Lopez, E. van Meijgaard, and M. Botzet, The HIRHAM4 regional atmospheric climate model, DMI Sci. Rep. 96–4, Dan. Meteorol. Inst., Copenhagen, Denmark, 1996.

Christensen, J. H., O. B. Christensen, J. P. Schulz, S. Hageman, and M. Botzet, High resolution physiographic data set for HIRHAM4: An application to a 50 km horizontal resolution domain covering Europe, DMI Tech. Rep. 01–15, Dan. Meteorol. Inst., Copenhagen, Denmark, 2001.

Christensen, J. H., and P. Kuhry, High-resolution regional climate model validation and permafrost simulation for the East European Russian Arctic, *J. Geophys. Res.*, *105*, 29,647–29,658, 2000.

Christensen, J. H., and E. van Meijgaard, On the construction of a regional climate model, DMI Tech. Rep. 92–14, Dan. Meteorol. Inst., Copenhagen, Denmark, 1992.

Clapp, R. B., and G. M. Hornberger, Empirical equations for some soil hydraulic properties, *Water Resources Research*, *14*, 601–604, 1978.

Cogley, J. G., GGHYDRO - Global Hydrographic Data Release 2.0, Dept. Geography, Trent University, Peterborough, Ontario, Climate Note 91-1, 1991.

Cosby, B. J., G. M. Hornberger, R. B. Clapp, and T. R. Ginn, A statistical exploration of the relationships of soil moisture characteristics to the physical properties of soils, *Water Resource Research*, *20*, 682–690, 1984.

Cubasch, U., G. A. Meehl, G. J. Boer, R. J. Stouffer, M. Dix, A. Noda, C. A. Senior, S. Raper, and K. S. Yap, Projections of Future Climate Change, in *Climate Change 2001: The Scientific Basis. Contribution of Working Group I to the Third Assessment Report of the Intergovernmental Panel on Climate Change*, edited by J. T. Houghton, Y. Ding, D. J. Griggs, M. Noguer, P. J. van der Linden, X. Dai, K. Maskell, and C. A. Johnson, pp. 525–582, Cambridge University Press, Cambridge, U.K., 2001.

Curry, J., On the formation of polar continental air, *J. Atmos. Sci.*, *40*, 2278–2292, 1983.

Davies, H. C., A lateral boundary formulation for multilevel prediction models, *Q. J. R. Meteorol. Soc.*, *102*, 405–418, 1976.

Denis, B., R. Laprise, and D. Caya, Sensitivity of a regional climate model to the resolution of the lateral boundary conditions, *Clim. Dyn.*, *20*, 107–126, 2003.

Denis, B., R. Laprise, D. Caya, and J. Cote, Downscaling ability of one-way nested regional climate models: The big-brother experiment, *Clim. Dyn.*, *18*, 627–646, 2002.

Dethloff, K., C. Abegg, A. Rinke, I. Hebestadt, and V. F. Romanov, Sensitivity of Arctic climate simulations to different boundary-layer parameterizations in a regional climate model, *Tellus*, *53A*, 1–26, 2001.

Dethloff, K., A. Rinke, R. Lehmann, J. H. Christensen, M. Botzet, and B. Machenhauer, Regional climate model of the Arctic atmosphere, *J. Geophys. Res.*, *101*, 23401–23422, 1996.

Dickinson, R. E., A. Henderson-Sellers, and P. J. Kennedy, Biosphere-Atmosphere Transfer Scheme (BATS) version 1e as coupled to the NCAR Community Climate Model, NCAR Technical Note NCAR/TN-387+STR, National Center for Atmospheric Research, Boulder, CO, 1993.

Dorn, W., Natural climate variations of the Arctic in a regional high-resolution atmosphere model (in German), Reports on Polar and Marine Research 416, Alfred Wegener Inst., Bremerhaven, Germany, 2002.

Dorn, W., K. Dethloff, A. Rinke, and M. Botzet, Distinct circulation states of the Arctic atmosphere induced by natural climate variability, *J. Geophys. Res.*, *105*, 29659–29668, 2000.

Dorn, W., K. Dethloff, A. Rinke, and E. Roeckner, Competition of NAO regime changes and increasing greenhouse gases and aerosols with respect to Arctic climate projections, *Clim. Dyn.*, *21*, 447–458, doi:10.1007/s00382-003-0344-2, 2003.

Dümenil, L., and E. Todini, A rainfall-runoff scheme for use in the Hamburg climate model, in *Advances in Theoretical Hydrology, EGS Series on Hydrological Science*, edited by J. P. O'Kane, pp. 129–157, 1, Elsevier Press, Amsterdam, the Netherlands, 1992.

Exner, F. M., Sitzungberichte der Mathematische-Naturwissenschaftlichen Klasse der Akad, Wissenschaften, 122 Abteilung 2a, Zweiter Halbband, 6(10)1165, 1913.

Farouki, O. T., The thermal properties of soils in cold regions, *Cold Regi. Sc. and Tech.*, *5*, 67–75, 1981.

Fortman, M., Influence of tropospheric aerosols on the Arctic climate (in German), Reports on Polar and Marine Research 486, Alfred Wegener Inst., Bremerhaven, Germany, 2004.

Foster, D. J., and R. D. Davy, Global snow depth climatology, USAFETAC /TN-88/006, Scott Air Force base,Illinois, 1988.

Fowler, C., J. Maslanik, T. Haran, T. Scambos, J. Key, and W. Emery, AVHRR Polar Pathfinder twice-daily 25 km EASE-Grid composites, Boulder, CO: National Snow and Ice Data Center, Digital media, 2002.

Gibson, J. K., S. Kållberg, S. Uppala, A. Hernandez, A. Nomura, and E. Serrano, ERA-15 Description, ECMWF Re-Analysis Project Report Series version 2, Eur. Cent. for Medium-Range Weather Forecasts, Reading, U.K., 1999.

Goudriaan, J., *Crop micrometeorology: a simulation study*, Wageningen Center for Agricultural Publishing and Documentation, 1977.

Gustafsson, N., HIRLAM2 final report, HIRLAM Tech. Rep. 9, Swed. Meteorol. and Hydrol. Inst., Norrköping, Sweden, 1993.

Hinkel, K. M., and F. E. Nelson, Spatial and temporal patterns of active layer thickness at Circumpolar Active Layer Monitoring (CALM) sites in north Alaska, *J. Geophys. Res.*, *108*, (D2),10.129/2001JD000927, 2003.

Houghton, J. T., Y. Ding, D. J. Griggs, M. Noguer, P. J. van der Linden, X. Dai, K. Maskell, and C. A. Johnson (eds.), *Climate Change 2001: The Scientific Basis. Contribution of Working Group I to the Third Assessment Report of the Intergovernmental Panel on Climate Change*, Cambridge University Press, Cambridge, U.K., 2001.

Hurrell, J. W., Decadal trends in the North Atlantic Oscillation: regional temperatures and precipitation, *Science*, *269*, 676–679, 1995.

Jones, R. G., J. M. Murphy, and M. Noguer, Simulation of climate change over Europe using a nested regional-climate model. I: Assessment of control climate, including sensitivity to location of lateral boundaries, *Q. J. R. Meteorol. Soc.*, *121*, 1413–1449, 1995.

Kahl, J. D., Characteristics of the low-level temperature inversion along the Alaskan Arctic coast, *Int. J. Climatol.*, *10*, 537–548, 1990.

Kanamitsu, M., C. H. Lu, J. Schemm, and W. Ebisuzaki, The Predictability of Soil Moisture and Near-Surface Temperature in Hindcast of the NCEP Seasonal Forecast Model, *J. Clim.*, *16*, 510–521, 2003.

Kiilsholm, S., J. H. Christensen, K. Dethloff, and A. Rinke, Net accumulation of the Greenland ice sheet: High resolution modeling of climate changes, *Geophys. Res. Lett.*, *30*, 1485, doi:10.1029/2002GL015742, 2003.

Køltzow, M., and S. Eastwood, Comparison between temperature dependent parameterization schemes for snow albedo and estimated snow albedo from AVHRR, Research Note 98, Norwegian Meteorological Institute, 2003.

Kushnir, Y., and J. M. Wallace, Low-frequency variability in the Northern Hemesphere winter-geographical-distribution, structure and time-scale dependence, *J. Atmos. Sci.*, *46*, 3122–3142, 1989.

Legates, D. R., and C. J. Willmott, Mean seasonal and spatial variability in global surface air temperature, *Theor. Appl. Climatol.*, *41*, 11–21, 1990.

Ling, F., and T. Zhang, Impact of the Timing and Duration of Seasonal Snow Cover on the Active Layer and Permafrost in the Arctic, *Permafr. Periglac. Proce.*, *14*, 141–150, 2003.

Louis, J. F., A parametric model of vertical eddy fluxes in the atmosphere, *Bound. Layer Meteor.*, *17*, 187–202, 1979.

Louis, J. F., M. Tiedtke, and J. F. Geleyn, 'A short history of the operational PBL-parameterization at ECMWF', in Proceeding of the ECMWF workshop on boundary layer parameterization 5, Eur. Cent. for Medium-Range Weather Forecasts, Reading, U.K., 1982.

Lunardini, V. J., *Heat transfer in cold climates*, Van Nostrand Reinhold Co, New York, 1981.

Machenhauer, B., The HIRLAM final report, HIRLAM Tech. Rep. 5, Dan. Meteorol. Inst., Copenhagen, Denmark, 1988.

Machenhauer, B., M. Windelband, M. Botzet, J. H. Christensen, M. Déqué, R. G. Jones, P. M. Ruti, and G. Visconti, Validation and analysis of regional present-day climate and climate change simulations over Europe, MPI Rep. 275, Max Planck Inst. for Meteorol., Hamburg, Germany, 1998.

Machenhauer, B., M. Windelband, M. Botzet, M. Déqué, and R. G. Jones, Validation of present-day regional climate simulations over Europe: nested LAM and variable resolution global model simulations with observed or mixed layer ocean boundary conditions, MPI Rep. 191, Max Planck Inst. for Meteorol., Hamburg, Germany, 1996.

Matsuura, K., and C. J. Willmott, Arctic Land-Surface Precipitation: 1930-2000 Gridded Monthly Time Series, Center for Climatic Research, Department of Geography, University of Delaware, Newark, DE 19716, 2004.

Olson, J. S., Global ecosystem framework-definitions, USGS EROS Data Center International report 1994a.

Olson, J. S., Global ecosystem framework-translation strategy, USGS EROS Data Center International report 1994b.

Pavlov, A. V., and N. G. Moskalenko, The Thermal Regime of Soils in the North of Western Siberia, *Permafr. Periglac. Proce.*, *13*, 43–51, 2002.

Putkonen, J., and G. Roe, Rain-on-snow events impact soil temperatures and affect ungulate survival, *Geophys. Res. Lett.*, *30*, 2003.

Rinke, A., K. Dethloff, and J. H. Christensen, Arctic winter climate and its interannual variations simulated by a regional climate model, *J. Geophys. Res.*, *104*, 19027–19038, 1999.

Rinke, A., A. H. Lynch, and K. Dethloff, Intercomparison of Arctic regional climate simulations: Case studies of January and June 1990, *J. Geophys. Res.*, *105*, 29669–29683, 2000.

Robock, A., The seasonal cycle of snow cover, sea-ice and surface albedo, *Mon. Weather Rev.*, *108*, 267–285, 1980.

Roeckner, E., K. Arpe, L. Bengtsson, S. Brinkop, L. Dümenil, M. Esch, E. Kirk, F. Lunkeit, M. Ponater, B. Rockel, R. Sausen, U. Schlese, S. Schubert, and M. Windelband, Simulation of the present-day climate with the ECHAM model: impact of model physics and resolution, MPI Rep. 93, Max Planck Inst. for Meteorol., Hamburg, Germany, 1992.

Roeckner, E., K. Arpe, L. Bengtsson, M. Christoph, M. Claussen, L. Dümenil, M. Esch, M. Giorgetta, U. Schlese, and U. Schulzweida, The atmospheric general circulation model ECHAM-4: Model description and simulation of present-day climate, MPI Rep. 218, Max Planck Inst. for Meteorol., Hamburg, Germany, 1996.

Roesch, A., M. Wild, R. Pinker, and A. Ohmura, Comparison of spectral surface albedos and their impact on the general circulation model simulated surface climate, *J. Geophys. Res.*, *107*, 10.1029/2001JD000809, 2002.

Roesch, A. C., *Assessment of the Land Surface Scheme in Climate Models with Focus on Surface Albedo and Snow Cover*, Ph.D. thesis, ETH Zürich, 2000.

Sellers, P. J., Y. Mintz, Y. C. Sud, and A. Dalcher, A simple biosphere model (Sib) for use within general cilculation models, *J. Atmos. Sci.*, *43*, 505–531, 1986.

Serreze, M. C., and R. G. Barry, Synoptic Activity in the Arctic Basin, 1979-85, *J. Clim.*, *1*, 1276–1295, 1988.

Serreze, M. C., J. D. Kahl, and R. C. Schnell, Low-Level Temperature Inversions of the Eurasian Arctic and Comparisons with Soviet Drifting Station Data, *J. Clim.*, *5*, 615–629, 1992.

Smith, S., Summary of Research Activities in 2002 at Baker Lake CALM site, Annual report, Environment Canada's Northern Ecosystem Initiatives, Maintaining the CANTTEX site at Baker Lake, 2003.

Smith, S. L., M. Burgess, and F. Nixon, Response of active-layer and permafrost temperatures to warming during 1998 in the Mackenzie Delta, Northwest Territories and at Canadian Forces Station Alert and Baker Lake, Nunavut, 2001-E5, Geological Survey of Canada Current Research, 2001.

Sturm, M., J. Holmgren, M. Konig, and k. Morris, The thermal conductivity of seasonal snow, *J. Glaciology*, *43*, 26–41, 1997.

Tao, X., J. E. Walsh, and W. L. Chapman, An assessment of global climate model simulations of Arctic air temperatures, *J. Clim.*, *9*, 1060–1076, 1996.

van Loon, H., and J. C. Rogers, Seasaw in winter temperature between Greenland and Northern Europe. 1. General description, *Mon. Weather Rev.*, *106*, 296–310, 1978.

Verseghy, D. L., CLASS– A Canadian Land Surface Scheme for GCMs. I Soil Model, *Int. J. Climatol.*, *11*, 111–133, 1991.

Viterbo, P., A. Beljaars, J. F. Mahfouf, and J. Teixeira, The representation of soil moisture freezing and its impact on the stable boundary layer, *Q. J. R. Meteorol. Soc.*, *125*, 2401–2426, 1999.

Walker, G. T., Correlation in seasonal variations of weather IX, *Memoris India: Meteorological Department*, *24*, 687–692, 1924.

Wallace, J. M., and D. S. Gutzler, Teleconnections in the geopotential height field during the Northern Hemisphere winter, *Mon. Weather Rev.*, *109*, 784–812, 1981.

Wallace, J. M., Y. Zhang, and L. Bajuk, Interpretation of interdecadal trends in Northern Hemisphere surface air temperature, *J. Clim.*, *9*, 249–259, 1996.

Webb, R. S., C. E. Rosenzweig, and E. R. Levine, Specifying land surface characteristics in general circulation models: soil profile data set and derived water-holding capacities, *Global Biogeochemical Cycle*, *7*, 97–108, 1993.

Willmott, C. J., and K. Matsuura, Smart Interpolation of Annually Averaged Air Temperature in the United States, *J. Appl. Meteorol.*, *34*, 2577–2586, 1995.

Willmott, C. J., and M. A. Rawlins, Arctic Land-Surface Air Temperature: Gridded Monthly and Annual Climatologies (Version 1.01), Center for Climatic Research, Department of Geography, University of Delaware, Newark, DE 19716, 1999.

Wilson, M. F., and A. Henderson-Sellers, A global archive of land cover and soils, data for use in general circulation climate models, *J. Climatol.*, *5*, 119–143, 1985.

Wolff, J.-O., E. Maier-Reimer, and S. Legutke, The Hamburg ocean primitive equation model, DKRZ Tech. Rep. 13, Dtsch. Klimarechenz., Hamburg, Germany, 1997.

Xie, P., and P. A. Arkin, Global Precipitation: A 17-year monthly analysis based on gauge observations, satellite estimates, and numerical model outputs, *Bul. Amer. Meteor. Soc.*, *78*, 2539–2558, 1997.

Yang, R., M. J. Fennessy, and J. Shukla, The Influence of Initial Soil Wetness on Medium-range Surface Weather Forecasts, *Mon. Weather Rev.*, *122*, 471–485, 1994.

Yershov, E. D., *General Geocryology*, Cambridge University Press, Moscow State University, 1st edn., 1998.

Zhang, T., K. Stamnes, and S. A. Bowling, Impact of the atmospheric thickness on the atmospheric downwelling longwave radiation and snowmelt under clear-sky conditions in the Arctic and Subarctic, *J. Clim.*, *14*, 920–939, 2001.

Acknowledgments

I would like to express my sincere thanks to Prof. Dr. Klaus Dethloff, the supervisor of this doctoral study programme, for his guide and encouragement. His deep insight into the Arctic climate system provided the potential to this thesis. I appreciate his sense of humour and the friendly atmosphere that he creates at the institute.

It is my great opportunity to get the guidance of Dr. Annette Rinke. Her encouragement and motivation during the work was my source of energy. Her understanding and collective approach showed me light at the time of crisis and helped me put things back in perspective. I thank her for her invaluable supervision and suggestions. I am grateful to her and her family for giving homely feeling during my stay in Berlin.

I sincerely thank Dr. A. C. Roesch from ETH Zürich for his support in understanding the spectral splitting of HIRHAM4 radiation scheme. It would not have been possible to run the NCAR LSM model without his kind help.

I would like to thank Prof. P. Kuhry who provided station data from Russian and Alaskan stations and valuable suggestions. Many thanks to Dr. J. Boike who provided station data and helped to understand the soil processes in the Arctic.

I am grateful to Dr. G. Bonan from NCAR USA who kindly provided me the Land Surface Model and Dr. W. Wu from University of Colorado for extending his help to run the Land Surface Model.

My thanks to Mrs. I. Hebestadt and Mrs. S. Erxleben for programming support. I would like to thank Mr. Heiko Gericke for his technical support and making computers available all the time at AWI.

I would like to thank Mr. Klaus Ketelsen from DKRZ for optimizing the HIRHAM4 code and helping to simulate several long simulations.

Many thanks to Dr. M. Lüter. I am grateful to him for his sincere help during my stay at AWI. He also helped me by giving useful information regarding the official formalities of Potsdam University.

I am grateful to Dr. W. Dorn who provided valuable help during preparation of boundary data for scenario simulations. I appreciate his help for writing thesis in Latex.

All the colleagues in our institute are appreciated for their family like atmosphere.

My thanks to Dr. C. Manoj and Dr. P. Kumar from NGRI, India who corrected my English.

Many thanks to Mr. Tapas Mitra (Manida) and his wife Mrs. Siegrid Mitra for giving homely feeling during my stay in Berlin. I will always remember Manida for his great sense of humour and his kind help in a foreign country.

My deepest sense of gratitude to my parents. It is their blessings and goodwill

which drive my life and it is their suggestions which lead me to the right path.

My special thanks to my wife, Pinki Saha for giving consistent assistance and moral supports during thesis writing. I appreciate her help for making several pictures and tables for my thesis.